

Thrombospondins -4 and -5 in Skeletal Development, Disease and Repair

Implications for bone tissue engineering



ENRIQUE ANDRÉS SASTRE

Colophon

Copyright © Enrique Andrés Sastre, The Netherlands, 2022

ISBN: 978-94-6361-684-3

All rights reserved. No parts of this thesis may be reproduced, distributed, stored in a retrieval system, or transmitted in any form or by any means, without written permission of the author or, when appropriate, the publisher of the publications.

The work presented in this thesis was conducted at the Department of Oral and Maxillofacial Surgery, Erasmus MC, University Medical Center Rotterdam, the Netherlands, and is part of the Medical Delta Regenerative Medicine 4D program. The research leading to these results was performed within the Connective Tissue Repair Lab and supported by the European Union's Horizon 2020 research and innovation program under Marie Skłodowska-Curie grant agreement no. 721432.

Cover design and illustrations: Enrique Andrés Sastre, Enrique Andrés Serra

Layout and printing: Javier Andrés Sastre, Optima Grafische Communicatie, Rotterdam, The Netherlands

Printing of this thesis was financially supported by:

Erasmus University Rotterdam

Dutch Society for Matrix Biology

Medical Delta

**Thrombospondins -4 and -5 in Skeletal Development, Disease and Repair
Implications for Bone Tissue Engineering**

**Trombospondines -4 en -5 in ontwikkeling, ziekte en herstel van het skelet
Implicaties voor tissue engineering van bot**

Thesis

To obtain the degree of Doctor from the
Erasmus University Rotterdam
by command of the
rector magnificus

Prof. dr. A.L. Bredenoord

and in accordance with the decision of the Doctorate Board.
The public defence shall be held on

Tuesday 31st May 2022 at 13:00

by

Enrique Andrés Sastre

Born in Valencia, Spain

DOCTORAL COMMITTEE

Promotor: Prof. dr. G.J.V.M. van Osch

Other members: Dr. B.C.J. van der Eerden

Prof. dr. R.A. Bank

Prof. dr. S. Grässel

Copromotor: Dr. E. Farrell

A mons pares, que sou definició
pura d'esforç i de voler

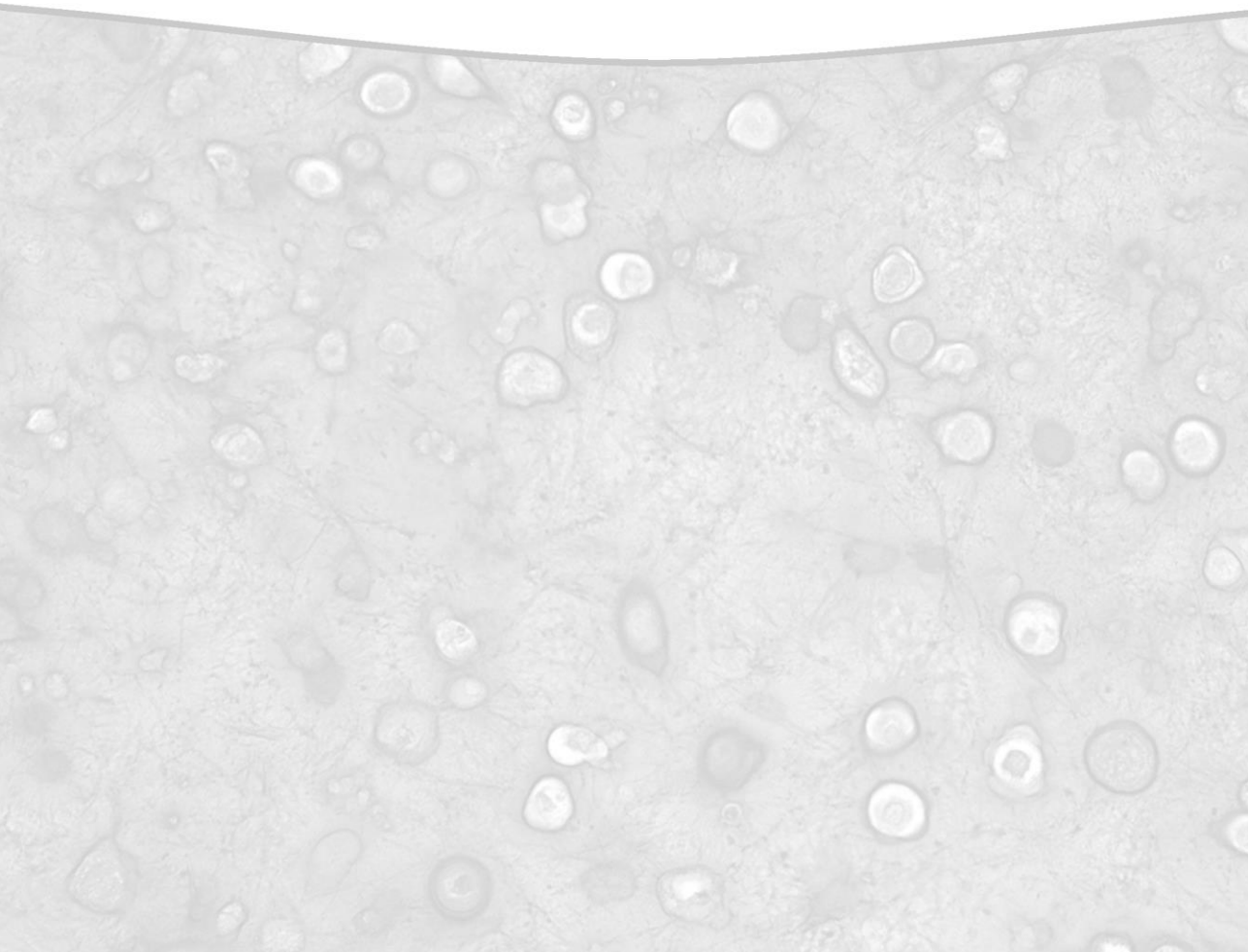
Als meus germans, que sempre
vos porte al cor allà on vaig

TABLE OF CONTENTS

Chapter 1	General introduction	9
Chapter 2	Spatiotemporal distribution of TSP-4 and TSP-5 during bone formation and repair	21
Chapter 3	TSP-5 and TSP-4: functional roles in articular cartilage and relevance in osteoarthritis	39
Chapter 4	TSP-5 derived peptides secreted by cartilage do not induce responses commonly observed during osteoarthritis	65
Chapter 5	A new semi-orthotopic bone defect model for cell and biomaterial testing in regenerative medicine	77
Chapter 5 Annex	TSP-4 potential for bone regenerative therapies	101
Chapter 6	General discussion and conclusions	109
Chapter 7	Summary	121
Chapter 8	References	127
Appendices		
	Nederlandse Samenvatting	147
	Resumen – Español	151
	Resum – Valencià	155
	List of publications	159
	Acknowledgements	161
	PhD portfolio	165
	Curriculum Vitae	167

CHAPTER 1

General introduction



THE SKELETON

Evolutionary origin of our skeleton

To understand the complex development and functions of the skeleton we possess it is key to place it in the context from which it first evolved (reviewed in [1, 2]). Our distant, long ago extinct marine ancestors possessed simple collagen-based endoskeletons which assisted their locomotion. During the Cambrian explosion, natural selection began to shape their skeletons in response to the new trophic relationships between the first complex predators and their prey. Improvements that made use of mineralised tissues in the head such as teeth and jaws rapidly spread, as well as protective exoskeletal bony shields in response. In parallel, by extending the use of those successful mineral elements to the existing collagenous endoskeletons, ossification gradually moved to the inside of the body, conferring structural strength and allowing rapid and massive growth. These two evolutionary innovations coexisted resulting in two converging redundant mechanisms through which bone formed, which have been retained until today. During our skeletal development, growth and healing, our bones form following both those two ancestral mechanisms namely intramembranous ossification and endochondral ossification (introduced later). However, failing to flawlessly execute those complex molecular processes is often at the basis of various skeletal diseases, and thus, understanding the two will be fundamental in assessing their causes and developing new treatments.

Intramembranous ossification

Most bones of the skull and the clavicles are formed from sheet-like connective tissue membranes, that contain undifferentiated mesenchymal cells (MSCs), via the process of intramembranous ossification (IO, Fig. 1) [2, 3]. These MSCs cluster to form centers of ossification, from which bone formation spreads. They differentiate into osteoblasts, cells

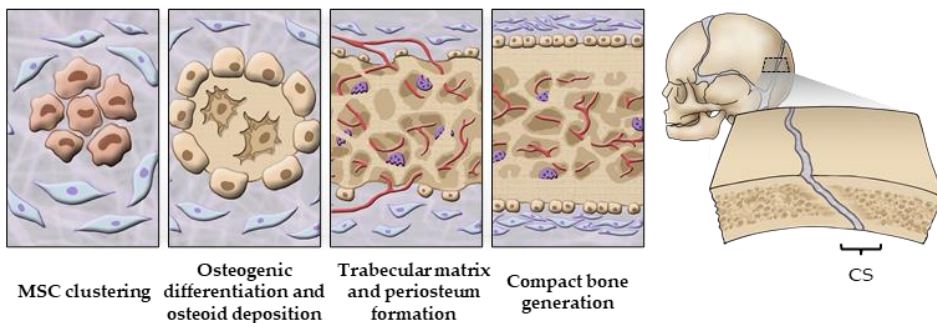


Figure 1. Steps of Intramembranous Ossification. Abbreviations: mesenchymal stem cell (MSC), cranial suture (CS).

specialised in forming the bone. These osteoblasts secrete osteoid, an immature collagen type I matrix that calcifies within a few days, hardening and entrapping the osteoblasts within. While those osteoblasts will transform into osteocytes, which will be responsible for maintaining the surrounding bone tissue, new osteoblasts at the edges of the bone will continue to arise promoting the growth of the trabecular bone. The periosteum produces cortical bone on the surface of the trabecular bone. Small junctions between the skull bones (cranial sutures) sustain a pool of progenitor cells to allow the growth of the skull until the end of the adolescence, moment in which the bones fuse together to conclude growth.

Endochondral ossification

In parallel to the bones formed via IO, the majority of bones start first as cartilage templates and are gradually replaced by bone, through a process known as endochondral ossification (EO, Fig. 2) [2, 4]. At the location of the new bone that will be formed, a group of progenitor cells condense, proliferate and differentiate into chondrocytes. These chondrocytes start producing an avascular cartilaginous matrix based on collagen type II and aggrecan, with the shape of the future bone. Meanwhile, the cartilage template undergoes a highly regulated process [5], with marginal proliferation and central maturation and cellular hypertrophy. The signals released by the hypertrophic chondrocytes attract blood vessels, causing the vascularisation of the diaphyseal perichondrium and its transformation into periosteum. Osteoblasts arise at the periosteum and secrete bone matrix against the cartilage forming the bone collar, which contributes to the growth of the bone in width. Meanwhile, the hypertrophic chondrocytes at the central area of the cartilage template calcify and degrade their extracellular matrix. After this, most of them commit programmed cell death (apoptosis), while a few of them transdifferentiate into osteoblasts to contribute to bone formation [6]. The porous, degraded matrix left behind facilitates the invasion of periosteal cells and blood vessels into the central area of the template, giving rise to the primary ossification center (POC). From this center, in an iterative cycle of chondrocyte

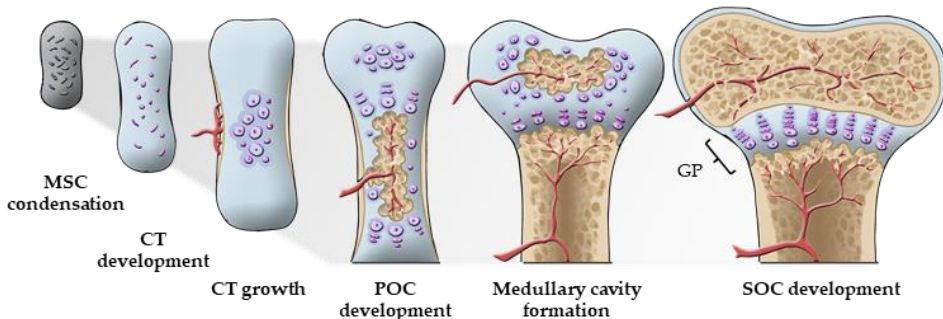


Figure 2. Stages of endochondral ossification. Abbreviations: mesenchymal stem cell (MSC), cartilage template (CT), primary ossification center (POC), secondary ossification center (SOC), growth plate (GP).

hypertrophy and invasion, bone is deposited over the cartilage surfaces. This center spreads along the diaphysis of the bone and aided by bone-resorbing cells, the osteoclasts, a medullary cavity is formed while the bone keeps growing in length. After birth, secondary ossification centers (SOC) form at the bone epiphyses and radiate from their centers. The most distal region of the bone will remain as articular cartilage, to allow easy motion between bones. The region where the primary and secondary ossification centers meet forms the growth plate (GP). There, a distal, thin plane of progenitor cells remains until adulthood and is responsible for the growth in length of the bone [7]. These cells divide and their daughter cells proliferate and undergo hypertrophy, and the cartilage that they had been producing is iteratively replaced by bone to elongate the diaphysis. Three distinct zones, containing chondrocytes at different maturation steps, are present on the GP: the resting zone (RZ), the proliferative zone (PZ) and the hypertrophic zone (HZ). Once sexual maturity is reached, the chondrocytes exhaust their proliferative potential and longitudinal bone growth is ceased.

NORMAL AND PATHOLOGICAL HEALING OF THE SKELETAL TISSUES

Normal and impaired fracture healing

Mobility is crucial for human quality of life. However, different traumatic injuries and diseases of the skeletal system affect many people and restrict their mobility. A systematic analysis of bone fractures pointed out that while the incidence, prevalence, and years lived with disability decreased slightly from 1990 to 2019, the absolute counts increased substantially (33.4%, 70.1% and 65.3% respectively), largely as a result of population growth and ageing [8].

In the event of a bone fracture, bone undergoes its regeneration by triggering a combination of the two mechanisms of bone formation previously described depending on the type, severity of the fracture and distance between bone fragments (reviewed in [9, 10]). When adequately stabilised, the broken ends may directly heal by fusing together (direct bone healing). However, this is rarely the case, and a callus is normally formed between the broken ends to stabilise the fracture (indirect bone healing). Through this mechanism, temporal cartilaginous patches form first, which ossify by recapitulating the EO program. In parallel, the IO also takes place to contribute to bone healing. The endochondral pathway is dominant in more severe fractures and, the healing process occurs in three stages that have significant overlap: the inflammatory phase, the reparative phase, and the bone remodelling phase (Fig. 3). Right after the fracture, blood released from broken vessels forms a haematoma at the site of injury (inflammatory phase). This event triggers cells from the periosteum and the bone marrow to commit to the chondrogenic lineage 48 hours after the fracture, which then secrete a transient fibrocartilaginous matrix between the two ends of the broken bone forming a soft callus that stabilises the broken ends (reparative phase). Following this, the newly formed

chondrocytes undergo hypertrophic maturation and the callus hardens as it is replaced by trabecular bone via EO, aided by the combined action of osteoblasts and osteoclasts. Last, over several months the bone formed slowly remodels to adapt to the mechanical forces (remodelling phase).

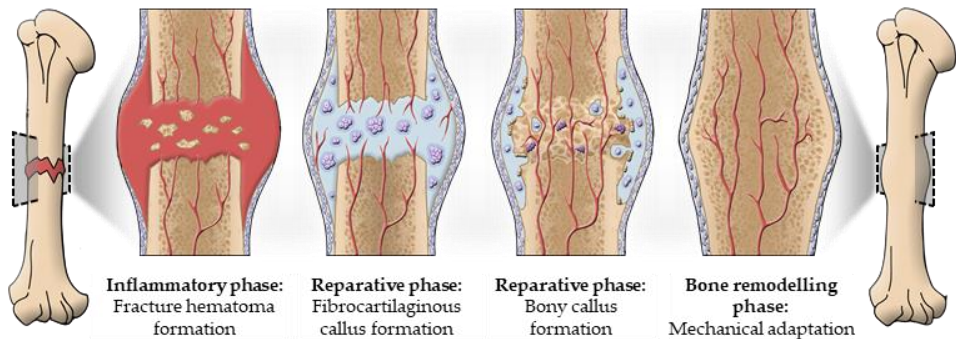


Figure 3. Stages in Fracture Repair

Unfortunately, failure of bone fracture healing occurs in 5% to 10% of all patients resulting in non-unions [11]. In most situations, patients can be treated with autologous bone grafts harvested from other locations of their body [12]. Nevertheless, this solution is far from optimal when the bone defect exceeds a critical size, since the amounts of harvestable bone are limited and the endogenous self-repair abilities of the body turn insufficient. This is often the case for patients with large bone defects resulting from tumour resection, where between one third and half of patients will develop complications and will require a second surgery [13]. To improve the treatment options available for large fractures, extensive research has focused on assessing which bioactive molecules present during skeletal development and fracture healing are able to induce bone formation at the site of injury [14]. By incorporating them to bone graft substitutes, bone healing can be promoted locally improving the prognosis and shortening the recovery times. Thus, the wide interest to study the series of events that lead to bone formation during health and disease.

Osteoarthritis, a joint disease with pathological bone formation

As previously introduced, bone and cartilage formation are intimately linked during embryologic development and fracture repair, making the transition of cartilage to bone in healthy individuals a tightly regulated process. It is no surprise then to observe the cellular and biochemical processes that gave rise to these tissues re-emerging during skeletal disease and repair [5, 15]. However, in certain pathologies of the adult cartilage unwanted bone formation might occur, which can reveal important regulatory elements of the EO process. Among them sits osteoarthritis (OA), a painful degenerative disease

that affects various tissues of the joints [16]. OA is characterised by the erosion of the articular cartilage, which over time leads to permanent disability [17]. Over 33% of people over 65 years of age suffer from OA [18], and there are currently no treatment options to cure or stop it once initiated. One of the hallmarks of this disease is the formation of osteophytes (bony projections) along the joint margins [19, 20]. During OA, the chondrocytes present in the articular cartilage experience the changes associated with hypertrophy leading to the vascularisation, mineralisation and eventual replacement of the cartilage by bone tissue [5]. At the end stage, the affected joint needs to be replaced by a prosthesis to deal with the chronic pain and to restore the motion lost due to the disease. In the skeleton, the control of the EO pathway is determined by a complex interaction of intrinsic and extrinsic factors, such as the mechanical environment, the local paracrine factors and extracellular matrix molecules [21]. Of these components, the cartilage extracellular matrix is one of the key players, since it contains the factors that control the chondrocyte function and fate [22]. Thus, the study of the changes the matrix experiences to orchestrate the EO is a necessary step to discover new therapeutic targets and drugs that can be used to treat bone defects, disturbed fracture healing or osteoarthritis.

SCAFFOLD-BASED THERAPIES FOR BONE TISSUE ENGINEERING

Large bone defects are serious complications resulting from traumatic injuries, the resection of bone tumours or infections. Although the use of autologous bone grafts is the preferred choice to treat small defects, it is limited to the amount of harvestable material of the patient [12]. For this reason, bone graft substitutes are being engineered to help increase the formation of new bone around fractures and surgical implants [23]. Since the repair of bone fractures recapitulates the biological events of skeletal development, tissue engineers aim to mimic that microenvironment. This is achieved with the use of scaffolds, which are used as a filling material that provides an appropriate three-dimensional structure to guide regeneration. The scaffolds provide a suitable biochemical environment and support, promoting the adhesion, migration, proliferation and differentiation of both progenitor cells and blood vessels. They can be produced with synthetic materials, ECM components, or a combination of both, and act synergistically to simulate the complex osteogenic microenvironment. In regards to the natural ECM-derived scaffolds, those can be produced either by decellularization of the bone ECM, or by building them up from the single components [24]. While the first strategy can produce scaffolds of a complex composition, the second strategy allows to control and fine-tune the composition and properties of the material.

As the major structural protein of the bone, collagen type I is widely used to produce highly porous osteoconductive sponges, which serve as the basic building block for different bone graft formulations [25]. Since pure collagen is unable to induce bone formation, additional biomolecules known to be present during bone formation and repair can be used to functionalise the scaffolds, such as growth factors, minerals and

extracellular matrix molecules and their fragments. These bone grafts, which follow under the regulatory classification of medical devices of class III, aim to guide and stimulate the activity of the patient's endogenous cells [23]. For example, collagen scaffolds functionalised with bone morphogenetic proteins (BMPs) have proven successful in the clinic to improve bone regeneration [26]. When surgically implanted, they release the osteogenic signals contained within to both attract cells from the surrounding tissues and to instruct them to form bone. However, the seek for simplicity in the scaffold's composition implies missing the multiple regulatory elements that are naturally present in the healing bones. To compensate for them, the administration of doses over a million times the physiological ones are necessary [27], which may cause diverse secondary effects such as inflammation, ectopic ossification, bone resorption, inappropriate adipogenesis and tumorigenic risk [28]. For this reason, multiple efforts are being made to find additional components that can fine tune the graft's formulations.

THE EXTRACELLULAR MATRIX OF THE HYALINE CARTILAGE

During bone formation, most of bones are formed from cartilage templates. Because of this reason, the cartilage matrix may contain variable amounts of bone-inducing elements that are interesting for bone tissue engineering. Thus, understanding the composition of the cartilage ECM and the role that each of its components play during bone formation and repair is fundamental to replicate the 3D environment for better bone repair. Not all cartilage in the body is equal though, since its function differs depending on the context where it is located. Accordingly, there are three types of cartilage: elastic cartilage, fibrocartilage and hyaline cartilage. They are present in multiple organs across the body, and possess different biochemical compositions and mechanical properties. Thus, not every type of cartilage is relevant to be used for bone tissue engineering purposes. Hyaline cartilage is the one that forms part of the skeletal system, where it lines the bones in the joints and forms the scaffolding templates involved in bone development and fracture healing. The cartilage present at this locations withstands mechanical compressive forces while allowing growth. This is achieved by a hardened gelatinous network of numerous ECM proteins, produced and maintained by the chondrocytes [22]. Mechanically, tensile strength is achieved via the collagen fibers (mainly collagen type II and collagen type IX) [29]. Simultaneously, resistance to compression is given by the presence of glycosaminoglycans (GAGs) thanks to their high charge density, which builds an osmotic pressure [30, 31]. Sulphated GAGs such as chondroitin sulphate and keratan sulphate can be bound to proteins, such aggrecan [32] and perlecan [33] and form proteoglycans. These proteoglycans, plus various other small leucine-rich proteoglycans (SLRPs), play not only structural roles but also possess cell-regulatory functions [22]. Last, additional non-collagenous matrix proteins such as those belonging to the families of matrilins and thrombospondins aid to stabilise the collagen network, linking it to the proteoglycan gel and promoting cell attachment or distributing diverse morphogens across the matrix.

Despite their common hyaline characteristics, the cartilage templates present during bone development and healing differ from the adult articular cartilage that lines the adult bones. While the first type forms transiently, the articular cartilage is meant to be retained during the lifetime. To achieve the transition towards bone, the hyaline cartilage matrix has to allow its progressive degradation, while maintaining the unity and mechanical function of the temporal chimeric osteochondral structure [34]. In order to orchestrate the endochondral ossification process, once the hyaline cartilage template has been deposited the chondrocytes within activate a specific terminal differentiation program towards ossification. Once it is triggered, chondrocytes stop proliferating and increase their intracellular volume up to 10-folds, thus becoming hypertrophic. In addition, their metabolic activity increases by 5-folds and the remodelling of their surrounding ECM begins [35]. At this point, while sustaining their structural collagen synthesis the chondrocytes produce for the first-time collagen type X (COL-X). Simultaneously, they increase the production of catabolic enzymes such as matrix metalloproteinases (MMPs) and aggrecanases (ADAMTS), and release enzymes such as alkaline phosphatase (ALP), which is responsible for the mineralisation of the cartilage template. As a result of the degradation of the cartilage matrix, fragments of ECM proteins are released. Some of these are bioactive (known as matrikines and matricryptins) and regulate a wide variety of cellular functions such as cell adhesion, migration, proliferation, angiogenesis, or apoptosis [36, 37].

The thrombospondin family in the skeletal system

The thrombospondin family is composed of five matricellular glycoproteins (Fig. 4), which has been related to the skeletal system both during biological development and disease [38, 39]. These proteins are secreted and possess a multimeric modular structure, and are involved in several processes, including angiogenesis, wound healing, cell proliferation and migration, and connective tissue organization [40]. Thanks to their multidomain structure, the thrombospondins can interact with a variety of ligands including cellular receptors, other extracellular matrix proteins, growth factors, cytokines and proteases [40, 41]. This allow them to have different activities depending on which domains, ligands and cell types are present and functional in a specific environment.

TSP-1 and TSP-2 belong to subgroup A of the thrombospondin family. They both form homotrimers and have comparable functional properties. For example, they possess potent anti-angiogenic activity [40, 42, 43], modulate collagen fibrillogenesis [44, 45], organise the ECM [44, 46] and inhibit both matrix metalloproteinase activity [47] and nitric oxide dependent signalling [48]. However, despite their structural similarities, TSP-1 and TSP-2 play opposing roles in the activation of the transforming growth factor beta (TGF- β), which plays multiple signalling roles in bone. While both bind latent TGF- β , TSP-1 activates it, while TSP-2 acts as a competitive antagonist of this activation [49]. TSP-1 is widely expressed during development, and localises in several tissues,

including bones [50-52]. In the adult skeleton, it forms part of the mineralised matrix, and it is produced by osteoblasts [51, 53-55]. On the other hand, TSP-2 expression is more restricted in the embryo and associated to areas undergoing vascularisation and in the developing cartilage and bone [52, 56]. In adult bone, periosteal MSCs and osteoblasts constitutively express TSP-2 [57-59], and increase their production during early fracture healing [59, 60].

The subgroup B of the thrombospondin family is comprised by TSP-3, TSP-4 and TSP-5 (also known as cartilage oligomeric matrix protein, COMP). The members of this group form pentamers and are differentially expressed in bones and cartilage of both embryos and adults [39, 40]. While TSP-5 has been widely studied mainly in cartilage, TSP-3 and -4 are less characterised. TSP-3 is expressed by chondrocytes in the developing skeleton as well as the adult bone, in particular in the early proliferative zone of the GP [50]. Unfortunately, little is known about TSP-3 role in tissue homeostasis and disease.

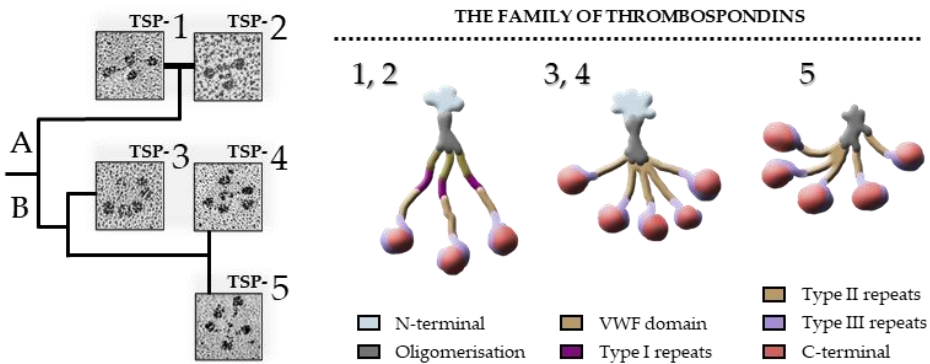


Figure 4. The thrombospondin family. Protein domains of the oligomers are represented by different colours. Rotatory shadow microscopy images reproduced from DiCesare *et al* [61], Lawler *et al* [62], Qabar *et al* [63] and Pellerin *et al* [64].

TSP-4 levels have been described to increase in various organs, including cartilage [65, 66] during tissue remodelling. Contrary to the thrombospondins of the subgroup A, TSP-4 mediates upregulation of angiogenesis [67], and it has been linked to the reduction of fibrosis and collagen production [66]. However, the location of TSP-4 during endochondral bone formation and bone repair is still unclear. TSP-5 is abundantly expressed in cartilage, although it is also found in other tissues, such as ligaments, tendons, synovium and bone, where it is produced by osteoblasts during the initial stages of osteogenesis [68]. TSP-5 is the most widely studied thrombospondin in cartilage, where it is involved in stabilizing the ECM, and modulating chondrocyte proliferation, collagen secretion and fibrillogenesis [69].

AIMS AND OUTLINE OF THE THESIS

During skeletal development and fracture healing, bone is mainly formed via endochondral ossification. During this process, temporal templates of hyaline cartilage arise which are later substituted by bone. For this transition to occur, the physical and biochemical composition of the cartilage matrix has to change following a well-defined sequence of events. The improper orchestration of those events however, can result in incomplete ossification and result in diseases that impair bone defect healing or result in osteoarthritis. In order to develop new therapies for the skeletal system, it is crucial to understand which are the series of events that drive bone formation and the individual roles of its elements involved. For this reason, in this thesis I aim to gain more insight into the role that two extracellular matrix proteins of the family of thrombospondins, TSP-4 and TSP-5, play in the skeletal system. Their presence and structural integrity during skeletal development, regeneration and disease are known to vary. However, their expression patterns and roles in transient cartilage are not fully understood. Once their roles are unravelled, I aim to determine if any of them may have the therapeutic potential to modulate bone formation.

First, **Chapter 2** is focused to understand the spatiotemporal location of TSP-4 and -5 during bone formation and fracture healing. For this purpose, I perform diverse immunohistochemical stains in young mice, as their skeleton is under development, and during fracture healing in adults. Then, I evaluate *in vitro* whether the two proteins can contribute to the process of EO by attracting cellular types known to invade the transient cartilage matrix, to determine if they may have potential to be used for bone tissue engineering approaches.

Next, **Chapter 3** investigates if TSP-4 and -5 might be produced too in a context where pathological EO is known to take place, to assess if the endogenous production of these proteins either promotes or prevents a regenerative response. For this, I focus on OA. During this cartilage disease, where an abnormal matrix remodelling takes place, the expression of TSP-4 and -5 is altered. In this chapter I assess the location of the two proteins in osteoarthritic human cartilage and analyse how they can modify the behaviour of chondrocytes *in vitro*. For this, I supplement chondrocyte cultures with the two proteins and investigate changes on their signalling, migratory behaviour and production of ECM components.

TSP-5 is long known to be degraded and released into the synovial fluid by osteoarthritic cartilage, in such high levels that its resulting products are used as biomarkers of the disease. However, it is unknown if such degradation products may act as signalling molecules. Therefore, in **Chapter 4** I explore if three known TSP-5 peptide fragments produced by damaged cartilage elicit responses commonly observed during OA, as those are relatively simple molecules that could be either inhibited or used as therapeutic agents in regenerative medicine approaches. In order to study the ability of these peptides to modify the behaviour of nearby cells and tissues of the joint, I use

synthetic versions of those peptides in different *in vitro* assays, to explore their possible effects on subchondral osteochondroprogenitor cells, endothelial cells and synovium.

Once a substance is suspected to have therapeutic potential in *in vitro* assays, it is then tested *in vivo* in order to assess its effects in a more biologically relevant environment. However, the current *in vivo* methodologies are far less efficient than *in vitro* techniques, and pose a big bottleneck to how many candidates can be tested. In order to improve the efficiency of the *in vivo* testing of osteogenic grafts, in **Chapter 5** a novel semi-orthotopic bone defect model for bone formation *in vivo* is developed. The chapter aims to standardise a methodology for an efficient testing of bone graft candidates with a low impact on animal welfare. I use this model to validate a methodology that allows the systematic evaluation of different grafts to undergo endochondral ossification. Next, in an addendum to this chapter, I functionalise a collagen-based biomaterial with TSP-4, as the results of the previous chapters led me to suspect that TSP-4 might be a novel agent capable to promote bone formation. Then, I test if this functionalised biomaterial is capable of promoting bone formation in the semi-orthotopic bone defect model developed at the beginning of the chapter.

Finally, in **Chapter 6** I summarise and discuss the findings of this work, and present the conclusions and the future perspectives for research.

CHAPTER 2

Spatiotemporal distribution of TSP-4 and TSP-5 during bone formation and repair

E. ANDRÉS SASTRE, K. MALY, M. ZHU, J. WITTE-BOUMA, D. TROMPET, A.M. BÖHM, B. BRACHVOGEL, C. VAN NIEUWENHOVEN, C. MAES, G.J.V.M. VAN OSCH, F. ZAUCKE, E. FARRELL

PUBLISHED AS: SPATIOTEMPORAL DISTRIBUTION OF THROMBOSPONDIN-4 AND -5
IN CARTILAGE DURING ENDOCHONDRAL BONE FORMATION AND REPAIR

BONE. 2021 SEP; 150:115999
DOI: 10.1016/j.bone.2021.115999

ABSTRACT

During skeletal development most bones are first formed as cartilage templates, which are gradually replaced by bone via the process of endochondral ossification (EO). In parallel, a smaller set of bones is produced by the direct deposition of bone via intramembranous ossification (IO). If later in life those bones break, both developmental programs will take place to guide the regenerative process. Bone formation and repair have been widely studied for their potential to reveal factors that might be used to treat patients with large bone defects. The extracellular matrix proteins thrombospondin-4 (TSP-4) and thrombospondin-5 (TSP-5/COMP) have been related to the skeletal system during biological development and disease. They organise the collagen fibers and interact with a variety of growth factors, matrix proteins and cellular receptors. However, very little is known about the skeletal distribution of TSP-4 in relation to its homologue TSP-5. In our study, we compared the spatiotemporal expression of TSP-5 and TSP-4 in EO and IO during postnatal bone formation and fracture healing. Our results indicate that during EO, TSP-5 distributes across all layers of the transient cartilage, while the localization of TSP-4 is restricted to the population of hypertrophic chondrocytes. Furthermore, TSP-5 is absent during IO while TSP-4 localises to the cranial sutures and to the activated periosteum in fractured bones. Last, we analysed the chemoattractant effects of the two proteins on endothelial cells and bone marrow stem cells and hypothesised that, of the two thrombospondins, only TSP-4 might promote blood vessel invasion during ossification. We conclude that TSP-4 is a novel factor involved in bone formation. These findings reveal TSP-4 as an attractive candidate to be evaluated for bone tissue engineering purposes.

INTRODUCTION

Bone formation involves the transformation of a pre-existing mesenchymal tissue into bone tissue, and takes place via two different mechanisms: intramembranous ossification (IO) and endochondral ossification (EO). Part of the skull and the clavicles are formed by IO, in which mesenchymal progenitors cluster together to begin the direct synthesis of bone. On the other hand, the rest of the bones of the body are produced via EO, in which a transient cartilage template forms prior to the deposition of bone. This latter process takes place during pre- and postnatal skeletal development in the growth plate (GP), the primary and secondary ossification centers (POC, SOC) [4], and as part of the bone fracture healing process in combination with IO [10]. To summarise, EO begins with the formation of a cartilage template, the macroscopic shape of which resembles that of the bone that will be formed. This template is initially comprised of small chondrocytes dispersed in an abundant extracellular matrix (ECM). Then, in order to prepare the ECM to be remodelled, chondrocytes undergo a series of maturation steps. First, they increase their anabolic activity, proliferate and synthesise new matrix with abundant collagen type II (COL-II). Once completed, chondrocytes undergo cell cycle arrest. At this stage, they become hypertrophic and start to express collagen type X (COL-X), while inducing the mineralisation and degradation of their surrounding ECM. Last, most of the chondrocytes undergo apoptosis, and their empty lacunae become invaded by the multiple cell types present in the marrow. Following this, the tissue is vascularised, the matrix degraded and the deposition of osteoid occurs.

The cartilage matrix that precedes bone formation contains numerous ECM proteins. Mechanically, collagen fibers confer tensile strength, and the major proteoglycan aggrecan provides resistance to compression via generation of an osmotic pressure by the high charge density of its glycosaminoglycan side chains. Apart from these components, additional non-collagenous matrix proteins form a complex network, aiding to stabilise the collagen network, linking it to the proteoglycan gel and promoting cell attachment or distributing diverse morphogens across the matrix. One family of such glycoproteins are the thrombospondins. This family is composed of 5 members all of which possess a modular structure, and assemble either as trimers (subgroup A, comprising TSP-1 and TSP-2) or pentamers (subgroup B, comprising TSP-3, TSP-4, and TSP-5) [40]. These proteins bind simultaneously to different ECM components and cellular receptors, to modulate cellular behaviour in a variety of contexts. The most studied member of this family in cartilage is thrombospondin-5 (TSP-5), also known as cartilage oligomeric matrix protein (COMP). During skeletal development, TSP-5 is present across the transient cartilage matrix, at both territorial and interterritorial locations [70, 71]. Among its known functions, TSP-5 assists collagen secretion [72] and fibrillogenesis [73] and interacts with and modulates the activity of different growth factors from the transforming growth factor beta (TGF- β) superfamily such as BMP-2 [74] and TGF- β 1 [75].

Thrombospondin-4 (TSP-4) is a protein structurally similar to TSP-5, which contains an additional N-terminal heparin-binding domain [76]. TSP-4 levels have been described to increase in various organs, including cartilage [65, 66] during tissue remodelling; and similar to TSP-5, TSP-4 binds collagen [77] and controls matrix assembly [78]. In fact, their structural similarities are such that the presence of TSP-5 and TSP-4 heteropentamers has been reported in tendon [79]. However, it is still unclear the location of TSP-4 during bone formation and bone repair, despite evidence supporting its presence during these processes. During *in vitro* chondrogenesis, both proteins become strongly upregulated [80], which also occurs during the establishment of the secondary ossification center of the mouse [81]. In addition, TSP-4 expression also increases during adult rat bone fracture healing, as documented by the microarray technique [82]. Nevertheless, the role of TSP-4 in the skeletal system has gained less attention than its counterpart TSP-5, and no accurate description of TSP-4 localisation during bone formation and fracture repair has been reported to date. Interestingly, unlike TSP-5 and the other three members of the thrombospondin family (TSP-1 to -3), TSP-4 is the only known proangiogenic thrombospondin [83, 84], which suggests that both proteins may play overlapping and yet distinct roles in the tissues where they are present.

To better understand the roles that TSP-4 and TSP-5 may play during bone formation and whether they might be related to matrix remodelling and vascularisation, it is essential to first assess the spatiotemporal location of the two proteins in various contexts where EO and IO take place. In the current study we first investigated the distribution of TSP-4 in relation to TSP-5 during bone development, and then if that distribution was maintained during fracture healing. Last, we assessed how the two proteins affect the migratory behaviour of endothelial cells and bone marrow stromal cells.

MATERIALS AND METHODS

Human digits

Whole toes were obtained as leftover material from 2 paediatric patients of 1 and 1.5 years old respectively affected by polydactyly undergoing removal of the extra digit. Acquisition was performed with implicit consent and according to the Code of Conduct for responsible use of human tissue in the context of health research by the Federation of Dutch Medical Scientific Societies www.federa.org.

Mouse tissue collection

C57BL/6N mice were bred in-house at the University of Cologne. They were housed in individually ventilated cages at 22 °C with a 12-hour light / 12-hour dark schedule. Water and food were constantly available and daily care was ensured by the animal facility. Only males were used for tissue collection. All animal experiments were

performed in accordance with the guidelines of the German animal protection law (institutional review board Landesamt für Natur, Umwelt und Verbraucherschutz Nordrhein-Westfalen).

Semi-stabilised bone fracture healing model

Animal care and experiments were performed in accordance with the guidelines of institutional authorities, and formally approved by the Animal Ethics Committee of the KU Leuven (licence agreement LA1210189). During the surgical procedure as described by Böhm AM *et al* [85], a transverse bone fracture was induced in the left tibia of 10- to 12-week-old male CD1 (CRL, from Charles River Laboratories) outbred mice under 100 mg/kg ketamine (EuroVet) and 10 mg/kg xylazine (VMD) anaesthesia. In short, a longitudinal incision was made in the skin to expose the proximal tibia. Then, after moving down muscles at the tibial crest, tibia fractures were made using a Comet diamant saw Miniflex (6.5 mm diameter), approximately at 2 mm distal to the growth plate. To stabilise the fracture, a 27 G needle was inserted into the medullary cavity through the proximal tibia, which extended beyond the fracture site into the distal diaphysis. After surgery, mice received a 3 mg injection of Vetergesic (Ecuphar). Detailed descriptions of the surgical procedure and healing process in this murine semi-stabilised tibia fracture model can be found in Maes C. *et al* [86, 87]. To study the different stages of fracture healing, mice were sacrificed at several time points after fracture induction, and the injured legs and non-injured contralateral tibias were collected for analysis.

(Immuno-)Histological analysis of samples

Samples from human origin were fixed for 24h in 4% formalin, and decalcified in 10% w/v ethylenediaminetetraacetic acid (EDTA) pH 7.4 at room temperature (RT) for three weeks with mild agitation. Samples from mouse origin intended to study bone development were fixed overnight in 4% formalin and decalcified in 10% w/v EDTA at RT for two weeks with mild agitation. Subsequently, in both cases samples were embedded in paraffin and 6 µm thick sections were collected for histology. Bone fracture samples were fixed overnight in 2% paraformaldehyde at 4°C, and decalcified in 0.5 M EDTA for two weeks, embedded in paraffin and sectioned at 5 µm. Next, TSP-4, TSP-5, COL-II and COL-X were detected by immunohistochemistry.

TSP-5 and TSP-4 immunohistochemical stainings. To improve antibody penetration and epitope unmasking, samples were treated with 10 mg/ml hyaluronidase [Sigma, Zwijndrecht, the Netherlands] in PBS (pH=5.5) at RT; 15 min for mouse, and 30 min for human samples. Prior to primary antibody incubation, the endogenous peroxidase activity was blocked with 0.3% H₂O₂ [Sigma, Zwijndrecht, the Netherlands] in dH₂O for 10 min at RT and blocked with 2.5% normal horse serum [ImmPRESS™ HRP Reagent Kit, Vector Laboratories, Burlingame, CA, USA] for 30 min at RT. Then, sections were incubated overnight at 4°C with rabbit anti-rat TSP-4 antibody [65] (1:1000), with rabbit

anti-bovine TSP-5 [88] (1:500) or with an equivalent 2 µg/ml concentration of rabbit immunoglobulin fraction [DAKO cytometry, cat no.X0903], as negative control. All antibodies were diluted in 1% BSA in TBS-Tween 0.1% (TBST). The next day, sections were washed three times with TBST and incubated with ImmPRESS™ (peroxidase) polymer anti-rabbit IgG reagent [ImmPRESS™ HRP Reagent Kit, Vector Laboratories, Burlingame, CA, USA] at RT for 30 min. After another three washes with TBST, slides were revealed. For antibody detection, the AEC-2-component kit [DCS, Hamburg, Germany] was used according to the manufacturer's instructions with 3-amino-9 ethylcarbazole as chromogen. Finally, sections were counterstained with Gill's haematoxylin, followed by a 10 min wash with running tap water. Slides were rinsed with dH₂O and covered with a glass coverslip and Kaiser's gelatine, prepared with 9% w/v gelatine type A (Sigma, Zwijndrecht, the Netherlands) and 45% v/v glycerol (Sigma, Zwijndrecht, the Netherlands) in dH₂O.

COL-X immunohistochemical staining. Endogenous peroxidase activity was first blocked with 1% v/v H₂O₂ in PBS for 30 min. Then, antigen retrieval was performed with pepsin 1 mg/ml in 0.5 M acetic acid pH=2 at 37°C for 2 h, followed by a 30 min incubation at 37°C with 10 mg/ml of hyaluronidase in PBS. Next, unspecific binding was prevented by 30 min incubation at RT with PBS containing 10% v/v normal goat serum, 1% w/v BSA and 1% w/v skimmed milk [ELK, FrieslandCampina, Amersfoort]. Then, either 5 µg/ml of mouse monoclonal antibody anti-COL-X [X53 clone, ThermoFisher, cat no. 14-9771-82] or 5 µg/ml of mouse IgG1 isotype control antibody [Dako cytometry, cat no.X0931] were added in PBS-1%BSA and incubated overnight at 4°C. Next day, slides were washed 5 times with PBS and a biotinylated goat anti mouse antibody [LINK, Biogenex, HK-325-UM) was incubated at 1:50 in PBS-1% w/v BSA supplemented with 5% v/v normal human serum for 30 min, which was then coupled to streptavidin-peroxidase [LABEL, Biogenex, HK-320-UK] for additional 30 min, 1:50 diluted in PBS. For antibody detection, the AEC-2-component kit [DCS, Hamburg, Germany] was used according to the manufacturer's instructions with 3-amino-9 ethylcarbazole as chromogen. Finally, slides were rinsed 5 times with PBS, revealed and mounted as with the TSP-4 immunostaining.

COL-II immunohistochemical staining. Endogenous peroxidase activity was first blocked with 1% v/v H₂O₂ in PBS for 30 min. Then, samples were treated for 30 min at 37°C with 1 mg/ml pronase [Sigma #P5147] and followed by 30 min at 37°C with 10 mg/ml hyaluronidase in PBS. Next, unspecific binding was prevented by 30 min incubation at RT with PBS containing 10% v/v normal goat serum and 1% w/v BSA. Then, either 0.4 µg/ml of mouse monoclonal antibody anti-COL-II [clone II-II-6B3, DHSB] or 0.4 µg/ml of mouse IgG1 isotype control antibody (Dako cytometry, cat no X0931) were added in PBS-1% w/v BSA and incubated overnight at 4°C. Next day, slides were rinsed 5 times with PBS and a biotinylated goat anti mouse antibody (LINK, Biogenex, HK-325-UM) was incubated at 1:50 in PBS-1%BSA supplemented with 5% v/v normal human serum for 30 min, which was then coupled to streptavidin-peroxidase (LABEL,

HK-320-UK, Biogenex) for an additional 30 min. For antibody detection, the AEC-2-component kit [DCS, Hamburg, Germany] was used according to the manufacturer's instructions with 3-amino-9 ethylcarbazole as chromogen. Finally, slides were washed 5 times with PBS, revealed and mounted as with the TSP-4 immunostaining.

Last, images were acquired with a microscope-mounted digital camera (SC-30, Olympus, UK). Hue and brightness were automatically adjusted after acquisition using Adobe Photoshop CC 2018, following the recommendations described by Sedgewick J. [89].

Production of recombinant TSP-4 and TSP-5

Recombinant production of full-length proteins was done similarly for TSP-5, as previously described by Ruthard *et al* (2014) [90], and TSP-4, as described by Crosby *et al* (2015) [91]. Rat cDNA sequences for TSP-5 (GenBank accession number NM_012834.1) and TSP-4 (GenBank accession no. X89963) were cloned into the episomal expression vector pCEP-Pu, N-terminally Strep II-tagged. The constructs were transfected into human embryonic kidney (HEK) 293 Epstein-Barr virus nuclear antigen (EBNA) cells with FuGENE HD Transfection Reagent [Roche, Basel, Switzerland] according to the manufacturer's instructions. Cells were selected with puromycin 1 mg/ml in DMEM/F12 GlutaMax [Gibco, Darmstadt, Germany] with 10% fetal calf serum [PAN, Aidenbach, Germany], 1% penicillin/ streptomycin [Gibco, Darmstadt, Germany] and 1% amphotericin B [Gibco, Darmstadt, Germany]. Protein production was done in DMEM/F12 with 1% FCS, 1% penicillin/streptomycin and 1% amphotericin B. Cell culture supernatants were harvested after 3–4 days, centrifuged to remove cell debris and stored at -20°C with 1.2 mM N-ethylmaleimide (NEM) and 1.2 mM phenylmethylsulfonyl fluoride (PMSF) to inhibit protease activity. For purification, supernatants were loaded onto a streptactin column [IBA, Goettingen, Germany] according to the manufacturer's protocol, and stored at -20°C . Last, purified protein concentration was assessed by the BCA assay, and molecular weight and structural integrity was assessed by polyacrylamide gel electrophoresis in non-reducing conditions and subsequent visualisation by Coomassie staining (data not shown).

Cell culture

Human endothelial cells (HUVECs) were purchased from Lonza and expanded in endothelial growth media (EGM-2), containing 2% FBS, 5 ng/ml EGF, 10 ng/ml bFGF, 20 ng/ml IGF, 0.5 ng/ml VEGF165, 1 $\mu\text{g}/\text{ml}$ L-ascorbic acid 2-phosphate, 22.5 $\mu\text{g}/\text{ml}$ heparin and 0.2 $\mu\text{g}/\text{ml}$ hydrocortisone [All from Promocell via Bioconnect, Huissen, the Netherlands].

BMSCs were isolated from leftover iliac crest bone chip material obtained from 3 paediatric patients undergoing alveolar bone graft surgery (with institutional consent for the use of waste surgical material with the option for parental opt-out and approval of medical ethics committee of Erasmus MC: MEC-2014-16; all male, age 9–10 years), as described previously [92]. Cells were expanded in α MEM [Gibco, Bleiswijk, the Netherlands] containing 10% FBS [Gibco, Bleiswijk, the Netherlands] and supplemented with 50 μ g/mL gentamycin [Gibco, Bleiswijk, the Netherlands], 1.5 μ g/mL amphotericin B [Gibco, Bleiswijk, the Netherlands], 25 μ g/mL L-ascorbic acid 2-phosphate [Sigma, Zwijndrecht, the Netherlands] and 1 ng/mL fibroblast growth factor-2 [Bio-Rad via Bioconnect, Huissen, the Netherlands] in a humidified atmosphere at 37°C and 5% CO₂.

Migration assays

Migration towards recombinant TSP-5 or TSP-4 was assessed with modified Boyden chambers (polyethylene terephthalate cell culture inserts with 8 μ m pore size) [Corning, Durham, NC, USA]. For this, the cells of interest were seeded on the upper insert membrane in 200 μ l of their specific basal media, and allowed to migrate towards 500 μ l of 10 μ g/ml of the recombinant proteins, diluted in the same basal media.

In the case of HUVECs, basal media was EBM-2; 5x10⁴ cells from passage 5 were used per insert. Recombinant protein testing was carried on endothelial basal media (EBM-2) [Lonza, Geleen, the Netherlands], supplemented with 1.25 mg/ml BSA [Product code 1002759876, Sigma, Zwijndrecht, the Netherlands]. Cells were allowed to migrate towards the lower chamber for 10 h at 37°C.

In the case of the BMSCs, 1.5x10⁴ cells from passage 4 were seeded on the upper insert membrane in α MEM. Recombinant protein testing was carried on α MEM supplemented with 50 μ g/mL gentamycin, 1.5 μ g/mL amphotericin B and 1.25 mg/ml BSA. Cells were allowed to migrate towards the lower chamber containing the recombinant proteins for 20 h at 37°C.

After the indicated incubation times, cells on the membrane were fixed for 10 min with 4% formalin and cells on the upper surface were removed with a cotton swab, followed by 5 min DAPI staining. Migrated cells on each membrane were imaged with a fluorescence microscope [Zeiss Axiovert 200M] in five random fields of 1.51 mm² each, and automatically counted using ImageJ software. Last, the average counts per membrane were expressed as cells/mm².

Proliferation assay

The number of HUVECs that proliferated after 24h was investigated with the EdU cell proliferation kit [Bascelik, Neuried, Germany]. First, 7500 cells/cm² were seeded in 48-well plates in EGM-2 and allowed to attach overnight. Then, cell cycles were synchronised by substituting the media with EBM-2 supplemented with 1.25 mg/ml BSA

for 8 hours. Next, cells were stimulated with 300 μ l of EBM-2 containing 10 μ g/ml of either recombinant TSP-5 or TSP-4, 1.25 mg/ml BSA and 10 μ M EdU for 24h, fixed with 4% formalin and stained according to the manufacturer's kit protocol. To quantify proliferation, positive cells were imaged with a fluorescence microscope [Zeiss Axiovert 200M] in five random fields of 1.51 mm² each. Total nuclei (DAPI) and EdU+ nuclei were automatically counted using ImageJ software. Percentage of proliferated cells per field was calculated as the number of EdU+ nuclei divided by total nuclei. Last, total proliferation per membrane was calculated as the average proliferation of its five fields.

Gene expression

For RNA isolation of callus tissue, samples were crushed while frozen in liquid nitrogen and homogenised in Trizol [Sigma-Aldrich]. RNA was separated from proteins, lipids and cellular debris using chloroform, and extracted with the RNeasy Mini kit. Then, 2 mg RNA were reverse transcribed into cDNA, by incubation with 0.15 mg/ml Random Primers and 10 ml cDNA synthesis mix consisting of 2.5x buffer, 25 mM dithiothreitol (DTT), 1.25 mM dinucleotidetriphosphates (dNTP) and 50 U/ml Superscript reverse transcriptase [all from Thermo Fisher Scientific] according to the manufacturer's protocol. Gene expression for *Comp*, *Thbs4* and *Hprt* was quantified using the Fast SYBR Green Master Mix [Thermo Fisher Scientific]. Gene expression of *Col2a1* and *Col10a1* on those same cDNA samples had been already published by Böhm AM *et al* [85], which we reproduced here. Primers used are listed on Table 1. Data was analysed with the Livak method ($2^{-\Delta\Delta CT}$), where normalisation was based on *Hprt* and then made relative to non-injured bones (day 0 baseline samples).

<i>Comp</i>	fw: 5'- GCGCCAGTGTGCAAGGACAA -3'	;	rv: 5'- TGGGTTTCGAACCAGCGGGC-3'
<i>Thbs4</i>	fw: 5'- GCCACAAGCACAGGAGACTTT -3'	;	rv: 5'- TGACCTGCTGCCTCAGAAGA-3'
<i>Hprt</i>	fw: 5'- TGCTGACCTGCTGGATTACA- 3'	;	rv: 5'- TATGTCCCCCGTTGACTGAT-3'

Table 1. Primer list used for cDNA quantification.

Statistical analysis

Experiments involving cell cultures were performed in technical triplicates, with the number of donors and repetitions indicated in the corresponding figures. Differences between *in vitro* experimental conditions were assessed using the linear mix model with Bonferroni correction. Longitudinal experiments of bone fracture healing were analysed by one-way ANOVA, with Kruskal-Wallis test and post-hoc Dunn's multiple comparison test. Statistics were performed with IBM SPSS Statistics (version 25.0.0.1 for Windows, IBM Corp., Armonk, N.Y., USA), and GraphPad Prism, while the latter was also used to create the graphs (version 8.0.1 for Windows, GraphPad Software, La Jolla California USA).

RESULTS

TSP-4 localises differently to TSP-5 in the human growth plate

The location of TSP-4 in comparison with TSP-5 was first analysed in two human growth plates, using sections of 1- and 1.5-year-old foot digits. Immunostainings confirmed the presence of COL-II across the entire cartilage, whereas the presence of COL-X was restricted to the hypertrophic chondrocyte zone (HZ) (Fig. 1A).

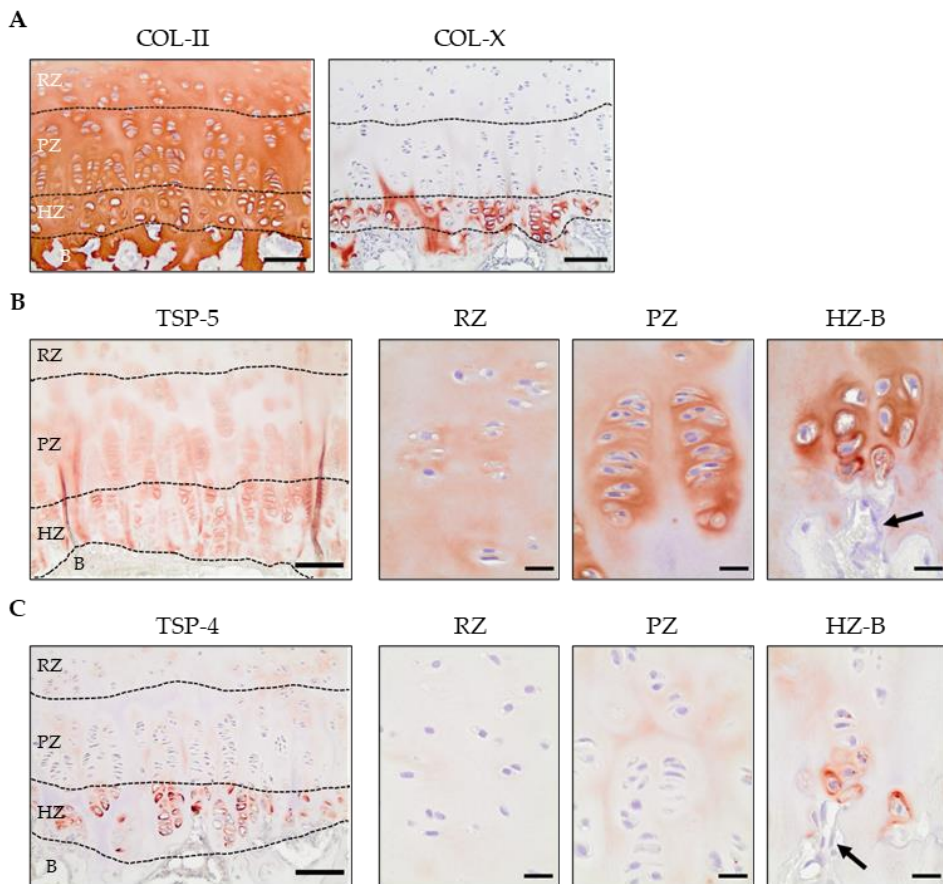


Figure 1. Localisation of TSP-5 and TSP-4 in the human growth plate. (A) Immunohistological staining of collagen type II (COL-II) and collagen type X (COL-X). (B, C) Immunohistological stainings of TSP-5 and TSP-4, including higher magnifications of the different zones of the growth plate. In all cases, detected proteins appear in red, while blue colour corresponds to the haematoxylin counterstain. RZ: Reserve zone. HZ: Hypertrophic zone. B: Bone. Dotted lines indicate the different layers of the growth plate. Arrows indicate cells from the marrow invading the empty chondrocyte lacunae. Scalebars: 200 μm and 20 μm (high magnification).

Immunostainings showed that TSP-5 and TSP-4 were both present yet exhibiting differential locations across the growth plate (GP). TSP-5 localised at the territorial matrix of all active chondrocytes –proliferative zone (PZ) and HZ–, with a faint interterritorial staining in the matrix of the reserve zone (RZ) (Fig. 1B). TSP-4 localisation on the other hand, was pericellular and present exclusively in the hypertrophic zone, following a similar distribution to that of COL-X (Fig. 1A, D). Neither proteins were detected in the newly formed bone.

Differential distribution of TSP-5 and TSP-4 during murine growth plate maturation and SOC formation

To assess TSP-4 and TSP-5 distribution during the maturation of the growth plate, we studied the location of these two proteins in the mouse proximal tibia from birth until skeletal maturity (Fig. 2). After birth (P-0), before the secondary ossification centers start to develop, the cartilaginous bone epiphyses are comprised of abundant reserve chondroprogenitors. At this stage of development, TSP-5 was found pericellularly around the chondrocytes of the columnar PZ and the HZ of the GP, while a very faint staining was detected in the RZ. No signal was present on the newly formed metaphyseal bone, but only on the cartilage remnants trapped inside. From the first week of age, TSP-5 was also observed in the RZ of the GP in addition to the PZ and the HZ, covering the totality of the cartilage. This distribution was maintained until skeletal maturity. TSP-4 on the other hand, was present exclusively in the HZ throughout all the stages analysed, and no signal was present in the newly formed bone. Only exception was observed at week 3, with few single positive cells for TSP-4 in the RZ, located at the outer perimeter of the adjacent secondary ossification center. Last, at 16 weeks of age once skeletal maturity was reached, the GP appeared disorganised and the TSP-4 signal was detected pericellularly on some cells across the cartilage matrix.

The differential expression of TSP-5 and TSP-4 during growth plate development indicated that these proteins could play a role in distinct stages of EO. Therefore, we analysed their expression in the SOC in more detail during its establishment and expansion on the femoral condyle, which occurs during the first 3-4 weeks of postnatal development in mice. For this analysis, we looked at the femoral condyle two weeks after birth. TSP-5 was detected across the entire epiphyseal cartilage, and was absent from the regions where ossification had concluded (Fig. 3). TSP-4 on the other hand, was only detected around the hypertrophic chondrocytes adjacent to the ossification front, and same as TSP-5, the staining signal disappeared after ossification. A closer look at the areas where bone formation had taken place revealed that, as in the GP, cells from the marrow entered in contact with both thrombospondins, which were present in the transient cartilage remnants.

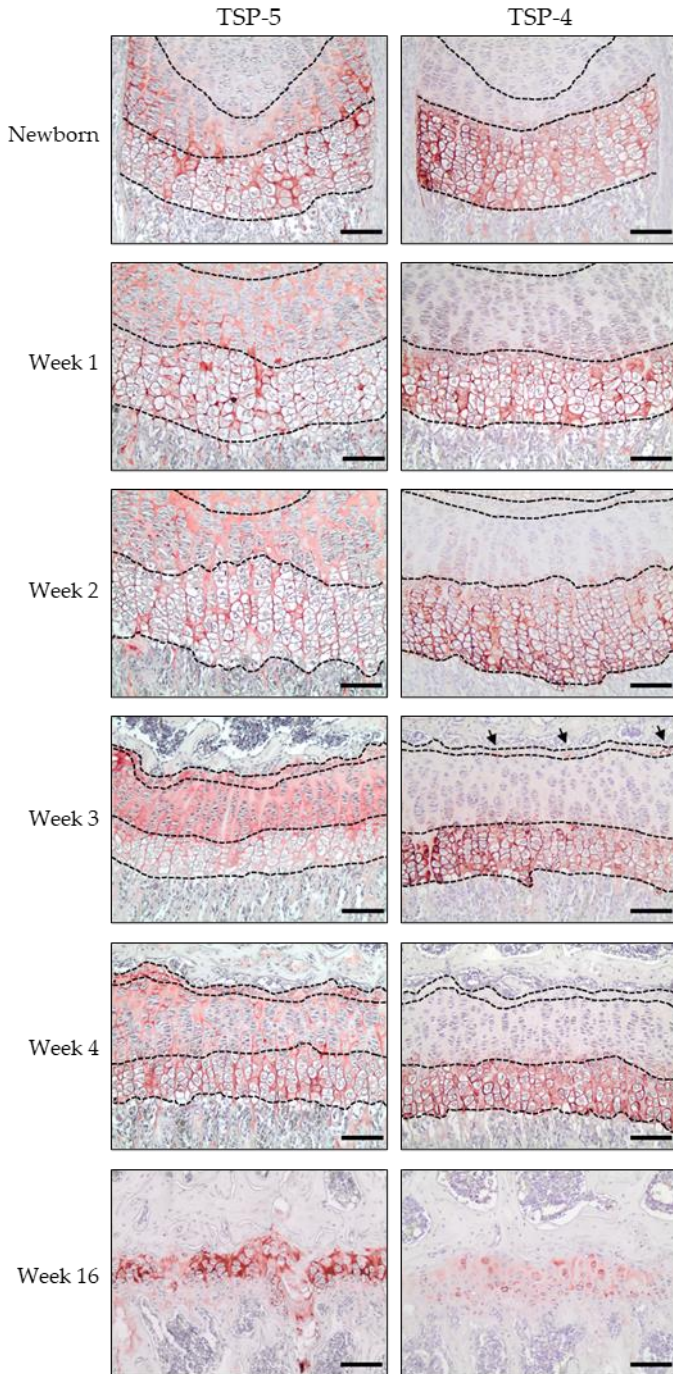


Figure 2. *Distribution of TSP-5 and TSP-4 during the maturation of the murine growth plate.* Immunohistological stainings of the mouse tibial growth plate from birth (P-0) until skeletal maturity (Week 16). Representative images of 3 mice per timepoint. Dotted lines indicate the different layers of the growth plate. Arrows indicate TSP-4 positive cells at the reserve zone. Scalebars: 100 μ m

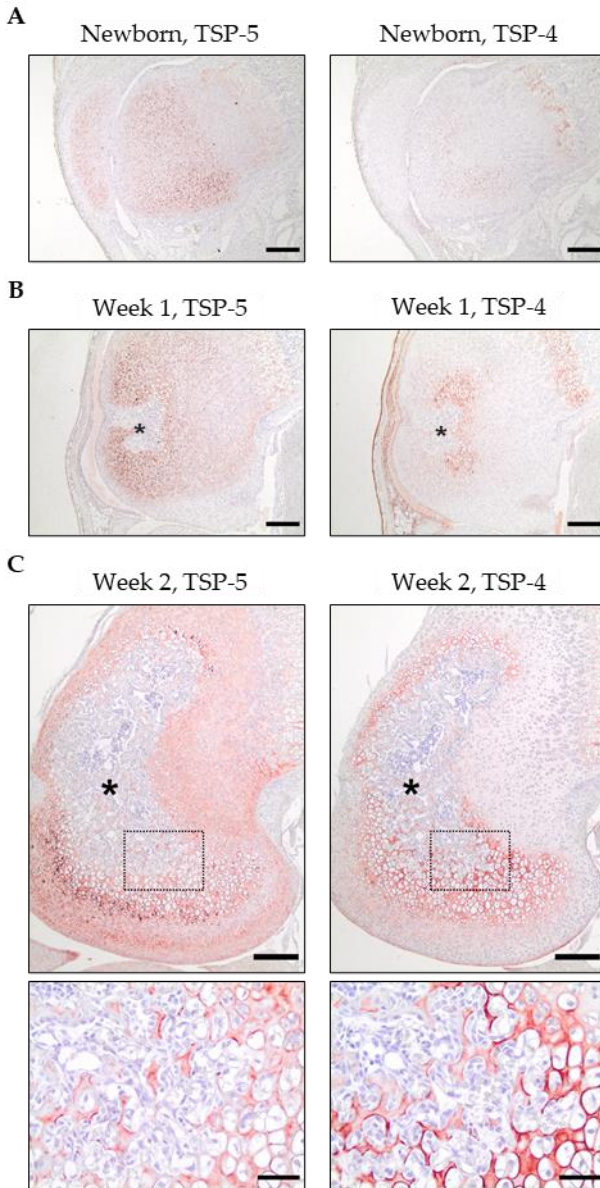


Figure 3. *Distribution of TSP-5 and TSP-4 during the expansion of the SOC.* Immunohistological stainings of the distal femoral condyle of (A) Newborn, (B) 1-week-old and (C) 2-week-old mice. Representative images of 3 mice per timepoint. (*) indicates SOC. Dotted box indicates region magnified on the right pictures. Scalebars: 200 μm (left) and 50 μm (right).

TSP-4, but not TSP-5, is present at the cranial sutures during bone development

Next, in order to assess the presence and distribution of TSP-5 and TSP-4 during IO, we analysed the two proteins at the coronal suture of newborn mice (Fig. 4). While we could not detect TSP-5, TSP-4 was exclusively present at the sutural mesenchyme, and absent in the newly formed bone.

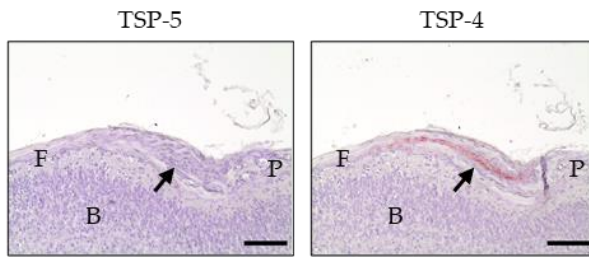


Figure 4. Distribution of TSP-5 and TSP-4 in the murine cranial sutures. Immunohistological stainings of the mouse coronal suture at birth (P-0) of 3 mice per timepoint. Arrow indicates the cranial suture. F: Frontal bone. P: Parietal bone. B: Brain. Scalebars: 100 μ m.

TSP-5 and TSP-4 are differentially present in the soft callus formed during bone fracture healing, and TSP-4 exclusively promotes the migration of endothelial cells

During bone fracture healing, part of the EO program is recapitulated and a transient cartilage template is formed as soft callus to bridge and stabilise temporarily the broken bone ends. Simultaneously, part of the IO program aids the healing process by depositing more bone. We hypothesised that both TSP-5 and TSP-4 might be differentially present at the corresponding regions of the soft callus, analogous to EO and IO during development. Gene expression analysis by qPCR of callus tissues harvested at different stages throughout the bone fracture healing process revealed that TSP-5 (encoded by the *Comp* gene) and TSP-4 (*Thbs4*) both demonstrated an expression profile similar to that of the chondrogenic markers collagen type II (*Col2a1*) and collagen type X (*Col10a1*), all showing a maximum expression at day 7 post fracture, and then gradually decreasing (Fig. 5A, data of collagens II and X reproduced from Böhm AM *et al* [85]). Interestingly, *Thbs4* also displayed an initial upregulation in the 24 hours post-fracture (Fig. 5A), suggesting that TSP-4 could be produced early during the regenerative response to the bone fracture. We next analysed the distribution of TSP-4 and TSP-5 by immunohistochemistry (Fig. 5B). While absent from the diaphysis of unfractured bones, presence of both TSP-4 and TSP-5 was evident during fracture healing. At day 7 after fracture, TSP-5 was located throughout the cartilage matrix within the soft callus regions, whereas TSP-4 was detected only around the hypertrophic chondrocytes in the callus (Fig. 5B). While TSP-5 located exclusively in the cartilage, TSP-4 was also detected in non-cartilaginous areas of the periosteum where IO was taking place. By 14 days post fracture, very sparse signal for the two proteins could be detected in the callus, limited to traces present within cartilage remnants that had not been remodelled yet into bone (data not shown).

Since TSP-5 and TSP-4 were both present during bone formation and fracture healing, we asked if any of the two proteins could act as a paracrine signal to promote cellular invasion of the surrounding cells responsible for ossification. To test this, we assessed bone marrow stromal cell (BMSC) and endothelial cell (EC) migration towards recombinant TSP-5 or TSP-4 in an *in vitro* transwell assay. Neither TSP-5 nor TSP-4 stimulated the migration of BMSCs. However, TSP-4 but not TSP-5 demonstrated the ability to stimulate migration of ECs ($p < 0.05$) (Fig. 5C).

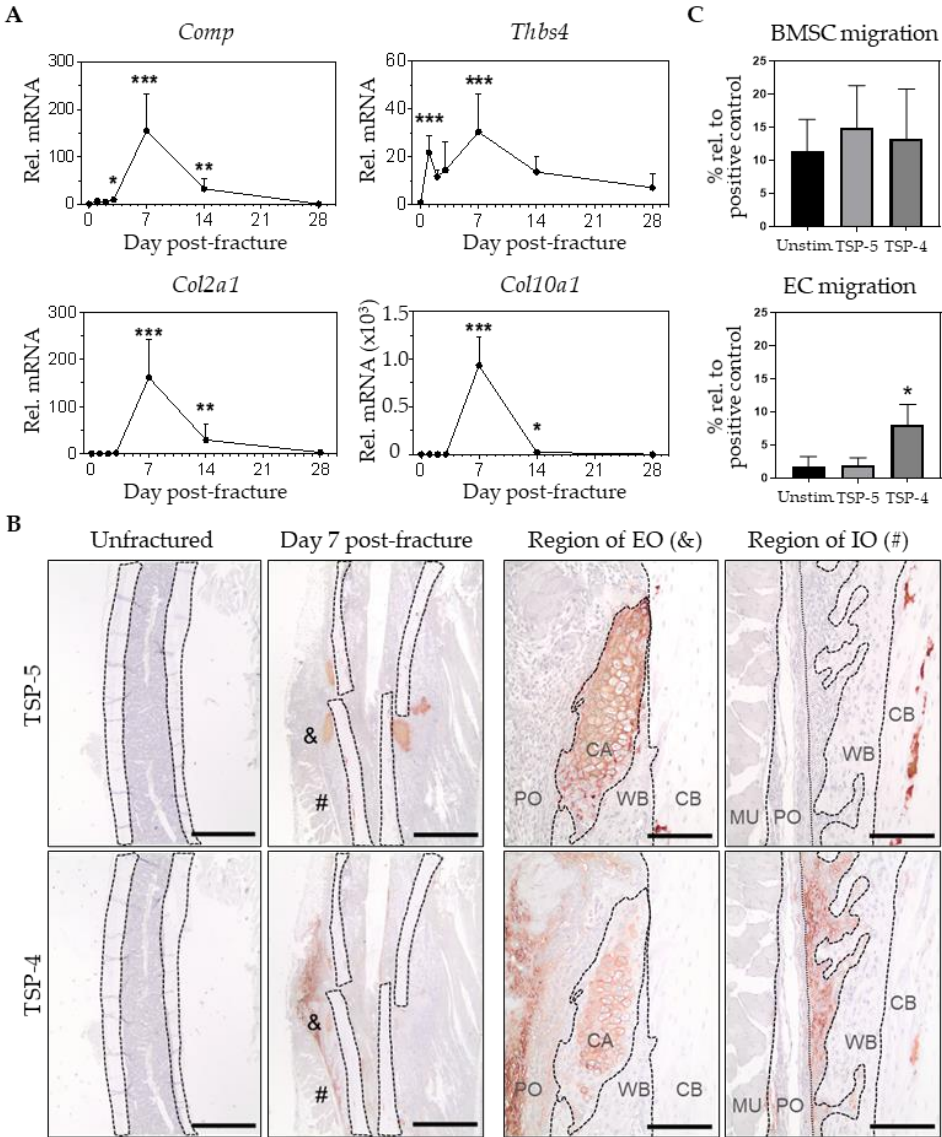


Figure 5. Gene expression and distribution of TSP-5 and TSP-4 during murine semi-stabilised tibia fracture healing. (A) qPCR on fracture calluses at various time points during bone healing, normalised to *Hprt* expression levels and expressed relative to expression levels in uninjured bones. For each time point analysed n= 4 to 6 mice. Error bars represent the SD. *p<0.05, **p<0.01, ***p<0.001 (vs. day 0). (B) Immunostainings of TSP-5 and TSP-4 showing representative images of fractures at post-fracture day 7. Representative images of 2 mice (unfractured) and 3 mice (post-fracture day 7). (&) Region of EO. (#) Region of IO. Dotted lines indicate the different tissues present on the image. PO: periosteum. CA: cartilage. WB: woven bone. CB: cortical bone. MU: muscle. Scalebars: 1 mm and 100 μ m. (C) Cellular migration of bone marrow stem cells (BMSC) and endothelial cells (EC) towards recombinant TSP-5 or TSP-4. In the case of BMSC, n=3 donors in triplicate. In the case of EC, n=3-4 repetitions in triplicate. Bars indicate the SD. *p<0.05 (vs. unstimulated).

DISCUSSION

In this study we have shown for the first time the localisation of the protein TSP-4, which we compared to that of TSP-5, during skeletal development and fracture healing. We have found that in cartilage undergoing EO TSP-4 is restricted to the hypertrophic zones, while TSP-5 is produced at all stages of chondrogenesis. In the cranial sutures producing bone via IO, TSP-4 locates at the osteoprogenitor niche while TSP-5 is absent. Furthermore, we observed this same distribution during the EO and IO events that take place in fracture healing. Last, of the two proteins only TSP-4 demonstrated proangiogenic functions, as deduced from its stimulatory effect on endothelial cell migration. Taken together, these findings indicate that TSP-4 is present at the cellular matrix that is about to transition into bone, while TSP-5 might have only cartilage-specific functions, suggesting that the two proteins may play different roles during bone formation.

While the location of TSP-5 was consistent with the previous descriptions in human [71] and mouse growth plates [70], to date, there is very limited information available about the expression and localisation of TSP-4 in transient cartilage. However, two key investigations approximated the location of TSP-4. In chick embryos *THBS4* mRNA transcripts were found adjacent to the mineralised spicules of bone of the growth plate, in “non-osteoblast alkaline phosphatase-positive cells” [93]. Furthermore, the presence of TSP-4 was detected in the mouse femoral head by mass spectrometry, and its production increased during the stages coinciding with the establishment of the SOC [81]. In line with those previous observations, we found that TSP-4 surrounded the growth plate chondrocytes, and that TSP-4 production increased at the femoral condyle during the establishment of the SOC. Nevertheless, no previous studies have reported yet the presence of TSP-4 in the cranial sutures.

Next, we asked if TSP-4 would be present in other situations where EO and IO are known to take place. Meyer MH *et al.* analysed the expression of an array of nerve-related genes in the fracture callus of rats. Their study showed that *Thbs4*, known to play roles in the nervous system [94], was upregulated during rat fracture healing with a maximum gene expression one week after fracture [95]. However, their study did not identify which tissue was responsible for *Thbs4* expression. In our work, we confirmed the upregulation of *Thbs4* during mouse fracture healing occurring 7 days post-fracture, which overlapped with that of *Comp* and other chondrogenic markers. Consistent with our results during developmental bone formation, TSP-5 was present across the cartilage matrix while TSP-4 was associated with the hypertrophic chondrocytes. Furthermore, TSP-4 but not TSP-5 was present in regions where newly bone was being produced via IO.

All five thrombospondins are indeed present at different steps on bone formation, and their multidomain structures allow them to simultaneously play both overlapping and opposing functions [38]. For example, TSP-1 and TSP-2 are both anti-angiogenic. On the other hand, while both bind latent TGF- β , TSP-1 activates it while TSP-2 acts as a

competitive antagonist of its activation [49]. Similarly, extracellular TSP-4 and TSP-5 are known to interact with integrins on the cellular surface [66, 96]. When we studied the direct effects of these two proteins on two cell types present in the marrow (BMSCs and ECs), the migratory behaviour of ECs was affected by TSP-4 but not by TSP-5, while none of the proteins induced the migration of BMSCs. Previous studies also demonstrated that both proteins have differential effects on cellular migratory behaviour. In cultured articular chondrocytes TSP-5 but not TSP-4 promotes chondrocyte attachment and migration [97, 98]. These results point to the functional differences between TSP-5 and TSP-4, which combined with their different location during ossification, suggests that despite their structural similarities the two thrombospondins may play mostly different roles during bone formation. The role of TSP-4 in the context of EO may thus be to facilitate the infiltration of other tissues into the cartilage template and to promote the remodelling of the matrix, similar as for what was observed at the blastema formed during axolotl limb regeneration [99]. Differently, in the context of IO TSP-4 might be related the maintenance of a niche of proliferating, undifferentiated progenitors [100], and further research should focus more closely on this possibility.

There have been limited studies that focused on how such differential effects of TSP-4 and TSP-5 on migration are achieved. Several receptors (including integrins) have been identified but a systematic comparison between different TSPs should be performed in future studies. TSP-4 is known to promote endothelial cell migration by binding integrin $\alpha 2$ [84]. In addition, TSP-4 has been reported to bind via its N-terminal domain NOTCH1, thereby activating the Notch signalling cascade [101]. Activation of this signalling on endothelial cells has been shown to increase endothelial cell migration and invasion distance [102, 103]. It is possible that, driven by TSP-4, both integrin and notch signalling pathways converge to promote cell migration. A similar double stimulation occurs with perlecan, another glycoprotein present in the cartilage matrix, but to negatively modulate angiogenesis by engaging simultaneously VEGFR2 and $\alpha 2\beta 1$ in endothelial cells [104]. Because the N-terminal domains of TSP-4 and TSP-5 are highly dissimilar, the differential modulation of endothelial behaviour between the two proteins might be something to explore in futures studies. Furthermore, indirect mechanisms altering the cellular migration *in vivo* may take place via the binding of TGF- β [67, 98], such as those known for TSP-5 [75]. However, those have not been yet characterised. It would be of great interest to identify the signalling pathways activated that leads to cellular migration in response to TSP-4.

In this work we exclusively compared the highly similar TSP-4 to TSP-5, as the latter has been the most characterised thrombospondin in cartilage. To date, no skeletal growth abnormalities have been reported on the knock-out mouse for TSP-5 (COMP) [105], while only a transient reduction of cartilage thickness has been observed in TSP-4 deficient animals [97]. The reason may be that their functions partially overlap with those of other thrombospondins, due to their modular similarities. Thrombospondin 3 (TSP-3) presents a similar expression pattern as TSP-5, particularly in the early proliferative zone of the

growth plate of long bones [50], and neither of them has been reported to have an angiogenic function. After studying the single knock-outs, Posey, K.L. *et al.* reported that skeletal growth was only retarded in the double knock-out for TSP-3 and TSP-5 [106], and suggested redundant roles for the two proteins. The thrombospondin 1 (TSP-1) knock-out, which was also analysed in that publication, did not seem to overlap in its functions with TSP-3 and TSP-5. Despite the lack of studies in fracture healing on TSP-3 and TSP-5 knock-outs, we can only hypothesise that by the loss of TSP-5, the expression of TSP-3 might either be enough to compensate for TSP-5 function in the cartilage present at the soft callus. On the other hand, the antiangiogenic thrombospondin-2 (TSP-2) is expressed by cells in the fracture mesenchyme, increasing during fracture healing to regulate callus formation, and the TSP-2 KO mice display increased vascularisation and enhanced bone formation during fracture healing [60]. However, opposite to our observation on TSP-4, TSP-2 is not present on the cartilage callus [59]. This suggests that TSP-2 and -4 may play opposite roles to orchestrate the vascularisation and bone formation during fracture healing. Future studies should focus on the systematic analysis of functional differences and similarities between the thrombospondin family members. Furthermore, it would be interesting to investigate fracture healing in TSP-4 knock-out mice with special attention paid to the different cell types involved that have been shown to respond to different TSPs, such as endothelial cells, macrophages and neurons.

CONCLUSIONS

We have demonstrated that TSP-4 is an ECM protein detected exclusively in the hypertrophic chondrocyte zone of transient cartilage during endochondral ossification and in the cellular population undergoing intramembranous ossification. This is different from the location of the structurally similar TSP-5, which is present throughout all the zones of transient cartilage and absent during intramembranous ossification. Its putative proangiogenic functions and ability to bind to different extracellular proteins, makes TSP-4 an attractive candidate to be considered as an accessory protein in biomaterials development for regenerative medicine-based applications focused on large bone defect repair.

ACKNOWLEDGEMENTS

We would like to acknowledge the additional funding by the Research Foundation Flanders (FWO #G0B5219N), KU Leuven (#C14/18/105) and a FWO PhD fellowship for Strategic Basic Research (SB). We also would like to thank N. Kops (Erasmus MC) for the support with the histological methodology.

CHAPTER 3

TSP-5 and TSP-4: functional roles in articular cartilage and relevance in osteoarthritis

K. MALY, E. ANDRÉS SASTRE, E. FARRELL, A. MEURER, F. ZAUCKE

PUBLISHED AS: COMP AND TSP-4: FUNCTIONAL ROLES IN ARTICULAR
CARTILAGE AND RELEVANCE IN OSTEOARTHRITIS

INT J MOL SCI. 2021 FEB 24; 22(5):2242

DOI: 10.3390/ijms22052242

ABSTRACT

Osteoarthritis (OA) is a slow-progressing joint disease, leading to the degradation and remodelling of the cartilage extracellular matrix (ECM). The usually quiescent chondrocytes become reactivated and accumulate in cell clusters, become hypertrophic, and intensively produce not only degrading enzymes, but also ECM proteins, like thrombospondin-5 (TSP-5/COMP) and thrombospondin-4 (TSP-4). To date, the functional roles of these newly synthesised proteins in articular cartilage are still elusive. Therefore, we analysed the involvement of both proteins in OA specific processes in *in vitro* studies, using porcine chondrocytes, isolated from femoral condyles. The effect of TSP-5 and TSP-4 on chondrocyte migration was investigated in transwell assays and their potential to modulate the chondrocyte phenotype, protein synthesis and matrix formation by immunofluorescence staining and immunoblot. Our results demonstrate that TSP-5 could attract chondrocytes and may contribute to a repopulation of damaged cartilage areas, while TSP-4 did not affect this process. In contrast, both proteins similarly promoted the synthesis and matrix formation of collagen II, IX, XII and proteoglycans, but inhibited that of collagen I and X, resulting in a stabilised chondrocyte phenotype. These data suggest that TSP-5 and TSP-4 activate mechanisms to protect and repair the ECM in articular cartilage.

INTRODUCTION

Articular cartilage consists of an extracellular matrix (ECM) with a unique composition and architecture, providing the biomechanical properties for frictionless motion [29, 107, 108]. The tissue is organised in four zones: the superficial zone at the top, the transitional zone, the deep zone and the calcified zone [29]. Also, the area around the chondrocytes is subdivided into a pericellular matrix directly surrounding the chondrocytes, a territorial matrix, surrounding the pericellular matrix and the interterritorial matrix, the area between the territorial matrices. The main components of the ECM are proteoglycans and collagens, responsible for elasticity and stiffness, respectively [29]. The predominant collagen II forms fibrils with collagen XI as a core and collagen IX on its surface [109-111]. The distribution of different collagen types depends on the zonal localization. Thinner collagen fibrils are associated with collagen IX [110, 111], while thicker fibrils are not [111, 112]. Fibrils in the superficial zone are also associated with collagen XII [113]. Collagen IX and XII both belong to the fibril-associated collagens with interrupted triple helices (FACIT). They are structurally similar [114] but, in contrast to collagen IX, collagen XII is noncovalently linked to fibrillar collagens [115]. Collagen X is restricted to the calcified zone and represents a transitional area, linking the articular cartilage to the bone [116-119]. To a minor extent, the ECM also contains noncollagenous proteins [107], e.g., the thrombospondin-5 (TSP-5, also known as cartilage oligomeric matrix protein, COMP), which promotes collagen secretion and assembly as well as ECM stability [73, 120]. Chondrocytes are surrounded by a dense ECM and remain quiescent in mature cartilage, mediating ECM homeostasis in a low turnover state [121]. In osteoarthritis (OA), alterations at the cellular and molecular levels cause a continuous degradation of the ECM, leading to joint failure and pain [122, 123]. Chondrocytes produce degrading proteases and are reactivated to synthesise ECM proteins, resulting in ECM remodelling [120, 122, 124-126]. The cause of chondrocyte reactivation is not completely understood, but might be regulated by cell-matrix interactions. Growth factors like the transforming growth factor beta 1 (TGF- β 1) [127-130], which are commonly stored in the ECM and released under certain circumstances, play an important role by regulating processes like cell proliferation and differentiation [131, 132], in particular via the SMAD and ERK signalling pathways [128, 133-136]. The level of activated TGF- β 1 is increased in the synovial fluid of OA patients [137], suggesting enhanced interaction with chondrocytes in cases of disease. During OA progression, the phenotype of chondrocytes becomes unstable [138], resulting in the loss of chondrogenic markers (collagen II, collagen IX and TSP-5) [139] and the synthesis of ECM components that are usually not expressed in articular cartilage, like collagen I and collagen X [140-142]. The ECM protein TSP-5 is a target of degradation in early OA, but is also re-expressed in later stages [120]. In contrast, its close family member, thrombospondin-4 (TSP-4), is hardly detectable in healthy cartilage, but its expression increases dramatically in OA cartilage and correlates with disease severity [65]. Both proteins have similar structures and binding partners [77, 143-148], suggesting similar or additive roles in articular cartilage. It has also been reported that TSP-5 binds TGF- β 1,

thereby promoting its transcriptional capacity [75], while this has not yet been shown for TSP-4. The re-expression of TSP-5 and the new synthesis of TSP-4 in OA was interpreted as an attempt to restore the integrity of the cartilage ECM [65, 120]. However, the effect of these ECM proteins on the chondrocyte phenotype and behaviour, as well as their contribution to OA relevant processes and ECM repair, have not yet been investigated in detail. Therefore, the present study focuses on the potential of TSP-5 and TSP-4 to promote repopulation of damaged cartilage areas by attracting chondrocytes, stabilizing their phenotype as well as inducing the synthesis and deposition of collagens and proteoglycans. The obtained data will contribute to a better understanding of the functional role of TSP-5 and TSP-4 in articular cartilage, and might help to improve and develop effective therapeutic applications.

MATERIALS AND METHODS

Collection and scoring of human osteochondral cylinders

Adult, human, anonymised cartilage samples were obtained from seven OA patients undergoing endoprosthetic knee replacement surgery at the Department of Orthopaedics (Friedrichsheim), University Hospital Frankfurt, Goethe University, and visually scored as described before [65]. Intact cartilage areas with a smooth and shiny surface were scored as grade 1 (G1), cartilage areas with superficial fissures and a rough surface were scored as grade 2, and areas with deeper fissures and/or exposure of subchondral bone as grade 3 to 4 (G3/4). Two non-OA cartilage sections staining were a gift from Gerjo van Osch [Erasmus University Medical Center, Rotterdam, the Netherlands] and used as healthy controls.

Chondrocyte isolation and culture from pig articular cartilage

Pig legs were obtained from the animal house at Goethe University Frankfurt, Frankfurt/Main, Germany from among animals sacrificed within the scope of other scientific projects. Legs from female, healthy pigs (three to six months old) were received immediately after sacrificing. Pig legs were processed to expose the knee and the knee joint was opened to scrape off the articular cartilage from the femoral condyles under sterile conditions. The cartilage was washed with phosphate buffered saline (PBS) [Thermo Fisher Scientific, Waltham, MA, USA] and cut into small pieces (2–3 mm³) to isolate chondrocytes. The cartilage pieces of pig knee joints were weighted, transferred into a sterile tube and digested with 0.2 % pronase [Roche Diagnostics, Mannheim, Germany] in DMEM/F12 medium containing 5 % FBS and 5 % pen/strep [all from Gibco, Karlsruhe, Germany] for 2 h at 37 °C with the agitation of 60 rpm. After incubation, cells and cartilage pieces were pelleted by centrifugation at 300 × g, 5 min at RT and the supernatant decanted. Cells and cartilage pieces were washed 3× with PBS and digested with 200 U/mL collagenase type II [Biochrom, Berlin, Germany] solution in DMEM/F12

medium (containing 5 % FBS and 5 % penicillin/streptomycin) overnight at 37 °C with the agitation of 60 rpm. The chondrocyte suspension was filtered through a 70 µm nylon cell strainer and centrifuged at 300 × g for 5 min at RT. The pelleted cells were resuspended, counted with a Neubauer chamber and seeded either in DMEM/F12 containing 5 % FBS or resuspended in medium containing 0.1 % bovine serum albumin (BSA) [PanReac, AppliChem, Darmstadt, Germany] for direct use in the migration assay. All cells were cultured at 37 °C, 5 % CO₂ and 20 % O₂ in a CO₂ incubator.

To analyse the production of matrix proteins and matrix formation via immunofluorescence staining and immunoblot analysis, 40,000 cells in DMEM/F12 containing 5 % FBS were seeded in each chamber of a Nunc™ Lab-Tek™ II four-well chamber slide [Thermo Fisher Scientific, Waltham, MA, USA]. Chondrocytes used for signalling experiments were seeded in a density of 300,000 cells in DMEM/F12 containing 5 % FBS per well of a six-well plate. The cells were allowed to attach to the bottom overnight. The following day, the cells were washed twice with PBS and starved in basic medium (DMEM/F12 containing 0.1 % BSA and 25 µg/mL ascorbic acid [Sigma-Aldrich, St. Louis, MO, USA]) for 24 h. Then, the cells were stimulated with recombinant proteins. Different concentrations of TGF-β1 [R&D Systems, Minneapolis, MN, USA] were used, depending on the downstream assay. In all assays, recombinantly expressed and purified TSP-5 and TSP-4 were used in a concentration of 10 µg/mL. The chondrocytes were treated with TGF-β1, TSP-5 or TSP-4 alone and in the combination of TGF-β1 with TSP-5 or TSP-4 in basic medium. When cells were stimulated in the combination of TGF-β1 with TSP-5 or TSP-4, the two components were mixed in a tube and pre-incubated for 20 min at RT, before applying to the cells.

Chondrocytes seeded in chamber slides were stimulated with 0.5 ng/mL TGF-β1, 10 µg/mL TSP-5, 10 µg/mL TSP-4 and in the combination of TGF-β1 with TSP-5 or TSP-4 for a period of seven days. The chondrocytes were first stimulated with recombinant protein in the basic medium for four days. The medium was changed at day 4 and recombinant proteins applied in a basic medium containing 5 % FBS. At day 7, the medium was replaced by a basic medium containing only 5 % FBS and chondrocytes cultured until day 10. The supernatants were collected after each medium change and stored at -20 °C.

For immunoblot analyses, chondrocytes were stimulated with 0.1 ng/mL, 0.25 ng/mL, 0.5 ng/mL, 1 ng/mL and 10 ng/mL TGF-β1, 10 µg/mL TSP-5, 10 µg/mL TSP 4 or a combination of all TGF-β1 concentrations with TSP-5 or TSP-4 for 30 min at 37 °C.

Expression and purification of recombinant proteins

Recombinant TSP-4 and TSP-5 were produced as described before [91, 149]. Shortly, HEK-293 EBNA cells were transfected with the pCEP-Pu V162 expression vector (generated by Prof. dr. Manuel Koch, University of Cologne) carrying the sequence of full-length rat TSP-5 and TSP-4 and cultured in DMEM/F12 medium containing 1 % FBS for a period of five days. The cell culture supernatant was collected daily and cleared by

centrifugation. The recombinant proteins were purified via the Strep-Tag affinity chromatography column [IBA, Goettingen, Germany] at day five. The protein concentration was measured with the Qubit fluorometer and protein fractions stored at $-20\text{ }^{\circ}\text{C}$ until use.

(Immuno)histological and immunofluorescence staining of cartilage samples and chondrocytes

Osteochondral cylinders were generated and processed as described before [65]. Samples were fixed in 4 % paraformaldehyde [Sigma-Aldrich, St. Louis, MO, USA] in PBS, pH = 7.4, overnight at $4\text{ }^{\circ}\text{C}$. After decalcification in 10 % ethylenediaminetetraacetic acid (EDTA) [VWR, Osterode am Harz, Germany], samples were embedded in paraffin. Then, $5\text{ }\mu\text{m}$ sections were generated, deparaffinised and rehydrated prior to antigen retrieval. Tissue sections were treated with 250 U hyaluronidase [Sigma-Aldrich] in PBS (pH = 5) before TSP-4 staining and with $20\text{ }\mu\text{g}/\text{mL}$ proteinase K [Qiagen, Hilden, Germany] in proteinase K buffer (10 mM NaCl, 50 mM Tris-base, 10 mM EDTA in ddH₂O, pH 7.4) before TSP-5 staining, for 15 min at $37\text{ }^{\circ}\text{C}$. Endogenous peroxidase activity was blocked with 0.3 % H₂O₂ [Carl Roth, Karlsruhe, Germany] in dH₂O for 10 min at RT and unspecific binding blocked with 2.5 % normal horse serum [included in the ImmPRESS™ HRP reagent kit, Vector Laboratories, Burlingame, CA, USA] for 20 min at RT. Primary antibodies (Table 1) were diluted in 1 % BSA and the tissue sections incubated at $4\text{ }^{\circ}\text{C}$ overnight. The primary antibodies were detected with the ImmPRESS™ (peroxidase) polymer anti-rabbit IgG reagent [included in the ImmPRESS™ HRP Reagent Kit, Vector Laboratories, Burlingame, CA, USA] at RT for 30 min. The AEC-2-component kit [DCS, Hamburg, Germany] was used according to the manufacturer's instructions to visualise the secondary antibody. Negative control staining without addition of the primary antibodies were carried out to exclude unspecific binding of the secondary antibody (data not shown).

Cultured chondrocytes in chamber slides were fixed with Shandon™ zinc formal-fix™ [Thermo Fisher Scientific, Waltham, MA, USA] for 20 min at RT, washed 3x with PBS. To stain proteoglycans cells were incubated with 0.1 % Safranin-O [Carl Roth, Karlsruhe, Germany] at RT for 15 min. Before antibody staining, cells were permeabilised with 0.3 % Triton X-100 [Merck, Darmstadt, Germany] in PBS for 10 min at RT. Unspecific binding sites were blocked with blocking buffer (1 % BSA and 1 % goat serum [Abcam, Cambridge, UK] in PBS) for 1 h at RT. Cells were incubated with the primary antibodies (Table 1) diluted in 1 % BSA in PBS at $4\text{ }^{\circ}\text{C}$ overnight. After three washing steps with TBST (PBS containing 0.1 % Tween-20 [Carl Roth, Karlsruhe, Germany]), cells were incubated with the corresponding secondary antibodies (Table 2) diluted in 1 % BSA in PBS at RT in the dark for 1.5 h. The cells were washed twice with TBST and once with PBS before mounting with the DAPI fluoroshield mounting medium [Abcam, Cambridge, UK]. DAPI was visualised at a wavelength of 461 nm, Alexa Fluor

488 at 516 nm and Alexa Fluor 594 at 617 nm with a fluorescence and Safranin-O with a light microscope [Nikon, Tokyo, Japan].

Protein extraction and analysis

Proteins from human cartilage samples were extracted as described previously [65]. Briefly, cartilage from areas showing different severity grades were scraped off and cut into pieces (1–3 mm³), and proteins were extracted with an extraction buffer (4 M guanidine hydrochloride, 50 mM Tris, 10 mM EDTA (pH = 7.4)) overnight at 4 °C. After precipitating the proteins with 96 % ethanol for 24h at –20 °C, the protein pellet was washed and resuspended in Laemmli buffer (250 mM Tris-HCl, pH 6.8, 40 % glycerol, 0.04 % bromophenol blue, 8 % SDS).

Cells in monolayer culture were washed with PBS and cell lysates collected by scraping the cells in 1x Laemmli buffer containing 4 % β -mercaptoethanol [Sigma-Aldrich, St. Louis, MO, USA] and phosphoSafe™ [Merck, Darmstadt, Germany]. Cell culture supernatants were mixed with Laemmli buffer with or without β -mercaptoethanol.

For quantification, proteins were separated by SDS-PAGE using 5%, 8% or 10% polyacrylamide gels as previously described [65]. The separation was carried out using a Mini-PROTEAN® Tetra-cell system [Bio-Rad, Munich, Germany] at 150 V and equal loading was demonstrated by PageBlue™ [Thermo Fisher Scientific, Waltham, MA, USA] or Roti®blue [Carl Roth, Karlsruhe, Germany] staining of total proteins. After electrophoresis, proteins were transferred onto a 0.45 μ m polyvinylidene fluoride (PVDF) membrane [GE Healthcare, Freiburg, Germany] using the mini Trans-blot® electrophoretic transfer cell [Bio-Rad, Munich, Germany] and unspecific binding sites

Target	Host	Dilution	Source or Supplier
Collagen I	rabbit	1:200 (IF), 1:1000 (IB)	Abcam (ab34710)
Collagen II	mouse	1:200 (IF), 1:1000 (IB)	Merck (CP18)
Collagen IX	guinea pig	1:200 (IF), 1:1000 (IB)	[150]
Collagen X	mouse	1:50 (IF), 1:100 (IB)	M. Zhou (University of Cologne)
Collagen XII	rabbit	1:200 (IF), 1:1000 (IB)	M. Koch (University of Cologne)
TSP-5	rabbit	1:100 (IF), 1:500 (IHC), 1:1000 (IB)	[61]
TSP-4	rabbit	1:100 (IF), 1:500 (IHC)	[65]
TSP-4	guinea pig	1:1000 (IB)	[77, 151]
SMAD2	rabbit	1:1000 (IB)	Cell Signalling (5339)
pSMAD2	rabbit	1:2000 (IB)	Cell Signalling (3108)
SMAD1/5/9	rabbit	1:500 (IB)	Santa Cruz (sc-6031-R)
pSMAD1/5/9	rabbit	1:1000 (IB)	Cell Signalling (13820)
ERK1/2	mouse	1:2500 (IB)	Cell Signalling (9107)
pERK1/2	rabbit	1:2000 (IB)	Cell Signalling (4370)
GAPDH	mouse	1:2000 (IB)	Thermo Fisher Scientific (MA5-15738)

Table 1. List of primary antibodies.

blocked in 10 % skim milk (TSP-5 and TSP-4) or 5 % BSA (signalling proteins and collagens) at RT for 1 h with gentle agitation. Membranes were incubated with the corresponding antibodies listed in Table 1 at 4 °C overnight. After washing, membranes were incubated with the corresponding secondary antibodies (Table 2) for 1 h at RT and the proteins visualised by using a mixture of ECL solution (0.1 M Tris-HCl, pH = 8.5; 225 mM *p*-coumaric acid and 1.25 mM luminol) with 3 % H₂O₂. The protein signals were analysed by the Chemi Doc™ XRS+ [Bio-Rad, Munich, Germany] molecular imager and the ImageLab™ software (<http://www.bio-rad.com/de-de/product/image-lab-software>). The band intensities were quantified with the ImageJ version 1.5 software (<http://imagej.nih.gov/ij>).

Target	Host	Conjugated	Dilution	Reference or producer
Rabbit IgG	goat	HRP	1:1000 (IB, IHC)	Agilent (P0448)
Guinea pig IgG	rabbit	HRP	1:1000 (IB, IHC)	Agilent (P014102-2)
Mouse IgG	goat	HRP	1:1000 (IB, IHC)	Agilent (P0447)
Rabbit IgG	goat	Alexa Fluor 594	1:500 (IF)	Invitrogen (A-11037)
Guinea pig IgG	goat	Alexa Fluor 488	1:500 (IF)	Invitrogen (A-11073)
Mouse IgG	goat	Alexa Fluor 488	1:500 (IF)	Invitrogen (A-11029)

Table 2. List of conjugated antibodies.

Migration assay

The transwell system with ThinCert™ cell culture inserts containing a polyethylene terephthalate (PET) membrane with a pore size of 8 µm was used in combination with 24-well plates to investigate the migration of primary pig chondrocytes. First, 400 µL DMEM/F12 containing 0.1 % BSA with either 10 µg/mL TSP-5 or 10 µg/mL TSP-4 were added to the lower compartment of the transwell system. As a positive control, chondrocytes were attracted with 10 ng/mL platelet-derived growth factor-BB (PDGF-BB) [Miltenyi Biotec, Bergisch Gladbach, Germany]. As a negative control, the plenty medium was added in the lower compartment. Chondrocytes were directly used after isolation from knee cartilage and washed twice with PBS before use in migration assays. Then, 50,000 cells in 200 µl medium were transferred to the upper compartment of the inserts. After 10 h incubation at 37 °C, 5% CO₂ and 20% O₂, the cells within and on the lower side of the PET membrane were fixed with Shandon™ zinc formal-fixx™ for 20 min at RT. Nonmigrated chondrocytes on the upper side of the PET membrane were removed using a cotton swab. After a brief rinse in dH₂O, the nuclei were stained with DAPI [Sigma-Aldrich, St. Louis, MO, USA] and imaged with a fluorescent microscope at a wavelength of 461 nm. Five pictures from different areas of the membrane were taken and the number of cells counted with ImageJ. The fold change of the number of cells which had migrated towards TSP-5, TSP-4 and the positive control were calculated based on the number of cells which had migrated towards the negative control. All technical replicates were performed at least in duplicate.

Attachment assay

Wells of a 96-well plate were coated with 10 $\mu\text{g}/\text{mL}$ TSP-5 and TSP-4 in PBS. As a negative control 100 mg/mL BSA and as a positive control 10 $\mu\text{g}/\text{mL}$ fibronectin [R&D Systems, Minneapolis, MN, USA] were used. The recombinant protein, in the indicated concentration, was added to each well and incubated overnight at 4°C. The following day, the wells were washed twice for 5 min with PBS and once for 5 min with DMEM/F12 containing 0.1% BSA. After blocking with 1% BSA for 3 h at RT, chondrocytes were added at a concentration of 50,000 cells in DMEM/F12 containing 0.1% BSA. Chondrocytes were incubated for 1 h at 37 °C and 5% CO₂ in a CO₂-incubator. Following the incubation, the supernatant was carefully removed and the wells briefly washed twice with PBS. Chondrocytes were fixed with Shandon™ zinc formal-fixx™ for 20 min at RT. Cells were washed three times for 5 min each with PBS and stained with 0.1% crystal violet for 30 min at RT. The cells were washed three times for 5 min each with ddH₂O and imaged with a light microscope. The number of cells was counted and the fold change to the negative control calculated. All technical replicates were performed in triplicates.

Surface plasmon resonance spectroscopy

The interaction between proteins was measured with the Biacore 2000 [Biacore AB, Uppsala, Sweden]. All experiments were performed at 25 °C and with a CM5 sensor chip coupled with 1500 U TGF- β 1. As a reference, a flow cell without an immobilised ligand was used. A 1:2 dilution series from a concentration of 160 nm to 0 nm of the analytes, TSP-5 and TSP-4, were prepared in a running buffer [Biacore AB, Uppsala, Sweden]. The system was equilibrated at a flow rate of 30 $\mu\text{l}/\text{min}$ with the running buffer, and the experiment started when a stable baseline was reached. The injection of the analyte was started and data were collected for kinetic analysis. One analyte concentration per cycle was injected, starting with the lowest concentration. The chip was regenerated after each cycle with 2 M NaCl.

The BIAevaluation software 3.0 [Biacore AB, Uppsala, Sweden] was used to create a sensorgram, showing the response against the time. By doing a multicycle kinetic, several analyte concentrations were induced in separate cycles, resulting in multiple curves in the sensorgram. By fitting the curves to the mathematical 1:1 model, the association rate (k_a), dissociation rate (k_d) and the dissociation constant (K_d) was evaluated.

Statistical analysis

The SigmaPlot version 13.0 software [Systat Software, Inc., San Jose, CN, USA] was used for statistical analyses. Differences between groups were evaluated by the paired t-test, One Way ANOVA or the Friedman test with either the Tukey, Student-Newman-

Keuls Method or Dunnett's post hoc test. Correlations between groups were analysed by using the Spearman rank test (r). A p -value < 0.05 was considered as significant difference ($p < 0.05$ *; $p \leq 0.01$ **; $p \leq 0.001$ ***).

RESULTS

TSP-5 and TSP-4 are differentially distributed in human healthy and OA knee articular cartilage

Healthy and osteoarthritic cartilage tissue was paraffin-embedded and sections were stained for TSP-5 and TSP-4 (Fig. 1A, B). In healthy cartilage, TSP-5 was ubiquitously and uniformly expressed throughout all layers. In the deep zone, the staining was mainly found in the interterritorial matrix. In addition, faint intracellular staining was observed. In OA cartilage, the staining in the superficial zone became weaker, and interterritorial TSP-5 seemed primarily to be degraded. Instead, a pronounced intracellular staining of

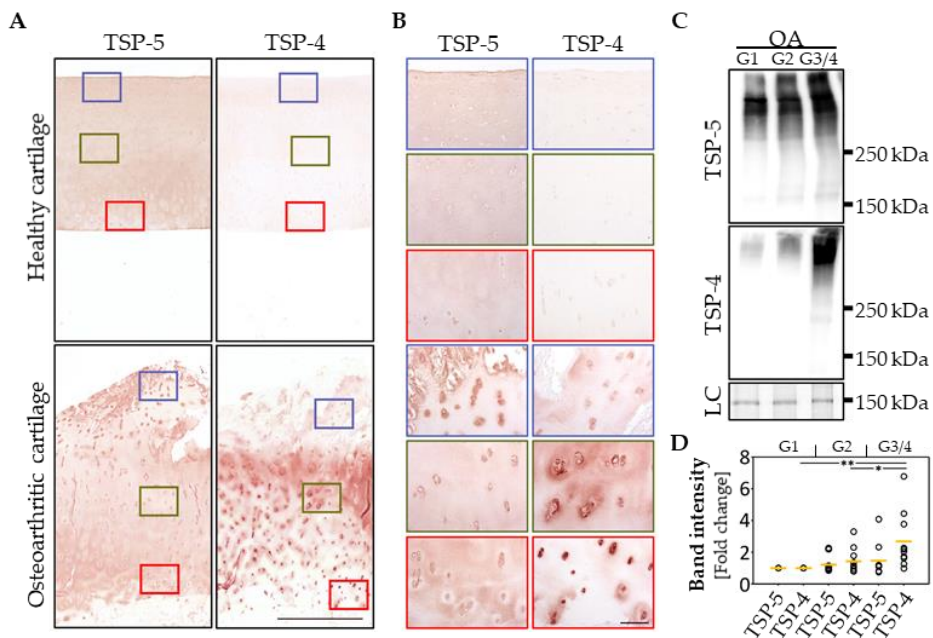


Figure 1. Localization and expression of TSP-5 and TSP-4 in human articular cartilage. (A) Articular cartilage sections from femoral condyles from healthy controls and OA patients were stained with TSP-5 and TSP-4 specific antibodies. Scale bar = 1 mm. (B) Magnifications of tissue areas indicated with the boxes in (A). Scale bar = 100 μ m. (C) Total TSP-5 and TSP-4 content was investigated via immunoblots, with proteins extracted from OA cartilage areas showing different degeneration grades (grade 1 (G1), grade 2 (G2) and grade 3/4). PageBlue™ staining was used as loading control (LC). Representative immunoblots from 10 different donors are shown. (D) Quantification and statistical analyses of the immunoblots. Values are represented as scatter plots with indicated mean as fold change versus G1. The significance of the increase in TSP-5 and TSP-4 is indicated ($p < 0.05$ *, $p < 0.01$ **).

TSP-5 was detected in the superficial zone, suggesting a re-expression of the protein. TSP-4 was hardly detectable in healthy cartilage, but could be detected in high levels in OA cartilage. While TSP-5 was predominantly re-expressed at the cartilage surface, increased expression of TSP-4 was found mainly in the middle and deeper zone of articular cartilage.

In order to get a deeper insight into the amounts and structural integrity of TSP-5 and TSP-4 in OA cartilage, total protein extracts from areas with different degradation stages were generated. Grade 1 (G1): smooth surface and no fissures, grade 2 (G2): superficial discontinuities and fissures and grade 3/4 (G3/4): deep fissures and visibility of the subchondral bone. An immunoblot analysis of these extracts (Fig. 1C) revealed that in the tissue TSP-4 was mainly present as a full-length pentameric protein, while TSP-5 already showed signs of degradation, indicated by bands of lower molecular weight. Further, the total amount of TSP-5 and TSP-4 was evaluated and the fold change in G2 and G3/4 samples related to G1 (set as 1) was calculated. The total amount of both proteins increased with disease severity. Interestingly, the increase in protein levels was much more pronounced for TSP-4 than for TSP-5. This increase was only significant for TSP-4 (Fig. 1D).

TSP-5 but not TSP-4 promotes chondrocyte migration and attachment

In order to analyse the function of TSP-5 and TSP-4 during OA progression, recombinant proteins were expressed and purified for downstream *in vitro* assays (Fig. 2A). Both recombinant proteins could be produced in sufficient amounts and showed a high structural similarity to the naturally occurring proteins in OA cartilage (Fig. 1C).

The immunohistochemical staining showed that the localization of TSP-5 and TSP-4 differs between healthy and diseased cartilage; while TSP-5 is re-expressed in superficial layers, TSP-4 is predominantly expressed in the middle and deep zones in OA conditions. To gain knowledge about the capacity of TSP-5 to attract chondrocytes and contribute to their migration into the areas of damage to support repair undertakings, transwell migration assays were performed. As attractants, TSP-5 (10 $\mu\text{g}/\text{mL}$) and TSP-4 (10 $\mu\text{g}/\text{mL}$) were added to the lower compartment, and porcine chondrocytes in the upper compartment were allowed to migrate for 10 h (Fig. 2B). PDGF-BB (10 ng/mL) was used as a positive and standard medium as a negative control. Both TSP-5 ($p = 0.014$) and PDGF-BB ($p = 0.012$) attracted chondrocytes compared to the negative control (Fig. 2C, D). The number of cells migrating towards TSP-4 was similar to the negative control. (Fig. 2C, D).

To determine whether TSP-5 could also facilitate the attachment and anchorage of the attracted chondrocytes, wells of a 96-well plate were coated with 10 $\mu\text{g}/\text{mL}$ TSP-5 and also TSP-4; 10 $\mu\text{g}/\text{mL}$ fibronectin was used as a positive control and 100 mg/mL BSA as a negative control. Chondrocytes were incubated in coated wells for 1 h, the attached cells were stained with crystal violet and analysed by light microscopy (Fig. 2E, F).

Chondrocytes attached to fibronectin ($p = 0.003$) and TSP-5 ($p = 0.012$) but not to TSP-4 ($p = 0.18$). Also, an increased attachment for TSP-5 compared to TSP-4 ($p = 0.007$) was observed. These data demonstrated that TSP-5 but not TSP-4 has the potential to attract chondrocytes and facilitate their attachment.

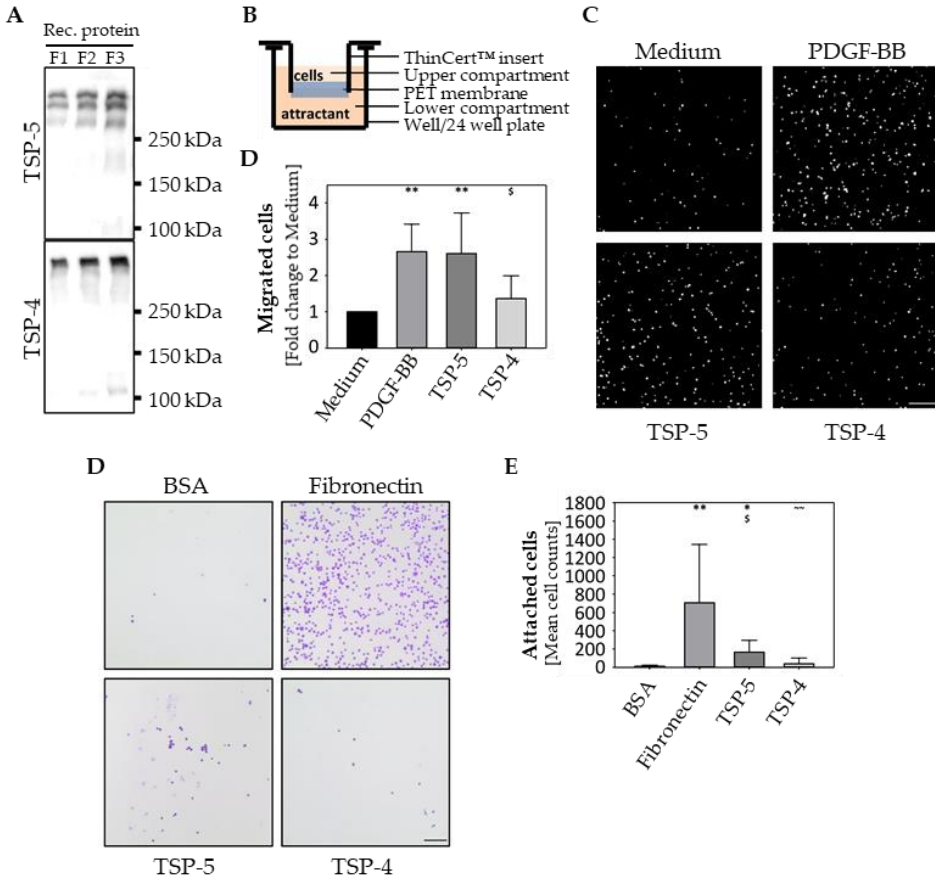
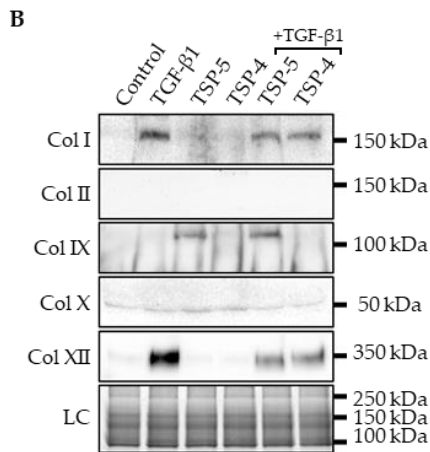
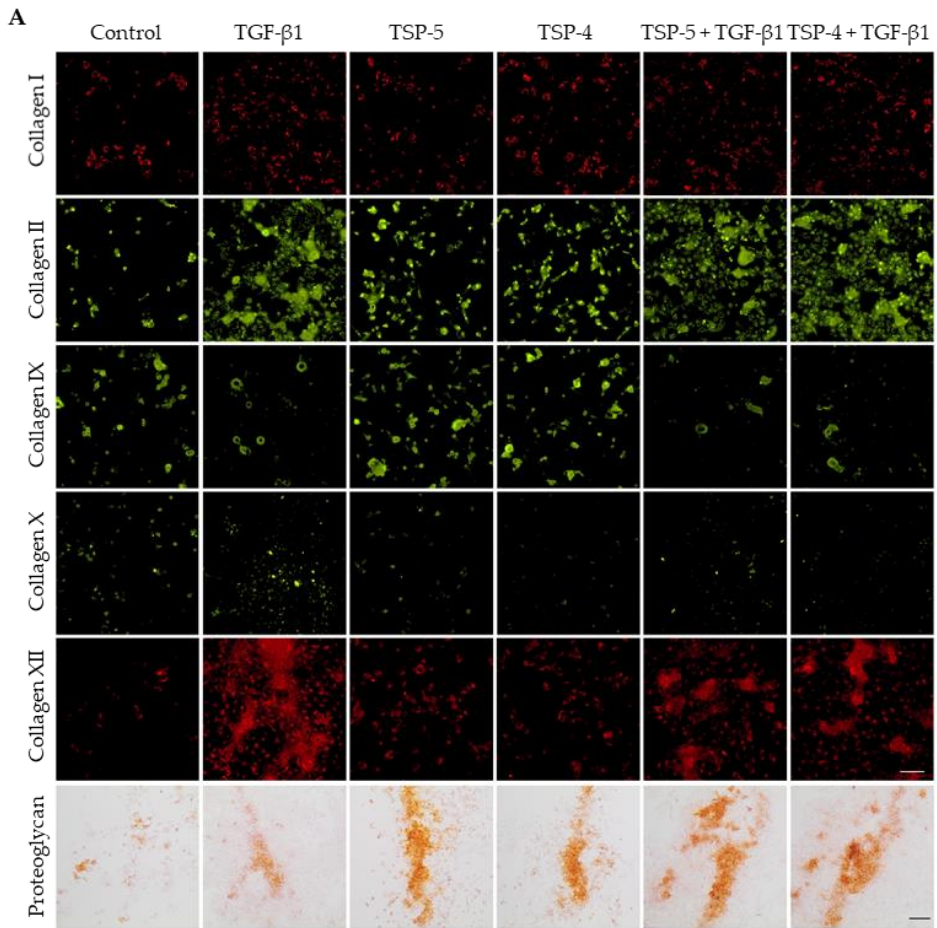


Figure 2. Chondrocyte migration and attachment to TSP-5 and TSP-4. (A) Recombinant (Rec.) TSP-5 and TSP-4 were eluted from the columns in several steps and every protein fraction [F] analysed by immunoblot. (B) Schematic illustration of the transwell system. Porcine chondrocytes were added to the upper compartment and allowed to migrate towards TSP-5 (10 $\mu\text{g}/\text{mL}$) or TSP-4 (10 $\mu\text{g}/\text{mL}$) for 10 h. (C) Representative images of migrated chondrocytes stained with DAPI. (D) Migrated cells were counted and cell numbers statistically evaluated. Each bar shows the mean + SD and significance (to medium: $p < 0.05^*$, $p < 0.01^{**}$ and to PDGF-BB: $p < 0.05^\$$) was analysed. (E) Representative images of attached chondrocytes stained with crystal violet. (F) Attached cells were counted and cell numbers statistically evaluated. Each bar shows the mean + SD and significance (to BSA $p < 0.05^*$, $p < 0.01^{**}$, to fibronectin $p < 0.05^\$$ and TSP-5 $p < 0.01^{**}$) was analysed. The standard medium was used as a negative and PDGF-BB (10 ng/mL) as a positive control for the migration assay. BSA (100 mg/mL) was used as a negative control and fibronectin (10 $\mu\text{g}/\text{mL}$) as a positive control for cell attachment. ($n = 4-5$); scale bar = 100 μm .

Both TSP-5 and TSP-4 modulate collagen and proteoglycan synthesis

To determine whether TSP-5 and TSP-4 could further stimulate chondrocytes to synthesise collagens and proteoglycans to rebuild the ECM in damaged areas and contribute to ECM remodelling in lower cartilage areas, chondrocytes were stimulated with TSP-5 (10 $\mu\text{g}/\text{mL}$), TSP-4 (10 $\mu\text{g}/\text{mL}$), TGF- β 1 (0.5 ng/mL) or in combination of TGF- β 1 with TSP-5 or TSP-4 for seven days. To ensure that the chondrocyte phenotype in monolayer culture remained stable, the stimulation experiments were stopped after three more days. TSP-5 and TSP-4 directly interact with TGF- β 1 (Suppl. Fig. 1), and TSP-5 is further known to modulate the transcriptional activity of TGF- β 1 [75]. Therefore, TGF- β 1 alone was used as an inducer of collagen synthesis (positive control), while the combination with TSP-5 and TSP-4 was used to observe their potential to modulate TGF- β 1-induced effects. As a negative control, chondrocytes were cultured in standard medium. Matrix-associated collagens were detected by immunofluorescence staining, and matrix-associated proteoglycans were stained with Safranin-O (Fig. 3A).

TSP-5 and TSP-4 stimulation resulted in an increased staining intensity of matrix-associated collagen II, IX, XII and proteoglycan, while no effect on collagen I and a slight decrease of collagen X deposition could be observed. TGF- β 1 enhanced the matrix formation of collagen I, II, XII and proteoglycan while reducing collagen IX levels and not affecting collagen X. Investigating the effect of TSP-5 and TSP-4 on TGF- β 1 induced matrix formation showed a decrease of collagen I, X and XII levels, as well as an increase of collagen II and proteoglycan. TGF- β 1 associated collagen IX reduction could not be reversed by TSP-5 or TSP-4. By investigating the effect of TGF- β 1 on the expression of TSP-5 and TSP-4, we showed that TGF- β 1 only induces the synthesis of TSP-5, but not of TSP-4 (Suppl. Fig. 2). Collagens that are not integrated into the matrix remain soluble and can be detected in the cell culture supernatant. Therefore, the amount of different collagen types was analysed by immunoblot assays (Fig. 3B). Soluble collagen IX could only be detected in supernatants of cells treated with TSP-5, either alone or in combination with TGF- β 1. This result showed that TSP-5 contributes to the synthesis of collagen IX, even though its deposition into the matrix seems not to be significantly increased. Elevated amounts of soluble collagen I and XII could be observed only in TGF- β 1 stimulated cells; this upregulation parallels the increase of the respective proteins in the matrix. Interestingly, the amount of the same proteins in the supernatant could be reduced by the addition of TSP-5 or TSP-4. The signals for collagen X and collagen II in the supernatant were either very weak or absent altogether, indicating that these proteins are quantitatively incorporated into the cell-associated matrix. Total levels of collagens (matrix-associated and soluble), detected by immunofluorescence staining and immunoblots (Fig. 3C), showed that TSP-5 and TSP-4 stimulation increased the total level of collagen II, IX and XII, and decreased that of collagen X. TGF- β 1 increased the expression of collagen I, II and XII while reducing that of collagen IX. These effects on collagen I and XII were weakened by the addition of TSP-5 and TSP-4, while the increase of collagen II expression was further enhanced.



C

	TGF- β 1	TSP-5	TSP-4	TSP-5 + TGF- β 1	TSP-4 + TGF- β 1
Col I	↑↑	-	-	↑	↑
Col II	↑↑	↑	↑	↑↑↑	↑↑↑
Col IX	↓↓	↑	↑	↓	↓↓
Col X	-	↓	↓	↓	↓
Col XII	↑↑↑	↑	↑	↑↑	↑↑

Figure 3. *The effect of TSP-5 and TSP-4 on collagen and proteoglycan production and deposition.* Chondrocytes were stimulated with TSP-5 (10 µg/mL), TSP-4 (10 µg/mL) alone or in combination with TGF-β1 (0.5 ng/mL) for seven days. (A) Immunofluorescence staining of collagen (Col) I, II, IX, X and XII as well as Safranin-O staining of proteoglycans at day 10. (B) Immunoblot assays of chondrocyte supernatants at day 10. Roti®blue staining of proteins was used as a loading control (LC). (C) Table summarizing the effect of TSP-5, TSP-4 and TGF-β1 on the total amount of different collagen types (matrix-associated and soluble). The amount of matrix-associated collagens was visually scored from IF staining and combined with band intensities for soluble proteins derived from immunoblots. The number of arrows indicates a strong, moderate or mild effect compared to the control. The direction of the arrows indicates an increase (↑) or decrease (↓) compared to control. No changes are indicated by a minus. The number of arrows indicates strong (three arrows), moderate (two arrows) or mild (one arrow) changes compared to control. (Immunofluorescence staining, $n = 3$; immunoblot $n \geq 2$ per group); unstimulated cells were used as a control; scale bar (collagens) = 100 µm; and (proteoglycans) = 200 µm.

TSP-5 and TSP-4 do not affect proliferation but suppress dedifferentiation of chondrocytes

Reactivated chondrocytes in OA proliferate and dedifferentiate to collagen I producing cells. TSP-5 and TSP-4 affect collagen II matrix deposition and suppress TGF-β1-induced collagen I expression. The primary aim of the following experiments was not to study the dedifferentiation process itself, but to determine whether TSP-5 and TSP-4 could directly or indirectly modulate this process. Chondrocytes were stained as described in Section 2.3 and studied in more detail by evaluating their proliferation and number of total, as well as the ratio, of collagen I and collagen II positive cells. These experiments were repeated three times with different batches of freshly isolated chondrocytes.

TGF-β1 served as an inducer of chondrocyte proliferation. TSP-5 ($p = 0.99$) and TSP-4 ($p = 0.86$) alone had no effect on cell proliferation, and cell numbers were comparable to the untreated control (Fig. 4A, B) after 10 days. TGF-β1 ($p = 0.003$) alone and in combination with TSP-5 ($p = 0.002$) or TSP-4 ($p < 0.001$) resulted in an increased cell number. The dual treatments with TGF-β1 also increased the cell numbers compared to the equivalent single treatments with TSP-5 ($p = 0.013$) and TSP-4 ($p = 0.023$). These data show that TSP-5 and TSP-4 do not affect cell proliferation, either directly or by modulating the TGF-β1 induced proliferation.

The percentage of cells expressing collagen I and collagen II, respectively, was investigated by immunofluorescence double staining (Fig. 4C). Collagen I and collagen II expressing cells were counted and the percentage of collagen expressing cells was calculated (Fig. 4D). The percentage of collagen I and collagen II expressing cells was comparable between the control ($p = 0.21$) and TGF-β1 ($p = 0.22$) treated cultures. For all other treatments, stimulation with TSP-5 ($p = 0.003$), TSP-4 ($p = 0.03$) or in combination with TGF-β1 (TSP-5: $p = 0.05$; TSP-4: $p = 0.02$) resulted in a shift towards collagen II producing cells. The percentage of unstained cells was comparable between groups, ranging from 3 to 11 %. Furthermore, the number of collagen I producing cells was lower

in cultures treated with TSP-5 ($p = 0.025$) and the co-stimulations of TGF- β 1 with TSP-5 ($p = 0.007$) and TSP-4 ($p = 0.004$). The stimulation with TSP-4 ($p = 0.056$) showed a tendency of a reduced number of collagen I positive cells. The opposite was observed for collagen II producing cells, whose numbers increased in cultures treated with TSP-5 ($p = 0.033$), TSP-4 ($p = 0.042$) and in the combination of TGF- β 1 with TSP-5 ($p = 0.034$) and TSP-4 ($p = 0.010$).

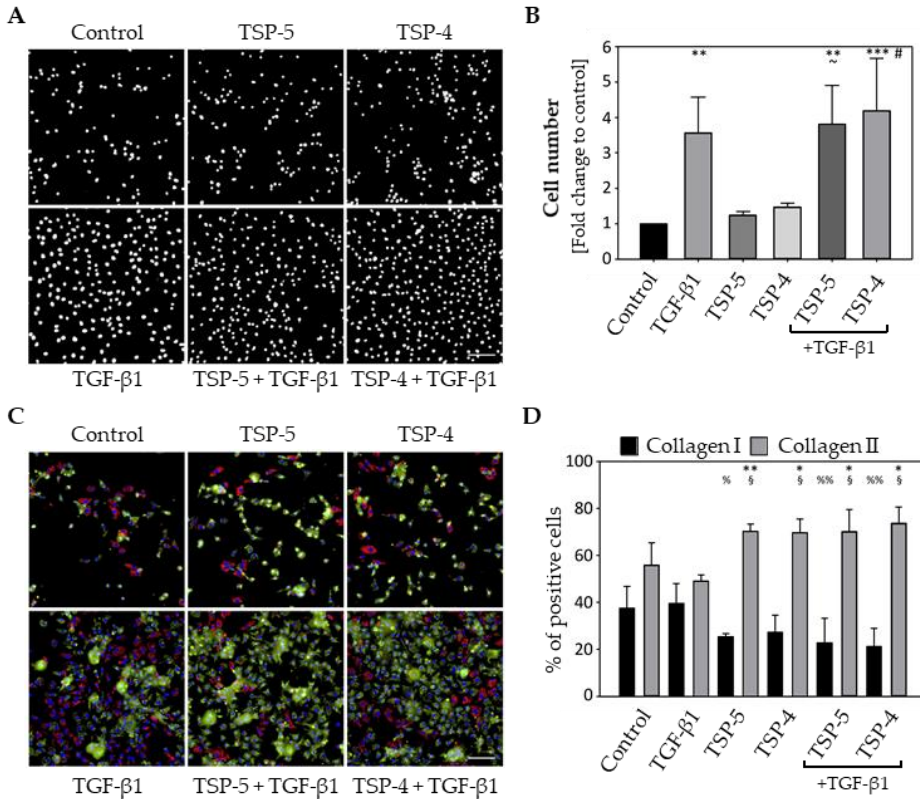


Figure 4. Effect of TSP-5 and TSP-4 on chondrocyte proliferation and dedifferentiation. Chondrocytes were stimulated with TSP-5 (10 μ g/mL) or TSP-4 (10 μ g/mL) for seven days. (A) Nuclei were DAPI stained at day 10. (B) The fold changes of the counted nuclei are represented and each bar shows the mean + SD. The significant differences between the control and all other conditions were calculated. Differences between TSP-5, TGF- β 1 and TSP-5 + TGF- β 1 as well as TSP-4, TGF- β 1 and TSP-4 + TGF- β 1 were calculated. Differences to the control are indicated by an asterisk *, to TSP-5 by waves ~ and to TSP-4 by rhombus #, as well as significance indicated by $p \leq 0.05$ #~; $p \leq 0.01$ **; $p \leq 0.001$ ***. (C) Immunofluorescence staining of collagen I (red), collagen II (green) and nuclei (blue) at day 10. (D) Percentages of chondrocytes expressing collagen I and II are represented and each bar shows the mean + SD. The significant difference between collagen I and collagen II positive cells was calculated and significance indicated as $p \leq 0.05$ *; $p \leq 0.01$ **. Differences of collagen I and collagen II positive cells to the control were calculated and significance indicated as $p \leq 0.05$ % or §; $p \leq 0.01$ %% or §§, respectively. TGF- β 1 (0.5 ng/mL) served as an inducer of proliferation and collagen synthesis and unstimulated cells as a control. ($n = 3$); scale bar = 100 μ m.

These results show that TSP-5 and TSP-4 are able to suppress chondrocyte dedifferentiation in monolayer culture.

TSP-5 and TSP-4 induce the phosphorylation of ERK1/2 while not affecting the SMAD pathways

TSP-5 and TSP-4 participate in cartilage maintenance and repair by stabilizing the chondrocyte phenotype and inducing the synthesis of important ECM components. To unravel potential signalling pathways involved, the phosphorylation of ERK and SMAD proteins was investigated after stimulation with TSP-5 and TSP-4, respectively.

Chondrocytes were treated with 10 µg/mL TSP-5 or TSP-4 for 30 min and phosphorylated ERK1/2, SMAD2 and SMAD1/5/9 detected by immunoblot analyses. Both TSP-5 and TSP-4 induced the phosphorylation of ERK1/2 (Fig. 5A). Even though the treatment with TSP-5 and TSP-4 seemed to slightly increase the level of total ERK1/2, the increase in phosphorylation was much more pronounced. None of the proteins affected the phosphorylation of SMAD2 or SMAD1/5/9 (Fig. 5B).

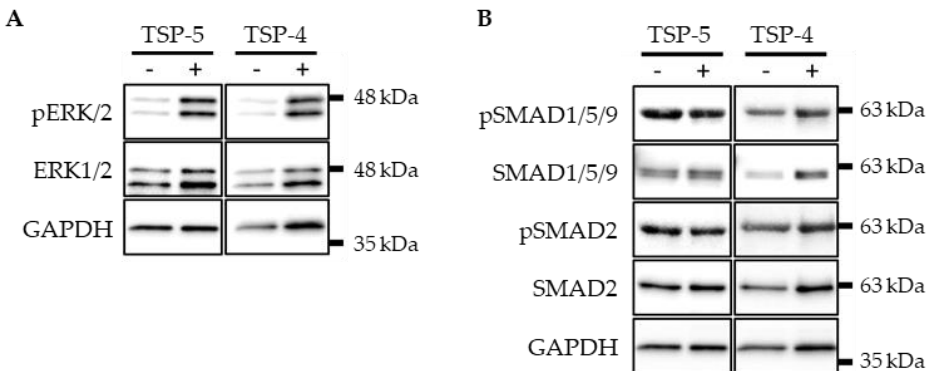


Figure 5. ERK and SMAD phosphorylation in chondrocytes after stimulation with TSP-5 and TSP-4. Chondrocytes were stimulated with 10 µg/mL TSP-5 or TSP-4. Cell extracts were harvested and SMAD as well as ERK proteins detected by immunoblot. (A) Representative immunoblots showing the detection of pERK1/2 and total ERK1/2. (B) Representative immunoblots showing the detection of pSMAD1/5/9, SMAD1/5/9, pSMAD2 and SMAD2. GAPDH was used as a loading control; ($n = 4$).

TSP-5 and TSP-4 can modulate TGF-β1 induced ERK1/2 signalling

The effect of TGF-β1 on matrix formation was modulated by the simultaneous addition of TSP-5 and TSP-4, respectively. Therefore, the capacity of TSP-5 and TSP-4 to modulate TGF-β1-induced ERK signalling was investigated. The phosphorylation of ERK1/2 was investigated 30 min after stimulation with 10 µg/mL TSP-5 or TSP-4 and different concentrations of TGF-β1 (0.1; 0.25; 0.5; 1 and 10 ng/mL). Maximal ERK1/2 phosphorylation was detected after treatment with 0.25 ng/mL TGF-β1 (Fig. 6A). The additional stimulation with TSP-4 shifted this phosphorylation maximum to a TGF-β1

concentration of 0.5 ng/mL (Fig. 6C). The most pronounced ERK1/2 phosphorylation with simultaneous TSP-5 treatment was found at 0.1 ng/mL TGF- β 1, and continuously decreased with increasing TGF- β 1 concentrations (Fig. 6B). The phosphorylation maximum at 0.1 ng/mL TGF- β 1 was weaker than that of TSP-5 alone. These results show that TSP-4 attenuates TGF- β 1 induced ERK1/2 signalling, in contrast to TSP-5, whose capacity to induce ERK1/2 phosphorylation is suppressed by TGF- β 1.

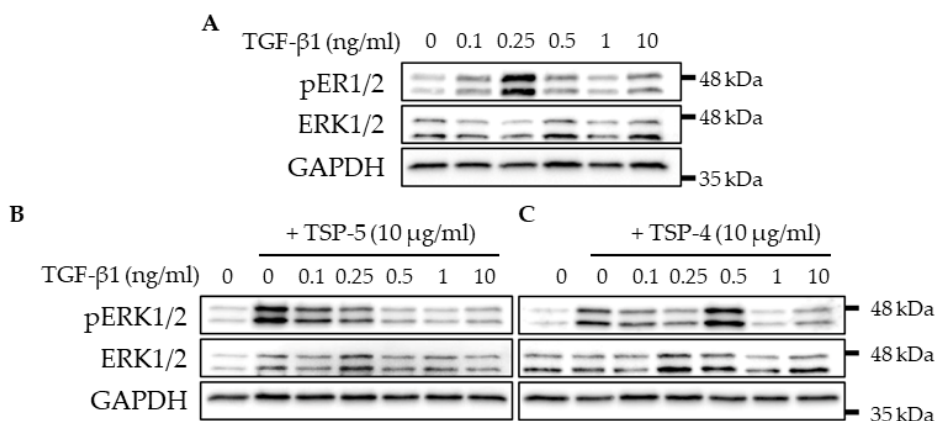


Figure 6. Modulation of TGF- β 1-induced ERK signalling in chondrocytes. Chondrocytes were stimulated with indicated concentrations of TGF- β 1 alone or in combination with TSP-5 (10 μ g/mL) or TSP-4 (10 μ g/mL) before ERK1/2 proteins were detected by immunoblot. (A) Representative immunoblots show the concentration-dependent TGF- β 1 induced phosphorylation of ERK1/2 (pERK1/2) and total ERK1/2. Representative immunoblots show the influence of TSP-5 (B) and TSP-4 (C) on the concentration-dependent TGF- β 1 induction of ERK1/2 phosphorylation. GAPDH was used as a loading control; ($n = 4$).

DISCUSSION

In the present study, we show that the presence and distribution of TSP-5 and TSP-4 are distinguishable, especially in healthy and OA cartilage, although both proteins are re-expressed during OA progression. While TSP-5 is ubiquitously expressed in healthy cartilage, TSP-4 is hardly detectable. In OA, TSP-5 was found to be degraded in early and re-expressed in late-stage OA [120]. In contrast, the TSP-4 level dramatically increased in an early OA stage, and was shown to be further elevated with OA severity [65]. This differential expression pattern indicates additive roles of extracellular TSP-5 and TSP-4 in articular cartilage that may depend on their zonal distribution.

In the past, it was shown that cells in the injured articular cartilage have the potential to migrate to the damage site, leading to a repopulation of these areas [152, 153]. TSP-5 re-expression was mainly found in the upper cartilage zones, where the structural damage was most severe, while TSP-4 was predominantly expressed in the middle and deep zone, below the layer where TSP-5 re-expression was detected. Therefore, we

hypothesised that the re-expression of TSP-5 might be an attempt to attract chondrocytes from the surrounding area to repopulate the defect site, and that interaction with TSP-5 and TSP-4 might induce mechanisms of ECM maintenance, protection and cartilage repair. Indeed, TSP-5, but not TSP-4, was demonstrated to attract chondrocytes and contribute to their anchorage [96, 97]. These data suggest that TSP-5 and TSP-4 interact with differential receptors on the chondrocyte surface and are distinguishable in their functional role. Although the presence of TSP-4 is insignificant for chondrocyte migration, its rapid upregulation in injury is associated with the regulation of matrix protein synthesis and ECM remodelling [78, 154, 155]; both processes are highly relevant in OA. Also, induction of ECM protein synthesis seems highly likely and beneficial for TSP-5 after mediating chondrocyte migration and attachment.

The effects of TSP-5-TGF- β 1 and TSP-4-TGF- β 1 complexes were also investigated, due to the important role of TGF- β 1 in healthy cartilage, its high abundance in OA and its susceptibility to modulation by TSP-5 after binding [75, 126, 137]. In our study, we showed, for the first time, that not only TSP-5, but also TSP-4 directly interacts with TGF- β 1 (Appendix A), although TGF- β 1 only induced the expression of TSP-5 and not TSP-4 (Appendix B). These findings, together with the low expression of TSP-4 under healthy conditions, suggest a minor role in the maintenance of healthy cartilage. In addition to TGF- β 1, TSP-5 synthesis can be increased by mechanical loading, as shown in cartilage explants [156, 157]. In the presence of cartilage lesions, the loading environment changes; this may lead to an altered response of chondrocytes, which deform less axially but are exposed to increased tensile strength compared to cells in an intact matrix [158, 159]. Therefore, an altered loading environment in articular cartilage might also affect the expression of TSP-4 and further increase the levels of TSP-5. At the cellular level, we could show that both TSP-5 and TSP-4 supported the synthesis and matrix deposition of collagen II, IX, XII and proteoglycans, while inhibiting those of collagen I and collagen X. The modulating effect of TSP-5 has also been described before, showing that the addition of TSP-5 or aggrecan suppresses the expression of hypertrophic genes in periosteal chondrocytes [160]. The increased expression of the main ECM components, collagen II and proteoglycans, as well as their potential to enhance TGF- β 1 induced collagen II and proteoglycan synthesis, strongly suggest an involvement of both proteins in cartilage repair by restoring an ECM composition that maintains original tensile strength and elasticity [29]. Collagen fibrils in articular cartilage consist mainly of collagen II [109], and their zonal specific biomechanical, as well as structural properties are achieved by its interaction with different ECM components such as collagen IX [109-111], resulting in a heterogeneity of collagen II cartilage fibrils [111-113]. Therefore, the effect of TSP-5 and TSP-4 on the expression of minor collagens, like collagen IX and XII, is also of great interest. While TSP-5 and TSP-4 can both bind fibrillar collagens [77, 143, 144], they behave differently in terms of their capacity to bind minor collagens. In that manner, TSP-5 was shown to interact with collagen IX [161, 162] and collagen XII [145], while TSP-4 cannot directly bind to collagen IX [163], and the binding to collagen XII has not yet been investigated. Collagen XII,

TSP-4 and TSP-5 are all localised in the superficial zone in healthy cartilage, which possesses properties, such as high tensile strength to withstand the immense forces of articulation [110, 113]. TSP-5 and TSP-4 induce the synthesis of collagen XII, and may therefore increase the tensile properties in the superficial zone and prepare the underlying tissue for increased loading. Especially in OA, affecting all cartilage layers, increased collagen XII levels may enhance the integrity of the ECM by strengthening collagen II fibrils. However, in combination with TGF- β 1, this increase seems reversed, maybe due to a negative feedback loop. TGF- β 1 stimulation resulted in high levels of immobilised and soluble collagen XII. These levels were much higher than those seen in TSP-5 and TSP-4 stimulated cells. Downregulation of collagen XII might be a consequence of the binding of TGF- β 1 to TSP-5 and TSP-4, blocking relevant binding sites, e.g., on growth factor receptors, as reported for a TSP-5-BMP-2 complex [164]. Conspicuously, collagen XII amounts were low in conditions where collagen IX was enriched. Also, collagen IX-KO mice showed an increased amount of collagen XII distributed in areas where collagen XII is usually not expressed [163]. Both FACIT collagens share sequence homologies and are associated with collagen organization [165], indicating a compensatory role of collagen XII in the absence of collagen IX. While collagen IX is rather associated with thinner collagen fibrils, lacking decorin [109, 111, 112], collagen XII is a known interaction partner, suggesting the involvement in the organization of collagen fibrils with larger diameter [166] and the tensile strength of articular cartilage. TSP-5 and TSP-4 stimulation had different effects on collagen IX expression, which was upregulated by both proteins. However, increased amounts of soluble collagen IX were only detected in the supernatant of TSP-5 stimulated cells, indicating an impaired matrix integration, maybe due to missing binding sites. Alternatively, the increased amounts of collagen IX could form complexes with TSP-5 in the supernatant. TSP-5 can directly bind to collagen IX with its C-terminal domain [161], suggesting a higher affinity of collagen IX to TSP-5 than to other binding partners in the matrix. Collagen IX is entirely integrated into the cell-associated matrix when stimulated with TSP-4. The reason for this might, therefore, be a lower expression capacity or the different binding properties to collagen IX in comparison to TSP-5 [163], excluding the possibility of a complex formation. Furthermore, the stimulation with TSP-5 and TSP-4 resulted in a partially reduced amount of collagen I, and led to a shift in direction collagen II positive cells. Several studies have reported that prolonged culture of chondrocytes in monolayer lead to dedifferentiation, characterised by an increase of collagen I expression and, at the same time, a loss of cartilage-specific markers, like collagen II, collagen IX and, in particular, TSP-5 [139, 167]. Therefore, it is tempting to speculate that stimulation with TSP-5 would counteract this dedifferentiation process. Indeed, our observations seem to confirm this hypothesis of chondrocyte phenotype stabilization after stimulation with TSP-5 and also TSP-4, though to a lesser extent. However, the loss of collagen IX, visible in TGF- β 1 stimulated cultures, could not be reversed by a simultaneous treatment with TSP-5 or TSP-4, demonstrating a dominant effect of TGF- β 1 on collagen IX expression and eventually also on the chondrocyte phenotype. A beneficial effect of TSP-5 in cartilage regeneration was demonstrated by

Wang C, *et al.* [168], showing that an overexpression of TSP-5 promoted chondrogenic differentiation of bone marrow derived stem cells, resulting in an increased formation of articular cartilage. Therefore, TSP-5 and TSP-4 might be promising factors for clinical applications, e.g., in maintaining the chondrocyte phenotype during *in vitro* expansion for autologous chondrocyte implantation (ACI) or incorporated into scaffolds, improving cell anchorage, protecting chondrocytes phenotype and inducing the production of proteins, essential for ECM properties.

After having demonstrated potential functional roles of TSP-5 and TSP-4 in articular cartilage, we aimed to gain more insight into the involved signalling pathways. Chondrocytes in mature cartilage facilitate the maintenance of the ECM in a low turnover state [121], which requires a delicate balance of catabolic and anabolic processes, which are regulated by, among other mechanisms, growth factors like TGF- β 1 [127, 128, 130]. The most relevant pathways to maintain cartilage homeostasis are the SMAD (small mothers against decapentaplegic homologs) and ERK1/2 signalling [130]. The counteracting SMAD2/3 and SMAD1/5/9 have different SMAD-binding motifs in the DNA sequence, resulting in the downstream transcription of differential genes [130, 169]. TGF- β 1 typically induce SMAD2/3 signalling, promoting matrix maintenance by inhibiting chondrocyte hypertrophy [133, 134] and inducing the expression of matrix proteins like aggrecan and collagen II [128], similar to ERK1/2 [128, 136]. SMAD1/5/9 phosphorylation results in the opposite, i.e., the expression of collagen X and MMP-13, causing chondrocyte hypertrophy and matrix degradation [135]. In OA, reactivated chondrocytes fail to regulate the metabolism properly, leading to an imbalance of anabolic and catabolic processes. For presently unknown reasons, chondrocytes favour SMAD1/5/9 and switch from an anabolic to a catabolic ERK1/2 signalling, in OA, leading to an unstable chondrocyte phenotype and ECM degradation [170-172]. The capacity of TSP-5 and TSP-4 to induce the ERK1/2 signalling pathway has already been demonstrated in other cell types, including primary hepatic stellate cells [173] and cardiomyocytes [174], respectively. Thereby, the ERK phosphorylation could be induced via the CD36 receptor [173], a receptor naturally expressed on healthy chondrocytes and even increasing in the pathology of OA [175]. In our study, we showed that TSP-5 and TSP-4 could also induce the phosphorylation of ERK1/2 in articular chondrocytes, while none of the proteins had an effect on SMAD1/5/9 or SMAD2/3 signalling. Interestingly, it has been shown earlier that other ECM components, like e.g., collagen II, were able to suppress hypertrophy in articular chondrocytes via the ERK1/2 signalling pathway [136]. The similar effects of TSP-5 and TSP-4 on protein synthesis and cell signalling indicate that the upregulation of proteoglycan and collagen II, as well as the downregulation of collagen X, might be mediated via ERK1/2 signalling, while migration is most likely performed by an ERK1/2-independent mechanism. Nonetheless, future studies are necessary to confirm the role of ERK1/2, as well as to identify the responsible receptors.

The present study was limited by the availability of healthy human articular cartilage samples. The distribution and expression of TSP-5 and TSP-4 was investigated in human

osteoarthritic and healthy cartilage samples. Thereby, we could show that the ECM composition had already been altered in an early OA stage (G1), i.e., at which obvious morphological defects were not yet detectable. Therefore, healthy pig cartilage was used to study the effects of TSP-5 and TSP-4 on chondrocytes *in vitro*. The effect of TSP-5 and TSP-4 on OA chondrocytes has to be investigated in more detail in future experiments.

In summary, these data demonstrate that chondrocytes in articular cartilage can activate mechanisms to protect and repair the ECM in injury and disease. TSP-5 and TSP-4, distributed in different cartilage zones, might contribute to the integrity and

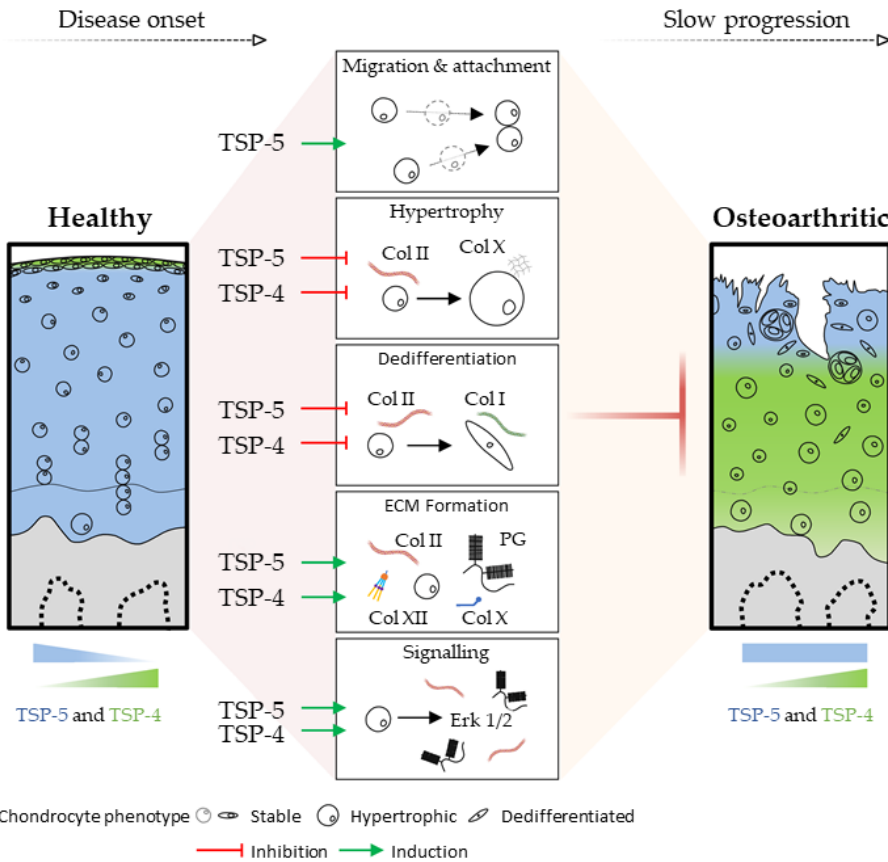


Figure 7. Functional role and distribution of TSP-5 and TSP-4 in articular cartilage. Schematic representation of TSP-5 and TSP-4 distribution, as well as protein levels in healthy and OA cartilage. Areas of TSP-5 and TSP-4 expression are indicated in blue and green, respectively. Their impact on cartilage and OA relevant processes is depicted in the middle. Green arrows indicate an induction, while red T arrows mean inhibition. PG = proteoglycan and Col = collagen.

repair of the ECM by promoting chondrocyte migration and ECM protein synthesis, as well as the stabilization of the chondrocyte phenotype (Fig. 7). Their involvement in direct and indirect cell signalling emphasizes the complexity of cell-matrix interactions and intracellular events in degenerative processes. Overall, OA leads to cartilage degradation, despite the protective effects of TSP-5 and TSP-4. However, these repair processes might help to slow the progression of OA, and thus pave the way for new treatment strategies.

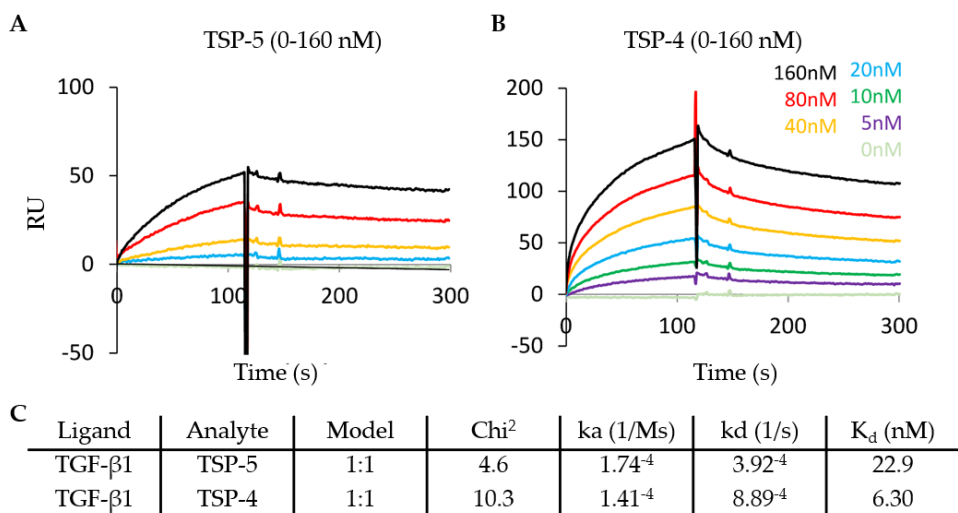
ACKNOWLEDGEMENTS

We would like to acknowledge the additional funding by the German Research Foundation through RU2722, project number 407168728.

SUPPLEMENTARY DATA

Both, TSP-5 and TSP-4 interact with TGF- β 1

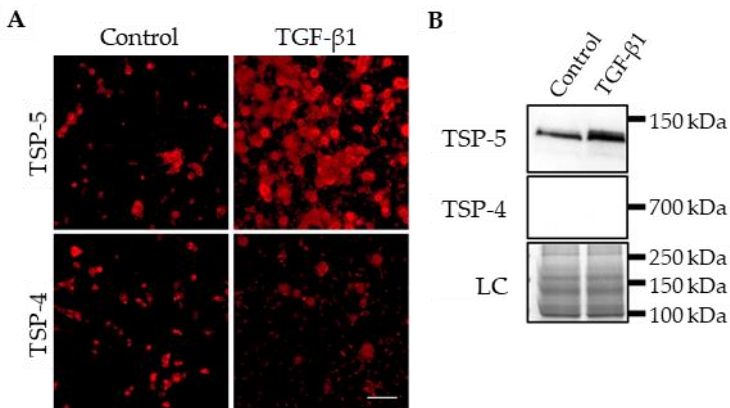
TSP-5 and TSP-4 had similar capacities to contribute to the ECM formation and could further modulate TGF- β 1 induced ERK1/2 signalling. A direct interaction of TSP-5 with TGF- β 1 has been described earlier. This interaction was shown to modulate the bioactivity of TGF- β 1 [75]. However, it was unclear if TSP-4 also directly interacts with TGF- β 1. Therefore, the interaction of both proteins with TGF- β 1 was characterised in surface plasmon resonance measurements using the Biacore system. The protein-protein interaction profiles show that both TSP-5 (Suppl. Fig. 1A) and TSP-4 (Suppl. Fig. 1B) interact with TGF- β 1. According to the calculated K_d value, the affinity of TSP-4 for TGF- β 1 seems to be slightly stronger than that of TSP-5. However, due to the low dissociation rate of TSP-5, a direct comparison is difficult (Suppl. Fig. 1C).



Supplementary Figure 1. Surface plasmon resonance measurements show a direct interaction of TSP-5 and TSP-4 with TGF- β 1. Protein-protein interaction profiles showing the binding of TSP-5 and TSP-4 to TGF- β 1. Surface plasmon resonance sensorgrams generated with the Biacore system are shown for TSP-5 (A) and TSP-4 (B). Resonance signals expressed as response units (RU), indicate the degree of binding TSP-5 and TSP-4 with TGF- β 1. TSP-5 and TSP-4 were used in concentrations ranging from 5 to 160 nM and injected to immobilised TGF- β 1 on a CM5 chip. (C) Summary of the data received from Biacore assays. The association rate (k_a), the dissociation rate (k_d), the dissociation constant (K_d) and the chi² are represented. A kinetic 1:1 model (Langmuir model) was used to calculate these parameters.

TGF- β 1 promotes the synthesis and deposition of TSP-5 but not TSP-4

Previously, it was shown that TSP-5 and TSP-4 could directly bind to TGF- β 1 and modulate its bioactivity. Further, Motaung SC, *et al.* [176] showed that TGF- β 1 could also induce the synthesis of TSP-5. To investigate if also TSP-4 is induced after TGF- β 1 treatment, primary chondrocytes were stimulated with 0.5 ng/mL TGF- β 1 for seven days in monolayer culture and the matrix deposition of TSP-5 and TSP-4 stained with specific antibodies at day 10. TGF- β 1 could induce the synthesis and matrix deposition of TSP-5 but not TSP-4 (Suppl. Fig. 2A). Soluble TSP-5 could be detected in the supernatant of controls and to a larger extend in the supernatant of TGF- β 1 stimulated cells, although in none of the cultures soluble TSP-4 could be detected (Suppl. Fig. 2B).



Supplementary Figure 2. *The effect of TGF- β 1 on TSP-5 and TSP-4 synthesis and deposition.* Chondrocytes were stimulated with TGF- β 1 (0.5 ng/mL) for seven days. TSP-5 and TSP-4 were detected with specific antibodies. (A) Immunofluorescence staining of TSP-5 and TSP-4 at day 10. (B) Immunoblot assays of chondrocyte supernatants at day 10. Roti[®]blue staining of proteins was used as a loading control (LC). ($n = 3$ per group); unstimulated cells were used as a control; scale bar = 100 μ m.

CHAPTER 4

TSP-5 derived peptides secreted by cartilage do not induce responses commonly observed during osteoarthritis

E. ANDRÉS SASTRE, F. ZAUCKE, J. WITTE-BOUMA, G.J.V.M. VAN OSCH, E. FARRELL

PUBLISHED AS: CARTILAGE OLIGOMERIC MATRIX PROTEIN DERIVED PEPTIDES
SECRETED BY CARTILAGE DO NOT INDUCE RESPONSES COMMONLY OBSERVED
DURING OSTEOARTHRITIS

CARTILAGE. 2020 SEP 29:1947603520961170
DOI: 10.1177/1947603520961170

ABSTRACT

The objective of this work was to evaluate if three peptides derived from the thrombospondin-5 (TSP-5/COMP), that wounded zones of cartilage secrete into synovial fluid, possess biological activity and might therefore be involved in the regulation of specific aspects of joint regeneration. To assess this, the three peptides were produced by chemical synthesis and then tested *in vitro* for known functions of the TSP-5 C-terminal domain from which they derive, and which are involved in osteoarthritis (OA): TGF- β signalling, vascular homeostasis and inflammation. However, none of the peptides affected the gene expression of TSP-5 in osteochondral progenitor cells ($p>0.05$). We observed no effects on the vascularisation potential of endothelial cells ($p>0.05$). In cultured synovium explants, no differences on the expression of catabolic enzymes or proinflammatory cytokines were found when peptides were added ($p>0.05$). For this, we concluded that the three peptides tested do not regulate TGF- β signalling, angiogenesis and vascular tube formation, or synovial inflammation *in vitro* and therefore most likely do not play a major role in the disease process.

INTRODUCTION

Osteoarthritis (OA) is the most prevalent chronic degenerative joint disease. It affects all tissues of the joint including the cartilage, synovium, vascular system and subchondral bone [16]. During OA, the cartilage matrix experiences degradative changes, resulting in the release of proteins and their fragments into the synovial fluid. OA can be diagnosed by detecting these degradation products in synovial fluid and serum, as biomarkers of the disease stage. For this reason, extensive research has focused on looking for more specific and reliable biomarkers associated with OA, in particular novel neopeptides produced during proteolysis [177]. However, little is known about possible biochemical functions that these fragments may still play during the onset of the disease and its progression. Bioactive fragments of extracellular matrix proteins, known as matrikines and matricryptins, are produced by limited proteolysis and can regulate a wide variety of cellular functions such as cell adhesion, migration, proliferation, angiogenesis or apoptosis [36]. Multiple matricellular proteins give rise to matricryptins. For example, the matricryptin PEX derives from the C-terminal domain of the matrix metalloproteinase-2 (MMP-2) and inhibits MMP-2 enzymatic activity in a negative feedback loop, blocking in turn angiogenesis [178]. Other matricryptins can promote catabolic and proinflammatory responses, such as the aggrecan 32-Mer fragment does in cartilage [179] or fibronectin fragments do on monocytes and cartilage [180, 181].

After joint injury and in early stages of osteoarthritis, increased amounts of thrombospondin-5 (TSP-5, also known as cartilage oligomeric matrix protein, COMP) fragments are released into synovial fluid [182]. TSP-5, which belongs to the family of thrombospondins, is currently being used as a biomarker of joint destruction [183], as its concentration correlates with both the severity of the disease as well as with the number of affected joints. An abstract published by Calamia *et al* in 2016 identified three specific peptides derived from TSP-5 that wounded zones of cartilage release into synovial fluid [184]. The three peptides reported originate from the multifunctional C-terminal domain of TSP-5, which plays diverse roles in cartilage homeostasis [146], inflammation [185] and TGF- β signalling [75, 164]. Previous research found that full-length TSP-5 was unable to modify the expression of proinflammatory markers in cartilage [90], unlike its binding partner matrilin-3 (MATN3) and its fragments [186]. However, we hypothesised that those TSP-5 fragments released by cartilage could have an OA-relevant biological function.

In this work, we asked if any of those three peptides is involved in responses associated to osteoarthritic joint disease; for example, by affecting vascularisation, by modulating downstream TGF- β signalling or by altering the expression of synovial catabolic enzymes.

MATERIALS AND METHODS

Peptides

Three peptides were produced by chemical synthesis [Peptide2.0, Chantilly, VA, USA], with the sequences ⁶³¹AEPGIQLKAV (Peptide 1) ⁶⁴²SSTGPGEQLRNA (Peptide 2) and ⁵⁵³VLNQGREIVQT (Peptide 3), reconstituted in DMSO and stored at -80°C. PBS was used to adjust the concentration and equivalent DMSO dilutions were used as controls on the experiments. To screen for the possible functions of the peptides, we selected a single concentration of 100 nM for most of the assays. We based our choice on the maximum amount of peptides that 10 µg/ml of the parent protein TSP-5 would release if TSP-5 was completely cleaved, as TSP-5 demonstrates bioactive effects *in vitro* at this concentration [187, 188] and TSP-5 is present in this concentration range in human serum [189].

Cell culture

HUVECs were purchased from Lonza, and expanded in endothelial growth media (EGM-2), containing 2% FBS, 5 ng/ml EGF, 10 ng/ml bFGF, 20 ng/ml IGF, 0.5 ng/ml VEGF165, 1 µg/ml L-ascorbic acid 2-phosphate, 22.5 µg/ml heparin and 0.2 µg/ml hydrocortisone [All from Promocell via Bioconnect, Huissen, the Netherlands]. Peptide testing was carried on endothelial basal media (EBM-2), which did not contain growth factors or supplements [Lonza, Geleen, the Netherlands].

Osteochondroprogenitor cells were isolated from leftover iliac crest bone chip material obtained from 4 paediatric patients undergoing alveolar bone graft surgery (following parental consent and approval of medical ethics committee of Erasmus MC: MEC-2014-16; age 9–13 years). Cells were expanded in α MEM [Gibco, Bleiswijk, the Netherlands] containing 10% FBS [Gibco, Bleiswijk, the Netherlands] and supplemented with 50 µg/mL gentamycin [Gibco, Bleiswijk, the Netherlands], 1.5 µg/mL amphotericin B [Gibco, Bleiswijk, the Netherlands], 25 µg/mL L-ascorbic acid 2-phosphate [Sigma, Zwijndrecht, the Netherlands] and 1 ng/mL fibroblast growth factor-2 [Bio-Rad via Bioconnect, Huissen, the Netherlands] in a humidified atmosphere at 37°C and 5% CO₂. Cells from passages 4-5 were used. For the following cell stimulation experiments, peptides were incorporated to α MEM supplemented with 50 µg/mL gentamycin, 1.5 µg/mL amphotericin B and 1.25 mg/ml BSA [Product code 1002759876, Sigma, Zwijndrecht, the Netherlands]. For those experiments involving cell stimulation with the peptides in combination with TGF- β , a dose of 0.1 ng/ml of TGF- β 3 [R&D, Abingdon, United Kingdom] was added to the stimulation media. This dose of TGF- β 3 was first determined experimentally and corresponded to the half-effective dose to upregulate the expression of the TSP-5 gene *COMP* in the osteochondroprogenitor cells (data not shown), which corresponded to a molar ratio of TGF- β 3:Peptide of 1:25.

Migration assay

Migration was assessed with modified Boyden chambers (polyethylene terephthalate cell culture inserts with 8 μm pore size) [Corning, Durham, NC, USA]. In brief, 5×10^4 HUVECs were seeded on the upper insert membrane in EBM-2 and allowed to migrate towards the lower chamber containing EBM-2 and the peptides for 10h at 37 °C. In order to ensure the ability of the cells to migrate, EGM-2 was loaded in parallel as a positive control and the basal medium EBM-2 was used as a negative control. Then, the cells on the membrane were fixed with 4% formalin and cells on the upper surface were removed with a cotton swab, followed by 5 min DAPI staining. Migrated cells on each membrane were imaged with a fluorescence microscope [Zeiss Axiovert 200M] in five random fields of 1.51 mm^2 each, automatically counted using ImageJ software, and the average counts per membrane expressed as cells/ mm^2 .

Proliferation assay

The number of HUVECs that proliferated after 24h was investigated with the EdU cell proliferation kit [Bioss, Neuried, Germany]. First, 7500 cells/ cm^2 were seeded in EGM-2 and allowed to attach overnight. Then, cell cycles were synchronised by substituting the media with EBM-2 supplemented with 1.25 mg/ml BSA for 8 hours. Next, cells were stimulated with the peptides in combination with EdU 10 μM in EBM-2. EBM-2 alone was used as a negative control for proliferation, and EGM-2 was used as a positive control. After 24h, cells were fixed with 4% formalin and stained according to the manufacturer's kit protocol. Finally, positive cells were imaged with a fluorescence microscope [Zeiss Axiovert 200M] in five random fields of 1.51 mm^2 each. Total nuclei (DAPI) and EdU+ nuclei were automatically counted using ImageJ software. Percentage of proliferated cells per field was calculated as the number of EdU+ nuclei divided by total nuclei. Then, total proliferation per membrane was calculated as the average proliferation of its five fields.

Tube formation assay

50 μl of Geltrex™ LDEV-Free Reduced Growth Factor Basement Membrane Matrix [Fischer Scientific, Landsmeer, the Netherlands] were allowed to polymerise for 30 min at 37 °C on a 96-well plate. Then, HUVECs were resuspended in EBM-2 containing the peptides seeded at a density of 2×10^4 cells per cm^2 and incubated at 37 °C. EGM-2 and EBM-2 were used as positive and negative controls, respectively. After 24 hours, 5 random images of the tubes formed (1.9 mm^2 each) were taken using an inverted microscope. Automatic measurements of the tubes were performed with the Angiogenesis Analyzer plugin for ImageJ to determine the average number of nodes per condition.

Viability assay

Osteochondroprogenitor cellular viability in presence of the peptides was assessed with the colorimetric MTT assay. This assay relies on the metabolic reduction of the tetrazolium dye MTT to formazan, which has a purple colour. 24,000 cells/cm² from one single donor were seeded in expansion media. Next day, media was replaced by α MEM supplemented with 50 μ g/mL gentamycin, 1.5 μ g/mL amphotericin B, 1.25 mg/ml BSA and with different peptides concentrations up to 1 μ M for 24 hours. MTT was added into the media at a final concentration of 0.9 mM during the 3 last hours. After a PBS wash, precipitated colorant was extracted with absolute ethanol. Absorbance was measured on a spectrophotometer [VersaMax, Molecular Devices], as A₅₇₀-A₆₇₀. Finally, viability was calculated as absorbance relative to the untreated condition.

Synovial explant culture

Synovial explants were obtained from leftover material from four patients undergoing total knee replacement surgery, both male and female and ranging from 67-77 years old, at the hospitals of Erasmus MC, Rotterdam; and Reinier de Graaf Gasthuis, Delft (The Netherlands). The patients gave implicit consent as stated by guidelines of the Federation of Biomedical Scientific Societies (www.federa.org) and with approval of the local ethical committee at Erasmus MC (MEC-2004-322). Explants were cut in pieces of similar size and washed with saline solution (0.90% w/v of NaCl). Then, they were cultured for 24h in low glucose DMEM containing 1:100 v/v insulin-transferrin-selenium [ITS+; Corning, Amsterdam, the Netherlands], 50 μ g/mL gentamycin and 1.5 μ g/mL amphotericin B. Peptides were supplemented twice during the following 48 hours. Explants were snap frozen and stored at -80°C for further analyses.

Gene expression

Frozen samples were microdismembrated and total RNA was isolated using the RNeasy® Plus Micro kit [Qiagen–Benelux, Venlo the Netherlands]. 300 ng RNA were reverse transcribed to cDNA using the RevertAid™ First Strand cDNA Synthesis Kit [Thermo Scientific, Bleiswijk, the Netherlands]. mRNA expression was measured for *COMP*, *B2M*, *TNFA*, *IL6* and *UBC* with qPCR™ Mastermix Plus for SYBR® Green I [Eurogentec, Nederland B.V., Maastricht, The Netherlands]. For *ADAMTS4*, *ADAMTS5*, *GAPDH*, *MMP1*, *MMP3* and *MMP13*, TaqMan Master Mix [ABI, Branchburg, NJ, USA] was used. Primer sequences are listed on Table 1.

Data was analysed using the Livak method ($2^{-\Delta\Delta CT}$). For the set of experiments of osteochondroprogenitor cells, the reference gene used was *GAPDH*. For the set of experiments using synovial explants, normalisation was based on the BestKeeper Index

(BKI) using the genes *GAPDH*, *UBC* and *B2M*. Gene expression was expressed relative to the untreated condition.

SYBR probes	
<i>COMP</i>	fw: 5'-CCCAATGAAAAGGACAACCTGC-3'; rv: 5'-GTCCTTTTGGTCGTCGTTCTTC-3'
<i>B2M</i>	fw: 5'-TGCTCGCGCTACTCTCTTT-3'; rv: 5'-TCTGCTGGATGACGTGAGTAAAC-3'
<i>TNFA</i>	fw: 5'-GCCGCATCGCCGTCTCCTAC-3'; rv: 5'-GCCGCATCGCCGTCTCCTAC-3'
<i>IL6</i>	fw: 5'-TCGAGCCCACCGGAACGAA-3'; rv: GCAGGGAGGGCAGCAGGCAA-3'
<i>UBC</i>	fw: 5'-ATTGGGTGCGGTCTTG-3'; rv: 5'-TGCCTGACATTCTCGATGGT-3'
TaqMan probes	
<i>ADAMTS4</i>	fw: 5'-CAAGTCCCATGTGCAACGT-3'; rv: 5'-CATCTGCCACCACAGTGTCT-3'; probe: FAM-5'-CCGAAGAGCCAAGCGCTTGGCTTC-3'-TAMRA
<i>ADAMTS5</i>	fw: 5'-TGTCCTGCCAGCGGATGT-3'; rv: 5'-ACGGAATTACTGTACGGCCTACA-3'; probe: FAM-5'-TTCTCAAAGGTGACCGATGGCACTG-3'-TAMRA
<i>GAPDH</i>	fw: 5'-ATGGGGAAGGTGAAGTGC-3'; rv: 5'-TAAAAGCAGCCCTGGTGACC-3'; probe: FAM-5'-CGCCCAATACGACCAAATCCGTTGAC-3'-TAMRA
<i>MMP1</i>	fw: 5'-CTCAATTTCACTTCTGTTTTCTG-3'; rv: 5'-CATCTCTGTCGGCAAATTCGT-3'; probe: FAM-5'-CACAAC TGCCAAATGGGCTTGAAGC-3'-TAMRA
<i>MMP3</i>	fw: 5'-TTTTGGCCATCTCTTCCTCA-3'; rv: 5'-TGTGGATGCCTCTTGGGTATC-3'; probe: FAM-5'-AACTCATATGCGGCATCCACGCC-3'-TAMRA
<i>MMP13</i>	fw: 5'-AAGGAGCATGGCGACTTCT-3'; rv: 5'-TGGCCCAGGAGGAAAAGC-3'; probe: FAM-5'-CCCTCTGGCCTGCGGCTCA-3'-TAMRA

Table 1. Primer list used for cDNA quantification.

Statistical analysis

Differences between treatments were assessed with one-way ANOVA, 2-sided with Dunnett's post hoc test. For those experiments involving multiple donor samples, data was analysed using the linear mix model with Bonferroni correction. In both cases, normality of the data was assumed. Statistics were performed with IBM SPSS Statistics (version 25.0.0.1 for Windows, IBM Corp., Armonk, N.Y., USA), and graphs were created using GraphPad Prism (version 6.1 for Windows, GraphPad Software, La Jolla California USA).

RESULTS

None of the peptides were able to modify the gene expression of *COMP*

TGF- β can trigger the expression of *COMP* [190], and the resulting TSP-5 protein can further enhance TGF- β activity in a positive feedback loop. Because the three peptides derive from the TSP-5 C-terminal domain, which is responsible for the binding to TGF- β [75], we hypothesised that the peptides could have a modulatory activity over this TSP-5-TGF- β -*COMP* feedback loop. Therefore, we investigated whether any of the peptides could modulate the expression of their parental gene *COMP*. For this, we used bone marrow osteochondroprogenitor stem cells, which have a moderate ability to differentiate and to repair damaged articular cartilage by depositing fibrocartilage [191]. After confirming that the peptides did not affect cellular viability (Fig. 1A), we evaluated whether any of the peptides could upregulate the expression of *COMP* at the mRNA level. Consequently, cells were stimulated with the peptides at 100 nM and *COMP* expression was assessed by qPCR. However, no significant differences were found in

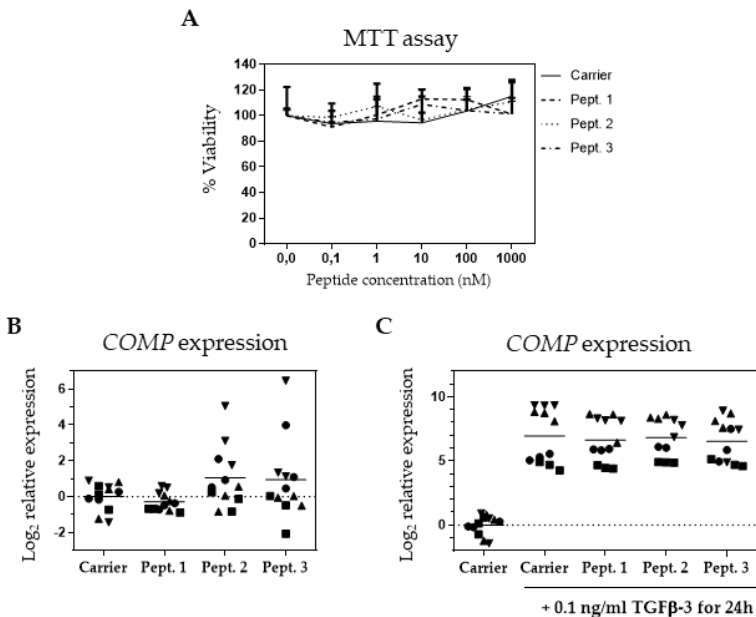


Figure 1. Effects of the three peptides on bone marrow osteochondroprogenitor cell viability and *COMP* expression. (A) Viability assay. Cells were incubated for 24 h in combination with the peptides, then viability was quantified by the MTT assay where the signal was normalised to the untreated cells (n=1 donor by quadruplicate) and each peptide concentration was compared to the equivalent carrier concentration; bars represent SD. (B, C) Gene expression of *COMP* (n=4 donors by triplicate) was measured by qPCR after 24 hours upon incubation with the peptides at 100 nM (B) or 100 nM peptides plus 0.1 ng/ml TGF- β 3 (C). In both cases, all treated conditions were normalised to *GAPDH*, and relative to the DMSO only condition; each donor is represented by a different symbol. Grand mean is represented.

COMP expression levels (Fig. 1B). Then, we asked if any of the peptides could modulate TSP-5 production when TGF- β signalling was triggered. Accordingly, *COMP* expression was measured after 24 hours peptide stimulation in presence of TGF- β 3. Despite *COMP* was being upregulated by TGF- β in a donor dependent manner, no differences in *COMP* expression were found in the presence or absence of the peptides.

None of the peptides affected vascular tube formation *in vitro*

During osteoarthritis, increased vascular remodelling is seen in the synovium [192] and in the cartilage, which is normally avascular in healthy adult joints [193]. In order to study if the peptides would be capable of modulating vascularisation, we performed different *in vitro* assays. First, we allowed endothelial cells (HUVECs) to migrate in a modified Boyden chamber assay with peptides, ranging in concentrations from 0.5 to 500

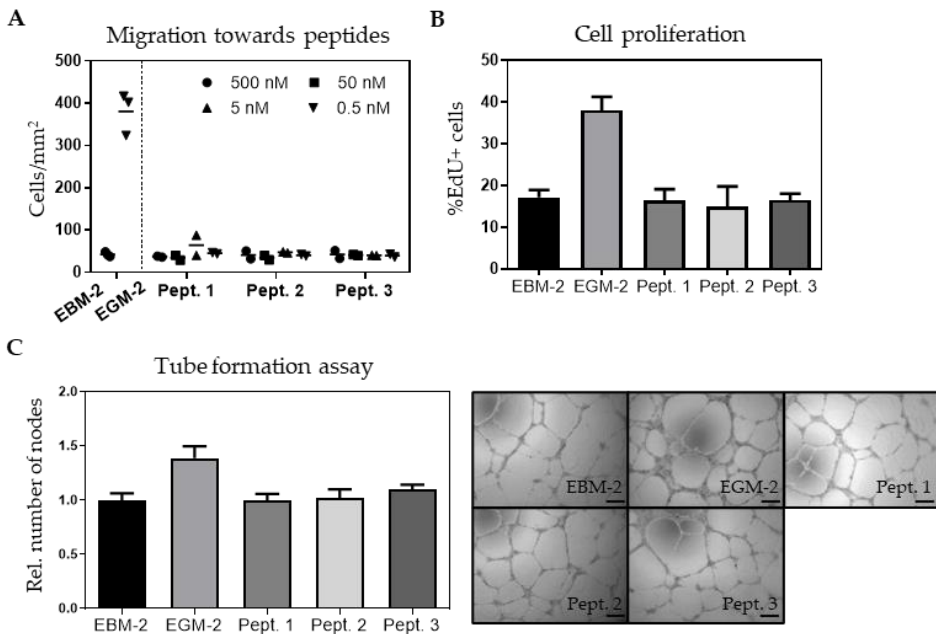


Figure 2. Assays to test the peptides influence on vascularisation potential by endothelial cells (HUVECs). (A) Migration assay. Cells were seeded on a microporous membrane and allowed to migrate towards a compartment with different concentrations of each of the peptides ($n=2$ /concentration). (B) Proliferation assay. Cells were incubated for 8 h in basal medium followed by a 24 h exposure to 100 nM peptides in basal medium ($n=3$ replicates). (C) Cells were seeded on Geltrex™ in combination with the peptides at 100 nM and allowed to form a tubular network for 24 h. Then, nodes formed were quantified ($n=3$ replicates). Scale bar = 200 μ m. In all experiments, both basal and growth media contained the same concentration of vehicle (DMSO), and growth media was used as a positive control. EBM-2: Endothelial Basal Media 2. EGM-2: Endothelial Growth Media 2. – (EBM-2), + (EGM-2). The bars represent the mean (A) and the mean \pm SD (B, C). All samples were compared to the untreated condition.

nM, and we observed that none of the peptides were chemokinetic for endothelial cells at the concentrations tested (Fig. 2A). Next, we asked if the peptides could stimulate endothelial cell proliferation, as it is one of the common responses to angiogenic stimuli. For this purpose, cells were stimulated for 24 hours in a media containing the nucleoside analogue EdU, which labelled the replicating cells. The peptides did not significantly increase the number of proliferating cells (Fig. 2B). Last, we performed a tube formation assay with HUVEC on a basement membrane coated plate stimulated with the peptides for 24 hours. In this case, peptides did not influence network formation (Fig. 2C).

None of the peptides altered gene expression of synovial catabolic enzymes or inflammatory mediators

As the peptides were found in synovial fluid, we asked if they could trigger an inflammatory response on the synovium. For this, synovial explants from patients

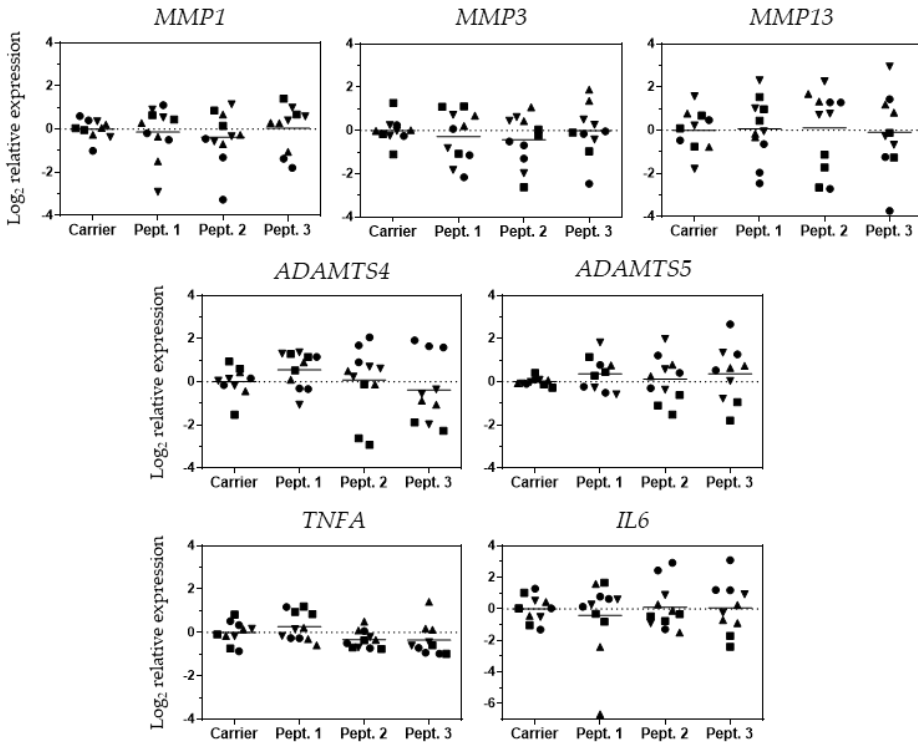


Figure 3. Effect of the peptides on gene expression of proteolytic enzymes in synovium. Synovial explants were treated for 48h with the peptides and gene expression of different proteolytic enzymes was measured by qPCR. Each gene expression measurement was first normalised to the BestKeeper Index (BKI). Each condition is relative to the carrier control, to which is compared; each donor is represented by a different symbol (n=4 donors in triplicate, one of them in duplicate) and grand mean is represented.

undergoing total knee replacement surgery were cultured with 100 nM of the peptides or with the carrier (DMSO) for 48 h, and gene expression of *MMP1*, *3* and *13*, and *ADAMTS4* and *5*, –proteases known to degrade extracellular matrix in osteoarthritis– was analysed. Gene expression of none of the proteases analysed was affected by the presence of the peptides. *IL6* and *TNFA*, which are potent regulators of catabolic processes in chondrocytes and synovial cells, were also unaffected by exposure to the peptides.

DISCUSSION

Our work has focused on the search for novel bioactive fragments of TSP-5, one of the main extracellular matrix proteins of the cartilage which is often used as a biomarker for OA. For this, we tested if any of the three TSP-5-derived peptides reported by Calamia *et al* in 2016 [184] could affect specific aspects related to osteoarthritis. We concluded that those three peptides are unlikely to be involved in the expression of *COMP*, vascularisation, or synovial expression of ECM proteases at the concentrations and time frames studied.

Identification of novel matrikines and matricryptins is challenging, as their functions can be similar, opposite or completely different to their parent protein. During OA, increased amounts of TSP-5 are released [194] and increased concentrations of monomeric forms of TSP-5 as well as smaller fragments appear as a result of proteolytic activity [195]. In a recent study, we showed that in the absence of its oligomerisation domain, which is required to form pentameric structures, TSP-5's angiogenic-related functions disappear [196]. Matrikines and matricryptins however, have been shown to have different biological functions to the protein from which they are derived, leading us to assess the effects of these identified peptides on processes crucial for the onset and development of OA.

The three peptides derive from TSP-5's C-terminal domain: ⁶³¹AEPGIQLKAV (Peptide 1), ⁶⁴²SSTGPGEQLRNA (Peptide 2) and ⁵⁵³VLNQGREIVQT (Peptide 3), and are well conserved across species. Peptides 1 and 2 are completely identical among mammals, while ⁵⁵⁸R in peptide 3 is exclusive for primates instead of the ⁵⁵⁸M found amongst other mammals. Interestingly, peptides with similar sequences can be potentially released from other proteins of the thrombospondin family, due to their high similarities. Although it is not clear which are the proteases responsible to produce these peptides, they might be related to OA-relevant proteases. ADAMTS-4 could be responsible for the production of ⁵⁵³V cleavage on peptide 3 [197]. These peptides are not likely to be involved in PSACH/MED, as none of the closest TSP-5 mutations fall on the peptides ⁵²⁹T, ⁵⁸⁵T and ⁷¹⁸R [198-200]. The three peptides span sequences where secondary structures initiate: beta sheets for peptides 1 and 3 and alpha helix for peptide 2. However, it is possible that the proteolytic events that release the peptides from the protein results on a peptide's secondary structure different to the one in the parent

protein. Our experiments were designed based on the known functions of the protein domain where the peptides are derived from. The main limitations for this study were that we could not account for the possible interactions between the peptides and other factors. In our screening approach, we assumed that cellular responses would be proportional to the peptide concentration, and that our selected single dose would be the highest possible within the physiological range. We cannot exclude, however, that other doses or experimental durations (though optimised previously) could have had an effect on the processes. Also, we could not account for the possibility that the synovial explants used may have already encountered the peptides *in vivo* which could have turned led to some level of desensitisation. In addition, we observed a high variability between donors and between explants of the same donor. This could be explained by the different degrees of inflammation and synovial damage of the patients, which could turn a patient unresponsive to our testing stimuli. In order to reduce interindividual variability, it would be advisable for future experiments to seek for sources of healthy synovium. Last, because matrikines and matricryptins may play different roles to their parent proteins, we cannot exclude their involvement on other processes in OA than those analysed. Following this research, Calamia *et al* (2019) identified more peptides derived from TSP-5, in parallel to multiple peptides derived from other matricellular proteins [201]. For future preselection of candidates, it might be advisable to prioritise those matrikines and matricryptins either known or strongly suspected to be biomarkers of diseases, in particular if containing certain motifs such as RGD or known interaction sites for growth factors. The reason is that, because diseased individuals possess those molecules in concentrations different than healthy individuals, those molecules are more likely to be actively involved into the pathogenesis of the disease, either by playing detrimental roles or by stimulating compensatory mechanisms.

CHAPTER 5

A new semi-orthotopic bone defect model for cell and biomaterial testing in regenerative medicine

E. ANDRÉS SASTRE, Y. NOSSIN, I. JANSEN, N. KOPS, C. INTINI, J. WITTE-BOUMA, B. VAN RIETBERGEN, S. HOFMANN, Y. RIDWAN, J.P. GLEESON, F.J. O'BRIEN, E.B. WOLVIUS, G.J.V.M. VAN OSCH*, E. FARRELL*

BIOMATERIALS. 2021 DEC; 279:121187
DOI: 10.1016/j.biomaterials.2021.121187

*These authors contributed equally

ABSTRACT

In recent decades, an increasing number of tissue engineered bone grafts have been developed. However, expensive and laborious screenings *in vivo* are necessary to assess the safety and efficacy of their formulations. Rodents are the first choice for initial *in vivo* screens but their size limits the dimensions and number of the bone grafts that can be tested in orthotopic locations. Here, we report the development of a refined murine subcutaneous model for semi-orthotopic bone formation that allows the testing of up to four grafts per mouse one order of magnitude greater in volume than currently possible in mice. Crucially, these defects are also “critical size” and unable to heal within the timeframe of the study without intervention. The model is based on four bovine bone implants, ring-shaped, where the bone healing potential of distinct grafts can be evaluated *in vivo*. In this study we demonstrate that promotion and prevention of ossification can be assessed in our model. For this, we used a semi-automatic algorithm for longitudinal micro-CT image registration followed by histological analyses. Taken together, our data supports that this model is suitable as a platform for the real-time screening of bone formation, and provides the possibility to study bone resorption, osseointegration and vascularisation.

INTRODUCTION

Bone has the ability to heal in most cases with minimal or no scar formation. However, after severe trauma or tumour resection surgery, bone might be unable to heal spontaneously in a reasonable amount of time. Above a critical size, bone defects exhaust their self-healing capacity. In these circumstances, there are many possibilities for intervention that use various grafts to support and promote the regeneration of the bone in the defects [202]. The use of autologous bone as a grafting material is the most successful method to achieve bone augmentation of defects. This strategy constitutes the current gold-standard, as autologous grafts are both osteoinductive and osteoconductive and have a low risk of immune rejection [203]. However, their use is limited to the available amount of harvestable material and often results in donor site morbidity. An alternative approach is to use tissue engineered grafts capable of promoting the bone healing response. In general, these grafts are based on a scaffold that may be combined with either pro-osteogenic agents, such as bone morphogenetic proteins (BMPs), stem cells, other cellular fractions or a combination thereof [23].

Assessing new potential therapies for bone defect repair begins with *in vitro* systems or *ex vivo* systems, since they are inexpensive and relatively simple [204]. However, they are limited since their simplicity comes with the price of excluding major cellular types involved in the process of bone regeneration. Thus, in order to further study the dynamics of bone formation and regeneration, the next step requires the use of preclinical animal models. These *in vivo* models are classified according to the site where bone formation takes place, at either orthotopic or ectopic locations [205]. In rodents, orthotopic locations such as at the radius, calvarium and the femur are nowadays the gold-standard for orthopaedic research as they are the most clinically relevant, in that they involve the creation and healing of a defect in a bony environment [206]. These studies are however time consuming, expensive, have a large impact on animal welfare due to the invasive nature of the model and require advanced surgical procedures. As an alternative, it is long known that *de novo* bone formation can be induced and studied at ectopic locations if three elements are provided: an inducing agent, an osteogenic precursor cell and an environment which is permissive to osteogenesis [207]. Common methods used for this purpose are based on intramuscular and subcutaneous implants, the latter being the easiest to perform surgically and having the lowest impact on animal welfare. Unlike orthotopic locations though, ectopic bone formation is not initiated by an established bony microenvironment, which poorly models some aspects of bone defect repair and an evaluation of the integrative repair capacity of the graft with the adjacent tissue is not possible.

Due to the increasing numbers of novel bone grafts being developed in the last years and the ethical concerns that animal experimentation raises, it is desirable to develop new experimental models aiming for surgical simplicity that improve the animal welfare and allow the simultaneous testing of multiple grafts in a controlled environment. To

address this, we hypothesised that a piece of bovine bone subcutaneously implanted in an immunodeficient mouse would retain the ability to regenerate -by recapitulating the events of bone repair- and thus, that it could be potentially used as a bone graft screening tool. For this reason, in this work we aimed to develop a new minimally invasive “semi-orthotopic” bone defect model for cell and biomaterial testing in regenerative medicine that would combine the advantages of ectopic and orthotopic bone repair models.

MATERIALS AND METHODS

Preparation of the bone ring constructs

Bone rings were prepared from freshly harvested distal epiphyses of the metacarpal bones of 3 to 8-month-old calves, which were purchased from a slaughterhouse and processed within 5 hours. To produce the rings, the metacarpophalangeal joint (MCP) was opened, and the cruciate ligaments sectioned, to expose the articular cartilage surfaces. Next, 10 hollow cylindrical osteochondral plugs per bone were drilled by using an 8 mm diameter trephine drill [MF Dental, Weiherhammer, Germany] in which a central canal was drilled using a 3-, 4- or 5-mm steel drills. Tissue damage was minimised by avoiding the heating of the explant through low speed drilling and simultaneous cooling with sterile PBS. Then, 4 mm height rings were made by removing the articular cartilage and the proximal bone ends using a circular table saw. In this way, 8-mm diameter × 4-mm height bone rings were obtained. Next, the bone rings were transferred to 12-well plates containing α -MEM supplemented with 10% v/v FBS, 100 μ g/mL gentamycin and 3 μ g/mL amphotericin B [all from Thermo Fischer, Bleiswijk, The Netherlands] and incubated overnight in a humidified atmosphere at 37 °C and 5% CO₂. The following day, immediately before implantation, the cores of the rings were filled with the different grafts. The top and bottom ends of the rings were closed with two circular 8 mm diameter dense polytetrafluoroethylene membranes (dPTFE) [PermaMEM®, Botiss biomaterials, Zossen, Germany], to prevent direct in-growth of host cells into the testing pocket and fastened with a single 6-0 non-resorbable polyamide suture Ethilon® [Johnson & Johnson Medical, Livingston, UK]. (Fig. 1A, B). The viability of the explants at the moment of implantation was assumed, since previously observed that comparable explants obtained in a similar manner remain viable *in vitro* for one month [208].

Preparation of the different grafts

To validate the model, different grafts were prepared to modulate bone formation inside the defect: cortical bone chips, tissue engineered cartilage constructs and cartilage grafts.

Cortical bone chips. The leftover bones used to produce the bone rings were used to harvest bone chips. After removal of the periosteum, the cortical surface of the diaphysis was scraped with a Safescraper® Twist [Geistlich Sons Lt., Manchester, UK][209], and the scraped chips were placed in α -MEM supplemented with heat inactivated 10% v/v FBS, 100 μ g/mL gentamycin and 3 μ g/mL amphotericin B [all from Thermo Fischer, Bleiswijk, The Netherlands], and incubated overnight in a humidified atmosphere at 37 °C and 5% CO₂.

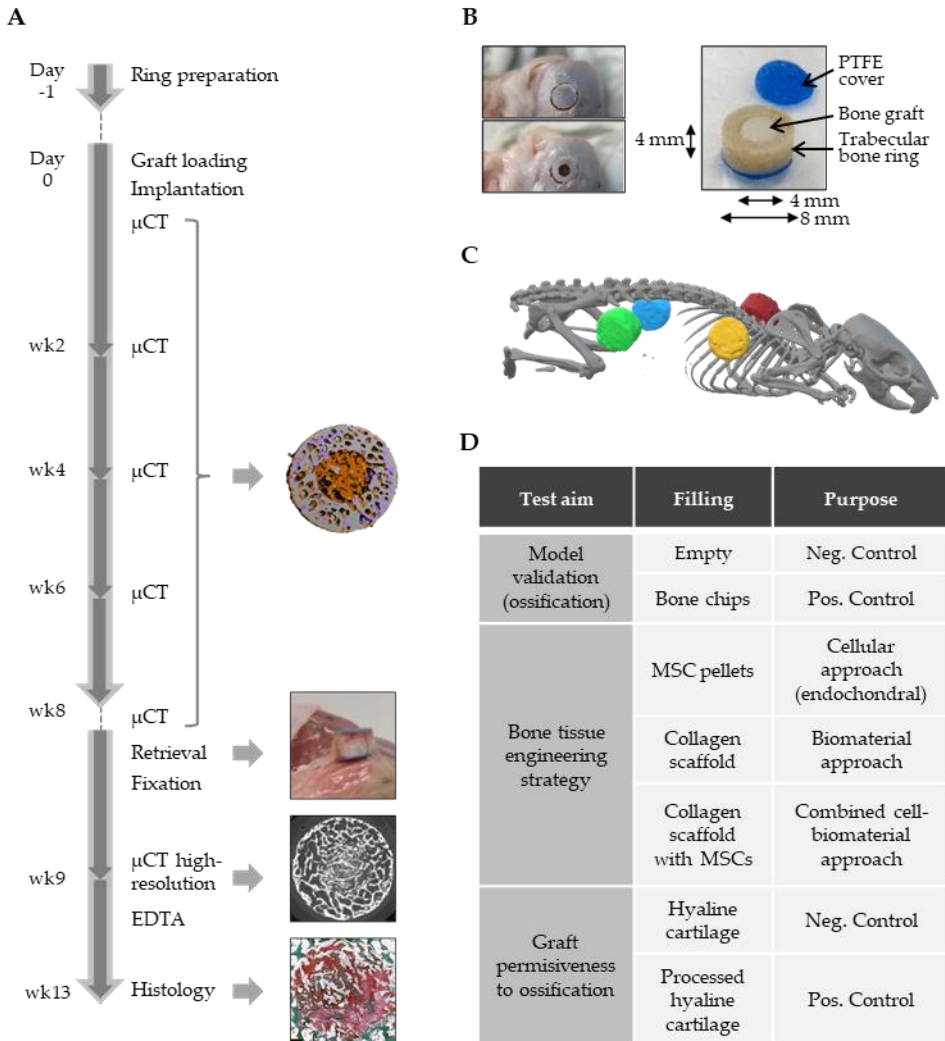


Figure 1. Preparation of the semi-orthotopic bone defect model. (A) Experimental timeline (B) Ring preparation and parts of the construct (C) Full-body micro-CT of a mouse hosting four constructs, highlighted in different colours (D) Construct fillings and purposes (E). Micro-CT (μ CT); Negative (Neg.); Positive (Pos.).

Tissue engineered cartilage constructs. Bone marrow stromal cells (MSCs) were isolated from leftover iliac crest bone chip material obtained from a 9-year-old male paediatric patient undergoing alveolar bone graft surgery (with institutional consent for the use of waste surgical material with the option for parental opt-out and approval of medical ethics committee of Erasmus University Medical Center: MEC-2014-16). Cells were expanded in α MEM containing heat inactivated 10% v/v FBS and supplemented with 50 μ g/mL gentamycin, 1.5 μ g/mL amphotericin B, 25 μ g/mL L-ascorbic acid 2-phosphate [Sigma, Zwijndrecht, the Netherlands] and 1 ng/mL fibroblast growth factor-2 [Bio-Rad via Bioconnect, Huissen, the Netherlands] in a humidified atmosphere at 37°C and 5% CO₂. The ability of these cells to differentiate into multiple tissues was confirmed by trilineage differentiation (data not shown), as described previously [92].

Generation of chondrogenic pellets. To generate the chondrogenic pellets, 2 x 10⁵ MSCs (passage 3) were suspended in 500 μ L of chondrogenic medium (high-glucose Dulbecco's modified Eagle's medium (DMEM) [Thermo Fischer, Bleiswijk, The Netherlands] supplemented with 50 μ g/mL gentamycin, 1.5 μ g/mL fungizone, 1 mM sodium pyruvate [Thermo Fischer, Bleiswijk, The Netherlands], 40 μ g/mL L-proline [Sigma, Zwijndrecht, the Netherlands], 1:100 v/v insulin-transferrin-selenium [ITS+; BD Biosciences], 10 ng/mL transforming growth factor β 3 [R&D systems], 25 μ g/mL L-ascorbic acid 2-phosphate, and 100 nM dexamethasone [Sigma, Zwijndrecht, the Netherlands]) in 15 mL polypropylene tubes [TPP via Westburg], and centrifuged at 300 g for 8 min. The pellets were chondrogenically differentiated for 23 days, where the chondrogenic media was replaced twice weekly.

Cell seeded scaffolds. To fabricate highly porous collagen-based scaffolds, a lyophilisation method previously described by O'Brien FJ *et al.* was used [210]. Type I collagen-GAG scaffolds were composed of type I collagen derived from bovine Achilles tendon [Collagen Matrix, USA] and chondroitin 6-sulfate (CS) derived from shark cartilage [C4384, Sigma-Aldrich, Ireland]. Briefly, collagen-GAG slurry was prepared by dissolving 3.6 g collagen and 0.32 g of CS in 360 ml of 0.5 M acetic acid using a blender [Ultra Turrax T18 Overhead Blended, IKA Works Inc., USA] at 15,000 rpm for 90 minutes at 4 °C. The final concentrations of the suspension were composed of 0.5% (w/v) collagen and 0.05% (w/v) CS. Subsequently, 0.3 ml of the slurry was pipetted into a stainless-steel tray (internal dimensions: 9.5 mm diameter and 4 mm height) before being freeze-dried [Virtis Genesis 25EL, Biopharma, UK] at a constant cooling rate of 1°C/min to a final temperature of -40°C. Next, the porous scaffolds were dehydrothermally crosslinked in a vacuum oven [VacuCell, MMM, Germany] for 24h at a pressure of 0.05 bar and temperature 105°C. In order to prepare the scaffolds to be seeded with cells, the scaffolds were rehydrated with graded ethanol series (100%, 90%, 70%) to dissolve acid residues. Then, they were washed with distilled water and PBS prior to cell seeding. The scaffolds, measuring dry 1 cm x 1.5 cm x 3 mm, were seeded each with a 0.5 ml suspension of 2x10⁶ MSCs (passage 3) while contained inside 50 ml polypropylene tubes. 30 min later, 4 ml chondrogenic medium was added to the tubes. Next day, the scaffolds were transferred

to polystyrene suspension culture plates [Greiner Bio-One] in chondrogenic medium. Media was refreshed twice weekly during the 23-day culture period. If cellular outgrowth was observed from the scaffold, the scaffolds were transferred to a new suspension plate. Since the cellular activity within the scaffolds during the culture time caused the scaffolds to contract reducing their volume, two cell-seeded scaffolds were implanted per bone ring to completely fill the defect.

Cartilage grafts. Tracheal explants were obtained from 3 to 8-month-old calves, purchased from a slaughterhouse. To prepare them, adjacent tracheal rings were dissected and sectioned sagittally at 4-mm intervals; then, transverse cylindrical biopsies were obtained with a 4-mm diameter biopsy punch [Stiefel Laboratories, Durham, NC] to obtain cartilaginous pieces that fit tightly into the whole volume of the bone defect. Viable cartilage samples were kept overnight until implantation in high-glucose DMEM supplemented with 100 µg/mL gentamycin and 3 µg/mL amphotericin B. In parallel, a set of explants were devitalised by performing 5 freeze-thaw cycles at -21°C, 60 minutes each and extracted for 16 h in 4M guanidine hydrochloride (GuHCl) [Sigma-Aldrich] under agitation at room temperature. Last, residual GuHCl was removed by three washes in PBS followed by a 4h incubation in PBS. One cylinder was implanted per bone ring.

Surgical implantation procedure and longitudinal micro-CT imaging

Animal experiments were conducted in the experimental animal facility of the Erasmus University Medical Center with approval of the local animal ethics committee (under licence number 101002015114 and protocol number 15-114-09), which comply with EU Directive 2010/63/EU, and were reported in compliance with the ARRIVE guidelines. The surgical procedure was performed on 10- to 14-week-old male immunodeficient NMRI-*Foxn1* nu/nu mice purchased from Janvier [Le Genest-Saint-Isle, France]. This strain has previously been shown to be capable of hosting similar xenogeneic implants [211-213]. 16 mice were used in total. This included experimental conditions from another study whereby the same control conditions were used in order to reduce total animal numbers. Of the 64 available subcutaneous pockets in these 16 mice, 40 pockets were used specifically for the study reported here. Mice were housed in groups of 3 and 4 in individually ventilated cages, and food was provided *ad libitum*. To avoid peri- and post-operative pain, mice received 0.05 mg/kg body weight of buprenorphine [Reckitt Benckiser, Hull, UK] 1 hour before the operation and 6-8 hours after implantation. The operation was performed under isoflurane inhalation anaesthesia. During the procedure, four incisions were made on the back of each mouse to create four subcutaneous pockets, where four constructs per mouse were placed bilaterally with respect to the thoracic and lumbar vertebrae. To prevent confounding effects, all experimental replicates and corresponding conditions for direct comparison were implanted in the same batch of surgeries and each treatment replicate was placed in each of the four pocket positions, ensuring that no more than two treatment replicates

were placed in the same mouse. No blinding was performed. After construct placement, 4-0 non-resorbable polyamide suture Ethilon® [Norderstedt, Germany] was used to close the wounds. While still under anaesthesia, the four implants were scanned by micro-CT [Quantum GX, Perkin Elmer, USA], with a 36 mm Field of View (FOV) and 72 µm isotropic voxel size. After the scan, the sutures were immediately replaced by clips [AutoClips®, Fine Science Tools, Heidelberg, Germany], since the clips would otherwise introduce artifacts into the scan, and the mice received an injection of 25 mg/kg of ampicillin [Dopharma, Raamsdonksveer, The Netherlands]. The clips were removed 8-10 days after the operation, when the wounds had healed. At 2, 4, and 6 weeks after the surgical procedure, mice were scanned again under isofluorane anaesthesia. After 8 weeks, mice were sacrificed by cervical dislocation under isofluorane anaesthesia, scanned again and the constructs retrieved. The bone rings were fixed in 4% buffered formalin at room temperature for one week. During fixation, the caps were removed and the constructs were scanned again by the micro-CT for 4 minutes with a FOV of 18 mm and 36 µm isotropic voxel size. During the entirety of the experiment, the health condition of the mice used was closely monitored, and a humane endpoint was established if there was a drop in body weight of 15% in 2 days or 20% from the moment immediately after implantation. Moreover, the exclusion of all constructs from analysis was set up *a priori* if the humane endpoint was reached. No signs of distress were evident, all the mice survived and all the conditions intended for this study were included for analysis.

Micro-CT analysis

Bone volume of the whole constructs. Bone morphometric analysis of the DICOM images generated was performed using specialised micro-CT software [SCANCO Medical AG, Brüttisellen, Switzerland]. Phantoms of known densities (0.25 g/cm³ and 0.75 g/cm³) were scanned at every measurement and used to convert pixel intensity into mineral density. To assess the total bone volume of each construct, the bone region was segmented from the neighbouring tissues using an automated contouring method. The resulting grey-scale images were Gaussian filtered with sigma of 0.8 and a support of 1 voxel, and the signal above a density threshold of 335 mg HA/ccm was used to produce binary images (Suppl. Fig. 1). Then, the bone morphometric parameter bone volume (BV) was evaluated using a three-dimensional analysis software [Image Processing Language, SCANCO Medical AG, Brüttisellen, Switzerland].

Automatic co-registration of follow-up scans and longitudinal bone morphometric analysis of the construct's testing pocket. Changes over time in the bone microarchitecture were determined by overlaying two consecutive data sets, provided that these have equal orientations. As the trabecular microarchitecture of the bone rings experienced only minor changes during the experiment, their 3D volumes were used to perform landmark-free alignments on the series of longitudinal scans (Suppl. Fig. 2). For this, the segmented binary images previously obtained were first used to create 3D

reconstructions. Then, each follow-up scan was aligned to its corresponding initial scan by automatic rotation and translation based on iterative transformations, so the overlapping volume was maximised between the two. This analysis was based on a previously described method [214, 215]. Following alignment, clusters of voxels were compared and categorised as either bone gain (only present in the follow up image), bone loss (only present in the baseline image) or unaltered bone volume (present in both images). Afterwards, color-coded images were created to represent those three categories. Next, in order to analyse the bone morphometric parameters of the testing pocket, the inner defect volume of the baseline scan was automatically segmented using a self-generated algorithm. Then, each of its follow-up scans was automatically aligned, and the baseline segmentation transferred to them. After calibration with hydroxyapatite (HA) phantoms of known density, the signal above a density threshold of 335 mg HA/ccm was used to produce binary images (Suppl. Fig. 1). The BV was calculated, and in order to compensate for minor differences in the manufacturing between the different rings, the ratio between the BV and the total volume of the defect (TV), the BV/TV, was calculated.

Histological assessment

After fixation, the constructs were decalcified in 10% w/v ethylenediaminetetraacetic acid (EDTA) pH 6.8-7.2 at room temperature for 4-5 weeks, where the EDTA was refreshed twice weekly. Subsequently, the samples were embedded in paraffin and 6 μm thick sections were collected for histology at different depths. Before histological assessment, sections were deparaffinised using a series of xylene, graded ethanol (100%, 96% and 70%) and distilled water.

H&E Staining. The histological sections were stained with Gill's haematoxylin [Sigma-Aldrich] for 5 minutes and incubated in 2% w/v eosin [Merck, Amsterdam, The Netherlands] in 50% v/v ethanol and 0.5% v/v acetic acid for 45 seconds. The sections were incubated in 70% ethanol for 10 seconds and afterwards dehydrated in 96% ethanol for 1 min, 100% ethanol for 1 min and two times xylene for 1 min, after which they were mounted with DPX, coverslipped and dried overnight at 37°C before imaging.

RGB Staining. RGB trichrome staining was performed as described by Gaytan F *et al* [216]. Briefly, sections were dewaxed using xylene and graded ethanol, rinsed in distilled water and stained for 20 minutes in 1% w/v Alcian Blue 8GX [Sigma] in 3% v/v acetic acid at pH 2.5. Then rinsed in tap water, followed by 20 minutes 1% w/v Fast Green [Sigma] in distilled water. Then, they were rinsed for 5 min in tap water, followed by 30 min 1% w/v Sirius Red [Direct Red 80, Sigma] in a saturated aqueous solution of picric acid. Then sections were carefully rinsed twice in 1% v/v acetic acid (3min each wash), followed by dehydration in subsequently 100% Ethanol (2x) and two times in Xylene. Slides were covered with DPX, coverslipped and dried overnight at 37°C before imaging.

Tartrate resistant acid phosphatase (TRAP) staining. Sections were incubated for 20 minutes at room temperature in freshly prepared 0.2M acetate buffer, 100mM L (+) tartaric acid pH 5.0. Then to this acetate buffer 0.5 mg/ml naphtol AS-BI phosphate [Sigma] and 6.4 mg/ml Fast Red TR salt [Sigma, 15% dye content] was added. Sections were incubated for 1- 1.5 h at 37°C and regularly checked until cells stained bright red. After staining sections were rinsed with distilled water and lightly counterstained with Haematoxylin (Gill's formula), followed by a 10 min wash with running tap water and dried overnight at 37°C. Sections were coverslipped with VectaMount® and imaged.

Safranin O staining. Sections were incubated in 0.1% Light Green solution [Sigma-Aldrich] in distilled water for 8 minutes. Afterwards they were rinsed with 1% acetic acid. Then, the slides were incubated with 0.1% Safranin O solution [Fluka] in distilled water for 12 minutes. They were rinsed two times with 96% ethanol for 30 seconds and afterwards dehydrated in 100% ethanol for 1 minute and two times xylene for 1 minute. Sections were coverslipped with VectaMount® and imaged.

Image acquisition

Composite tile scans from stainings were obtained with a NanoZoomer HT microscope (C9600-12) using the software NDP.scan v2.5.90 [Hamamatsu Photonics]. Hue and brightness were adjusted after acquisition using Adobe Photoshop CC 2018, following the recommendations described by Sedgewick [89].

Statistical analysis

Each construct was treated as a separate unit for means of measurement, independently of the position and the identity of the host mouse. Mice were considered as carriers of the constructs, and their interindividual variability assumed to play a negligible role into the construct's response to the graft. Normality of the data was not assumed for the analysis of longitudinal micro-CT measurements. Longitudinal measurements versus the initial timepoint within same sample were analysed by Kruskal-Wallis test with Dunn's correction. Single terminal time point data was compared via Mann-Whitney two-tailed test. Longitudinal measurements where the change in the bone filling of the defect in time of two conditions was compared, were analysed by paired analysis by two-way ANOVA with time matching. Sphericity was assumed and Sidak correction for multiple comparisons was performed. A p-value of <0.05 was considered significant. GraphPad Prism (version 8.0.1 for Windows, GraphPad Software, La Jolla, California USA) was used to perform the statistics and to create the graphs.

RESULTS

Bone rings can recapitulate critical size defects *in vivo*

In order to determine what defect size could be considered as critical in our model, we assessed the spontaneous ossification taking place in constructs containing different defect sizes over a period of 8 weeks. For this, we implanted different constructs incorporating empty defects of 3 mm, 4 mm and 5 mm following the methodology described in Fig. 1. No noticeable adverse effects occurred on these mice, nor the rest used for this study. Following implant placement and until termination of the experiment, all the mice of the study increased their weight by $7.6\% \pm 5\%$ (Suppl. Fig. 3). After 8 weeks, the micro-CT images and histological inspection revealed that *de novo* bone formation had taken place inside the defects, although the bone deposition was limited to the inner edges of the ring (Suppl. Fig. 4). Since the 3 mm defect was mostly occluded by the new bone formed, and to maximise the amount of marrow to better replicate the bone microenvironment, the 4 mm defect was selected to be used in further experiments. Next, we assessed in more detail the biological processes taking place *in vivo* in those constructs. After 8 weeks, mineralised projections of the ring into the defect could be observed by micro-CT at different depths, indicating that new calcified tissue was being formed inside the defect adjacent to the inner ring surface (Fig. 2A). In addition, the total mineral content of the implanted ring increased on average around 15% during the 8-week period of implantation (Fig. 2B). The histological analysis after comparison to the construct pre-implantation (Fig. 2C) revealed that vascularised fibrous tissue had formed inside the ring during implantation, initiating the closure of the defect (Fig. 2C). A closer look at the defect site revealed that the bony projections observed with the micro-CT images corresponded to newly formed mineralised matrix. The histology suggested that bone was forming via endochondral ossification (Fig. 2D). The newly formed bone was well-integrated to the bone ring and had formed vascularised marrow compartments. In addition, more bone had formed inside the trabecular space of the ring too (Fig. 2D), which also contributed to the increase of the total calcified volume of the construct. In conclusion, these observations indicated that the bone rings retained their inherent ability to regenerate, but to a level insufficient to heal the full defect during the 8-week timeframe. Consequently, this opened the possibility that bone formation could be stimulated if a suitable bone graft was placed into the defect.

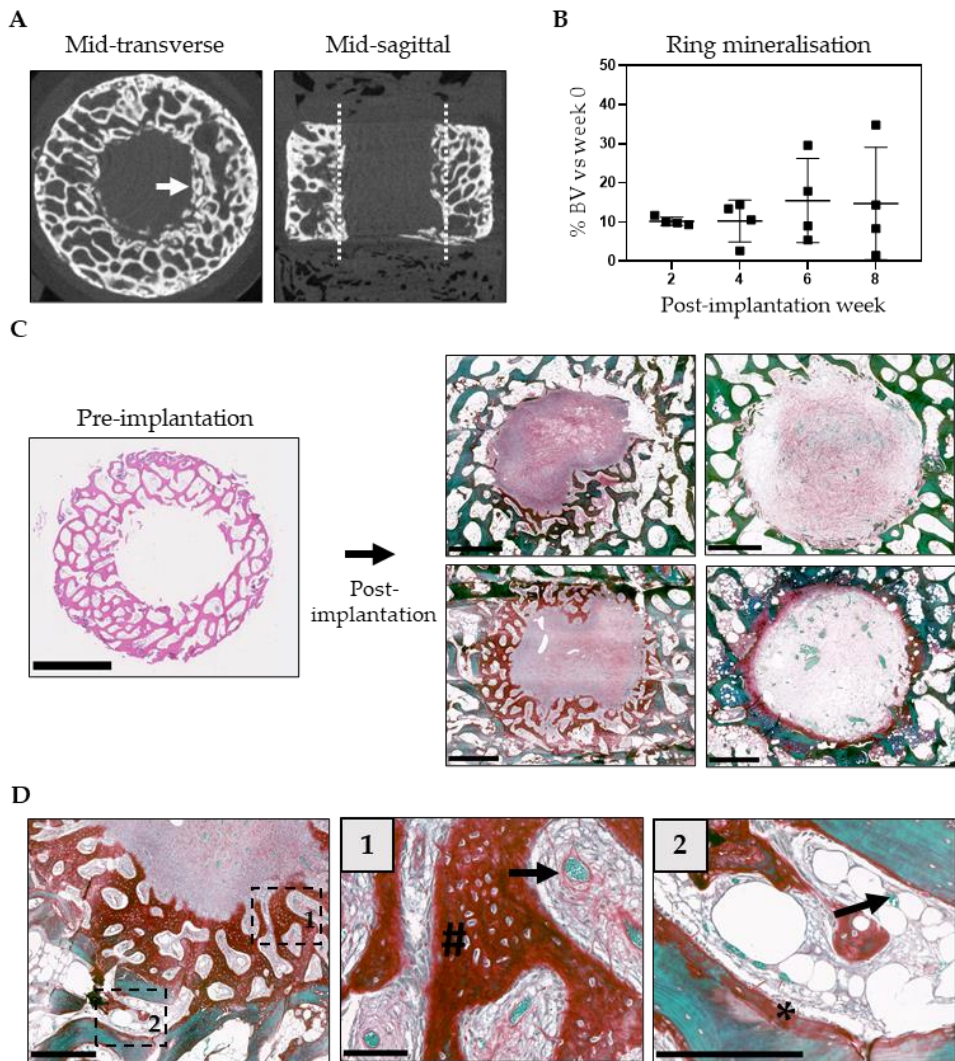


Figure 2. Bone formation into an empty defect in the semi-orthotopic bone ring healing model after 8 weeks *in vivo*. (A) Micro-CT showing the mid-transverse and mid-sagittal planes of one construct 8 weeks post-implantation. White arrow and dotted lines indicate a region with newly formed bone. (B) Percentage of the whole cylinder's bone volume (%BV) over time versus the bone volume at the time of implantation. N=4 constructs per condition. (C) H&E staining showing the rings pre-implantation and RGB staining showing different degrees of closure in representative sections of 4 different constructs 8 weeks post-implantation. Scale bars: 1mm. (D) RGB staining showing bone formation taking place both inside the defect (1) and on the pre-existing bone of the ring (2). The hash (#) indicates calcified cartilage undergoing endochondral bone formation. In green the mature bone; the asterisk (*) marks the osteoid and the black arrows mark the presence of blood vessels in light green. Scale bars: E: 500 μ m, E₁: 250 μ m, E₂: 100 μ m.

Bone formation is stimulated when a suitable graft is placed into the defect

In clinics, autologous bone chips are the gold standard used for bone augmentation due to their osteoconductive, osteoinductive, and osteogenic properties. For this reason,

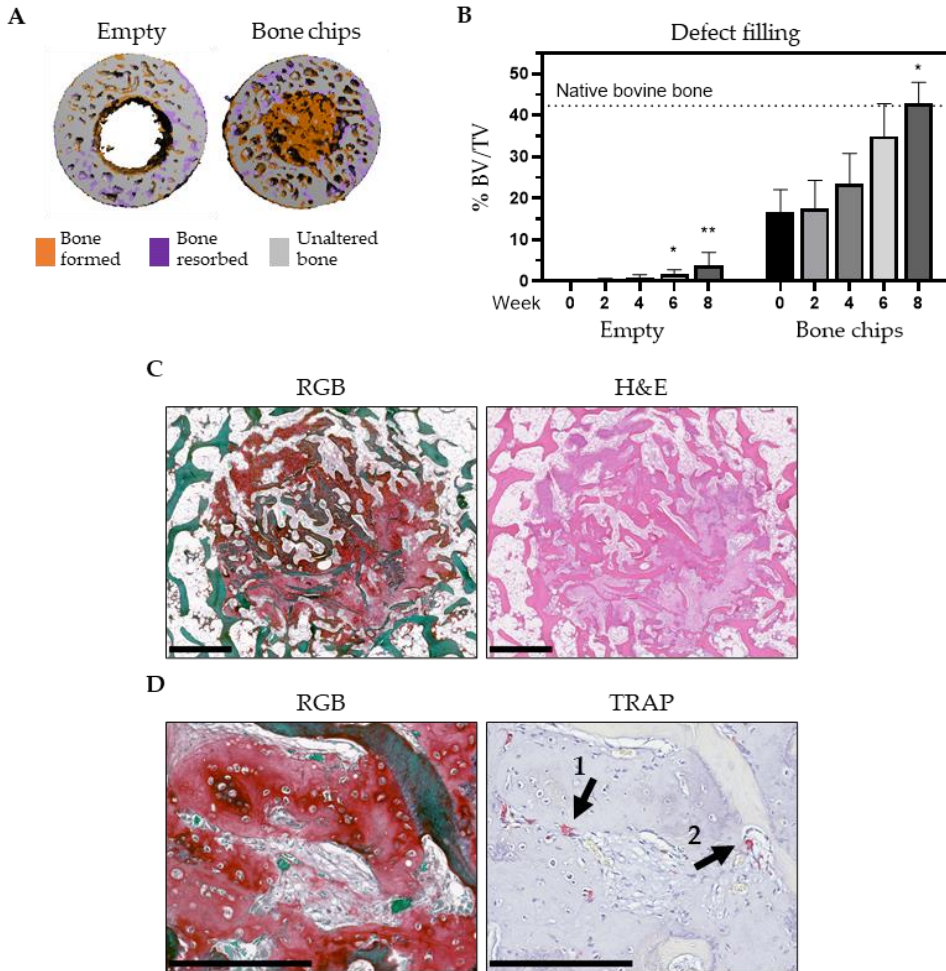


Figure 3. Assessment of the healing capacity of the construct in the semi-orthotopic bone defect healing model. (A) Pre- and post-implantation overlays of micro-CT 3D image reconstructions. (B) Quantification of mineralization over time per volume unit (% BV/TV) inside the defect when empty and when cortical bone chips are used as grafting material. Dotted line indicates the average undamaged bovine bone pre-implantation % BV/TV. The two conditions were analysed separately, and time points were compared by one-way ANOVA. N=4 constructs per condition. Bars indicate average + SD. * p < 0.05, * p < 0.01 (vs. week 0). (C) Serial sections with RGB and H&E stainings showing the presence of mature bone and forming bone inside the defect post-implantation via endochondral ossification. Scale bar 1 mm. (D) Serial sections with RGB and TRAP stainings. Arrows point at TRAP+ cells remodelling the newly-formed matrix (1) and the cortical bone used for grafting (2). Scale bar 250 μ m.

we next validated the model by testing if a graft composed of bovine cortical bone chips would have the ability to increase the rate of bone formation inside the ring's defect more than if left empty. The micro-CT overlay of the constructs before and after implantation indicated that most of the newly calcified tissue in the condition containing the bone chips localised inside the defect (Fig. 3A). This result suggested the ability of the defect to regenerate when a suitable graft was placed inside. In order to assess the net gain in bone volume experienced over time, the amount of calcified tissue present in the defect was quantified by applying the analysis algorithm described in Suppl. Fig. 2. After 8 weeks, while the empty defects filled their mineralised bone volume by $4 \pm 3 \%$, the defects that were implanted with bone chips (corresponding to an initial $17 \pm 5 \%$ filling) experienced a net bone volume increase of $26 \pm 8 \%$, reaching in total the same average level of bone volume per volume unit as the native bovine bone used to manufacture the rings, $42 \text{ mm}^3/\text{mm}^3$ (Fig. 3B). This was further confirmed by histology (Fig. 3C), where large amounts of forming bone via endochondral ossification (in red) and mature bone (in green) were present inside the defect and surrounded by a newly formed marrow containing blood vessels, adipocytes and other cell types. Among those, multinucleated bone lining TRAP+ cells, indicative of osteoclasts, were observed remodelling both the newly formed matrix and the cortical bone used for grafting. In order to ensure that the signal measured on micro-CT corresponded to that of the histological observations, the resulting signals at matching locations were compared (Suppl. Fig. 5). From all the above, we concluded that it is possible to evaluate the healing dynamics of the bone ring defect when a suitable graft is placed inside.

Bone formation occurs in tissue engineered constructs

Cell based tissue engineering approaches, particularly focused on the developmental process of endochondral ossification are a very commonly used method for bone defect repair. Next, we further tested the feasibility of the model by investigating cell-based and cell-free approaches for bone defect repair. We first evaluated if small spheres of hypertrophic cartilage grafts derived from bone marrow stem/stromal cells (MSCs) could undergo endochondral ossification. To produce such grafts, MSCs were chondrogenically differentiated in the pellet system [92, 217]. The histological analysis confirmed that chondrogenic differentiation had taken place, by the blue coloration of the RGB staining (Fig. 4a), by the cellular hypertrophy and by Safranin O staining (not shown). Then, 9 to 11 of those spherical pellets were placed inside each bone defect to fill the maximum volume possible. After 8 weeks *in vivo*, it was possible to observe with micro-CT that the cartilaginous constructs had induced mineralised tissue formation inside the defects (Fig. 4B, 4C). Histological assessment revealed that bone formation was taking place both between and within the pellets (Fig. 4D). Since different rates of ossification took place between constructs, the differences in colour unveiled that the spaces between pellets ossified at a faster pace than the pellets themselves. In addition, TRAP+ cells could be identified remodelling the cartilage matrix of the MSC constructs (Fig. 4E). In a second group, highly porous scaffolds prepared with collagen type I in

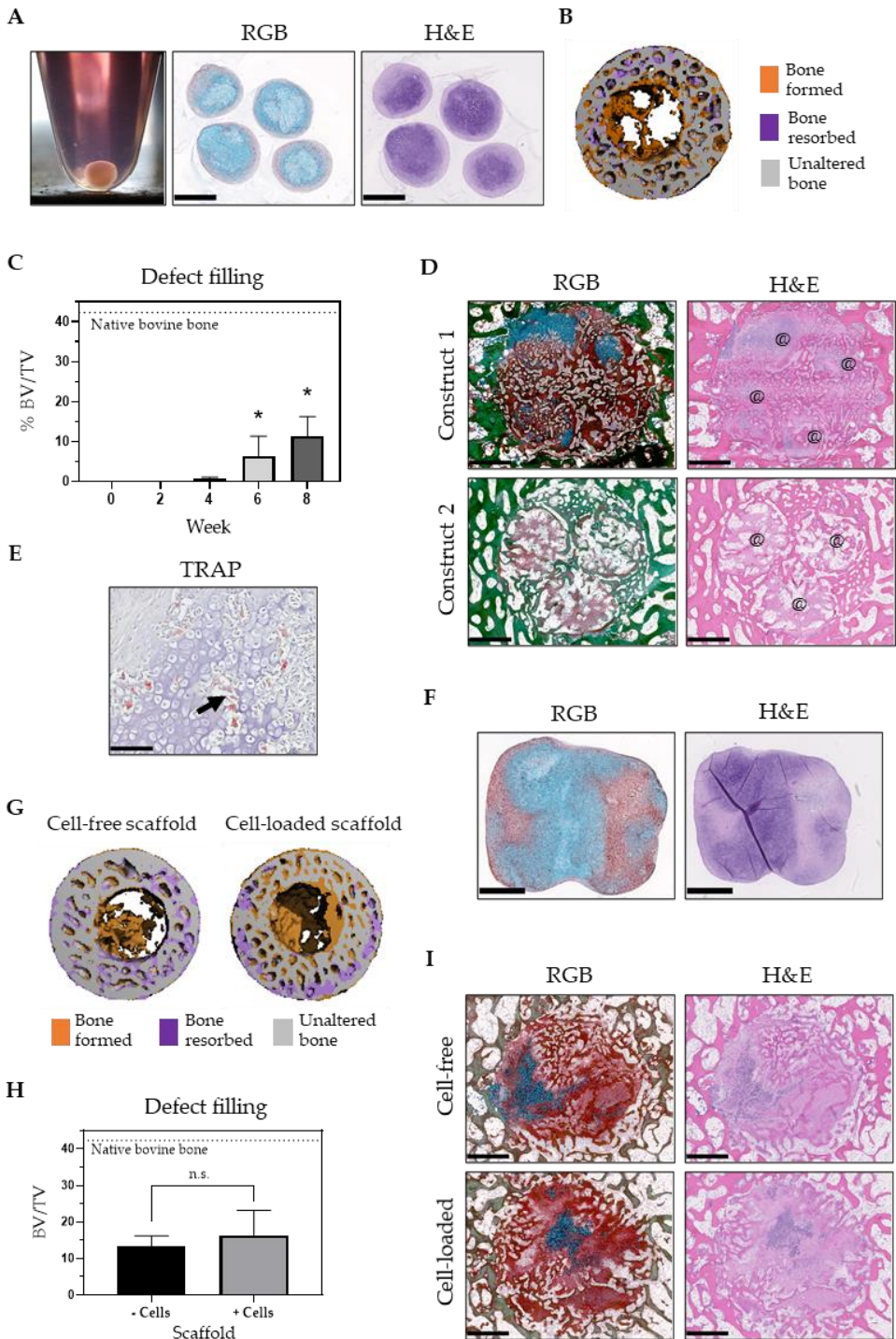


Figure 4. Different tissue engineering approaches grafted in the semi-orthotopic bone defect healing model. (A) Macroscopic view and RGB and H&E stained chondrogenically primed (for 23 days) MSC pellets prior to implantation. (B) Pre- and post- implantation overlays of micro-CT 3D image reconstructions. (C) Quantification of mineralization measured by micro-CT over time per volume unit (% BV/TV) inside the defect when pellets were used as grafting material. (D) RGB and H&E-stained sections showing two different constructs post-implantation that are at different stages of ossification. @ Indicates the location of the pellets. (E) TRAP staining demonstrating active remodelling of the pellets inside the defect. Arrow indicates a group of TRAP+ cells resorbing the matrix (F) RGB and H&E-stained cell-seeded scaffolds chondrogenically primed for 23 days prior to implantation (G) Pre- and post- implantation overlays of micro-CT 3D image reconstructions of cell-free and cell-loaded scaffolds (H) Quantification of mineralization per volume unit (% BV/TV) inside the defect 8 weeks post-implantation (I) RGB and H&E-stained scaffolds showing the healing defects post-implantation. Scale bars, A, D, F, I: 1mm, E: 100 μ m. Bars indicate the SD. In C, N=4; in H, N=6. * $p < 0.05$ (vs. week 0); n.s. (non-significant) $p < 0.05$.

combination with chondroitin sulphate, which have previously shown potential for bone regeneration when implanted [218-220]. Scaffolds were seeded with MSCs and cells chondrogenically differentiated *in vitro*. After confirmation of the deposition of a cartilaginous matrix (Fig. 4F), the constructs were implanted for 8 weeks *in vivo* in parallel to the same cell-free scaffold, in order to compare a cell-free and a cell-seeded scaffold. The CT analysis at 8 weeks revealed that both, the cell-free and cell-seeded scaffolds had calcified and performed similarly with regard to bone formation (Fig. 4G, 4H). This was further verified by histology, suggesting that bone was forming via endochondral ossification in both conditions (Fig. 4I). These experiments supported that the osteogenic performance of grafts composed of solely biomaterial, solely cells, or a combination of biomaterials and cells can be studied effectively in our model.

Graft permissiveness to ossification

Since the bone ring demonstrated the ability to possess intrinsic osteoinductive properties, we then explored if our model could be used to assess graft's permissiveness to osteogenesis and vascularisation. For this, tracheal cartilage was used. Contrary to the transient cartilage constructs produced with MSCs, young tracheal cartilage remains phenotypically stable by actively preventing blood vessel invasion and subsequent ossification [221]. In order to produce comparable tracheal grafts that permit ossification, we hypothesised that devitalising and extracting a subset of these tracheal grafts would result in the loss of their anti-invasive properties. Then, the rings were loaded with both vital and devitalised-extracted tracheal cartilage grafts. Eight weeks post-implantation, the devitalised-extracted cartilage showed a significant increase of mineralisation on micro-CT in comparison to the vital cartilage, suggesting that the devitalised-extracted cartilage was undergoing remodelling (Fig. 5A, B). Histological analysis revealed that the vital cartilage grafts had remained phenotypically stable, as demonstrated by the strong GAG staining, the absence of blood vessels and bone projections (Fig. 5C). In contrast, the devitalised-extracted grafts displayed extensive remodelling originated from the bone ring (Fig. 5C). Large number of erythrocytes were visible in the

devitalised-extracted cartilage graft, indicating it had spontaneously vascularised. In addition, new marrow compartments and mineralised structures had occurred. These observations demonstrated that this model can be used to assess the permissiveness of grafts to vascularise and undergo osteogenic remodelling.

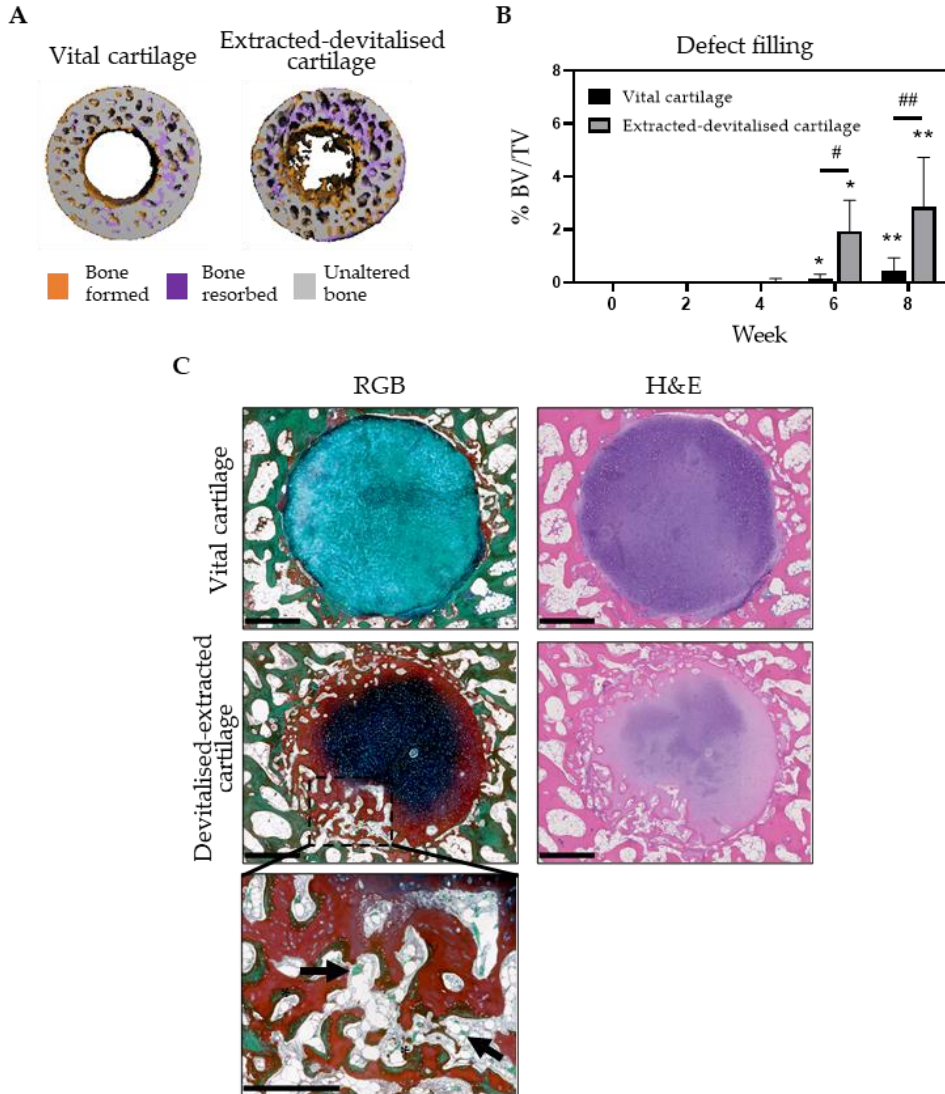


Figure 5. Evaluation of graft permissiveness to ossification in the semi-orthotopic bone defect healing model. A) Pre- and post- implantation overlays of micro-CT 3D image reconstructions. B) Quantification of bone volume over trabecular volume in the defect area filled with vital or extracted cartilage. N=4 constructs per condition. Bars indicate the SD. * p < 0.05, ** p < 0.01 (vs. week 0); # p < 0.05, ## p < 0.01 (matched timepoints). C) RGB and H&E stainings after 8 weeks of the vital or extracted cartilage. The asterisk (*) marks the newly deposited bone and the black arrow marks the presence of a blood vessel in light green. Scale bars, 1mm and 500 μ m. E: 100 μ m.

DISCUSSION

In this work we have developed a new *in vivo* semi-orthotopic bone defect healing model for the purpose to test cell, bioactive molecules, biomaterials –and combinations thereof– for regenerative medicine. By ectopically implanting bovine bones containing a critical-size defect in a mouse, we have demonstrated the potential for at least four standardised osteoinductive microenvironment in a single animal. This will allow the evaluation and comparison of desirable biological processes that take place during graft-mediated bone healing, opening the possibility to be used as a new *in vivo* medium throughput screening platform. Since this platform offers great reproducibility, can be automated and thus, lower costs, it is expected to allow a more efficient testing of bone grafts in rodents, with special emphasis on the principles of the 3Rs (reduction, replacement and refinement) [222].

Traditionally, fracture healing has been studied in large animals such as dogs, rabbits and sheep due to their large skeletal size and similar bone structure to humans. Due to the excessive costs, research started to move first to rats and then further to mice [223], since these animals offered technical advantages such as easy handling, reduced prices and a large *repertoire* of genetically modified strains. Nevertheless, the reduced size of the mouse limits the volume of the graft that can be tested. Our semi-orthotopic *in vivo* model suggests however that it is possible to overcome some of the current limitations that mice pose. In particular, regarding the number and size of bone grafts that can be tested simultaneously at orthotopic locations, and allowing the evaluation of 4 grafts per mouse, each containing a 50 mm³ bone defect. By contrast, previous mouse critical-size defect models were reported as single 3 mm length defects (<3 mm³) [224], while double calvarial defects were produced by drilling two 3.5 mm diameter defects (<3.4 mm³, as calculated from the values provided in [225]). By comparison, our model is closer to the orthotopic bone defect sizes used in rabbits (70 – 100 mm³) [226-229]. With our new model, we have the added beneficial capability of not only testing bigger constructs in mice –allowing to replace larger animals for smaller ones in specific set-ups– but also having controls within the same animals as a treatment condition, thus reducing inter-animal variability and potentially the number of animals required. Moreover, the ectopic location of the four testing units constitutes a refinement of the current orthotopic surgeries, since the implanted constructs lack functional pain receptors and the animal locomotion remains unaffected. An additional advantage of our model is the possibility to generate micro-CT scans *in vivo*. As the same animal can be imaged at different time points, this limits the number of animals needed and enables the use of image registration to increase the sensitivity of the results. It should be noted that in this study a relatively low threshold was used (335 mgHA/ccm) that not only segments bone but also low-mineralised tissue. Using this low threshold makes the model more sensitive for the detection of mineralisation in the defect region, but also results in an overestimation of trabecular thickness and the bone volume fraction in the ring of

original bone. It would be possible, however, to use a dual-threshold to differentiate between low-mineralised and fully mineralised bone.

The capacity of a human bone construct to initiate its regenerative program *in ovo* was demonstrated by Moreno-Jimenez *et al.* [230], in a system limited to a one-week time frame. In our model the time frame was extended to 8 weeks, since bone formation is commonly assessed over a time frame of 8-12 weeks [205]. This allowed us to replicate four freshly created bone defects, with the ability to produce a rapid interaction and response to a variety of bone grafts. Similar models include an osteochondral model aimed at assessing cartilage repair developed by colleagues in our group [231], while another group recreated a necrotic bone defect environment to study bone repair [232-234]. However, since the osteochondral model contained both bone and cartilage tissues, its complex cellular cross-talks prevented analysis of the specific contribution of the bone fraction. In the second case, the bone construct did not replicate an osteoinductive bone microenvironment at the moment of implantation, the model required a complex surgery and was limited to one construct per animal. It is worth noting that in all these models, ours included, bone formation occurs in non-mechanically loaded environments, which are important factors during of skeletal regeneration [235]. However, all large bone defects in humans and animals require some kind of mechanical stabilisation/fixation in order for healing to take place. For this reason, our model best replicates these type of clinical situations.

In our model, constructs were created by sandwiching a bone ring between two PTFE caps, in order to create a core region only accessible for cells passing through the trabeculae of the bone ring. PTFE membranes are clinically used for alveolar ridge preservation [236], their biocompatibility is comparable to that of collagen membranes [237] and the beneficial effect on bone repair is mostly achieved by physically excluding unwanted connective tissue from the defect site. While we expect that this physical effect was key in producing a hypoxic bony microenvironment, depending on the scientific questions the absence of membranes or the use of alternative ones might allow to study different aspects relevant to bone regeneration, such as blood vessel attraction and invasion.

Vascularisation is a key event during bone formation. In the model for the necrotic bone mentioned above [34-36], angiogenesis was initiated in a comparable shaped devitalised bone ring construct by placing an arteriovenous bundle inside. The construct was then isolated from the surrounding tissues with a silicon-based membrane, causing vascularisation to occur from the inside outwards. However, the lack of peripheral vascularisation limited bone formation [232]. Since in our model the bone ring was not connected to the mouse blood supply at the moment of implantation, re-vascularisation occurred from the outside inwards, eventually reaching the whole volume of the construct. We thus hypothesised that the construct's core transiently accommodates a microenvironment with reduced oxygen, comparable to that present in a freshly-created

bone defect. Studying the process and timing of revascularization and its possible implications for bone repair would be interesting for future experiments.

Due to the xenogeneic nature of the constructs, immunodeficient NMRI-*Foxn1* knock-out mice were used to prevent an immune rejection. These mice lack the T cell component, while maintaining the rest of immune system lineages. Although the T cell component plays a role in bone formation [238-240], our model unfortunately excludes this variable. On the other hand, these mice still possess macrophages and neutrophils, which allows several inflammatory processes relevant to callus formation during bone healing such as macrophage polarisation and their interaction with blood vessels to be studied [241-243].

To validate this new model, we tested several types of graft commonly used in the clinic and in small animal defect models. Clinically, the use of bone chips is the gold standard for the treatment of bone defects, thanks to their osteoinductive, osteoconductive and osteogenic properties. For this reason, a bone chip-based graft was first tested, and our observations of bone formation, bone resorption and vascularisation, indicated active remodelling of the graft. Next, we tested a tissue engineered strategy in order to further validate the model. When chondrogenically differentiated MSC pellets were added, whose ability to undergo endochondral ossification is known to occur even in the absence of a bony environment [244], we observed that the pellets ossified as well as the regions within the defect between the pellets. This observation highlighted the ability of the ring to osseointegrate the graft contained inside independent of its shape. The collagen-based scaffolds used are known to ossify ectopically when harbouring chondrogenically differentiated MSCs [245]. However, when comparing the scaffolds, with and without cells, we observed that both scaffolds ossified to comparable levels, which matched the previous observation in rat calvarial defects [218, 219]. Since the bone ring demonstrated the capability to initiate and sustain the ossification of its core, we further validated the model by assessing permissiveness to ossification of two grafts. On one hand, vital cartilage resisted calcification, as has been reported previously [246, 247]. On the other hand and in line with the expected permissiveness to vascularisation described by Eisenstein *et al.* [221], the treated cartilage constructs permitted ossification as seen by the mineralised tissue, blood vessels and marrow formed inside. This observation further opens the possibility for our model to be used in studies that assess cartilage integrity. For all of this, we concluded that the bone microenvironment generated in the construct matches that of orthotopic *in vivo* models. Newer bone grafts formulations with improved properties are continuously being developed, based on natural and synthetic materials such as calcium phosphate-based fillings, bioactive glass, ceramics, or devitalised bone [248]. Thus, the semi-orthotopic bone presented here could be used to study and improve the osteogenic properties of those graft formulations such as cellular ingrowth capacity, stability and degradability, ability to osseointegrate or to induce bone formation.

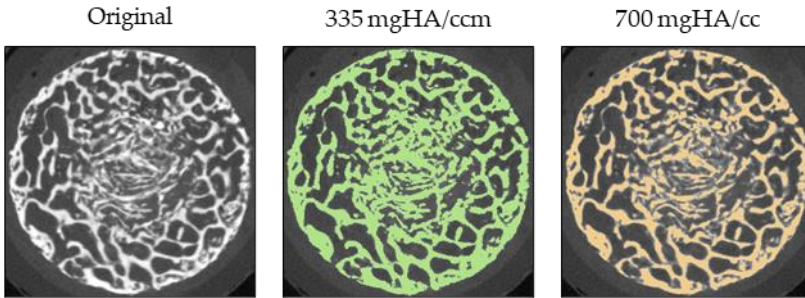
CONCLUSION

In this study we conclude that the semi-orthotopic model developed recapitulates the graft-mediated healing response of a critical size bone defect, to a level accurate enough to make it suitable as a bone graft screening platform. Therefore, the model could be of interest in further experiments that study the interaction between the bone microenvironment and biomaterials (e.g., metal implants, a variety of scaffolds), which may contain bioactive substances (e.g., growth factors, drugs or small molecules including genetic cargos) and/or cells (stromal cells, osteoblasts, etc.). Although we focused on the main outcome of bone formation of our model, further uses could be extended to situations where the cellular interactions with a bone microenvironment are key, as in the case of bone tumours. In addition, future modifications of the model may consider including micro-CT-based quantitative measurements of vascularisation, even in combination with mouse reporter strains.

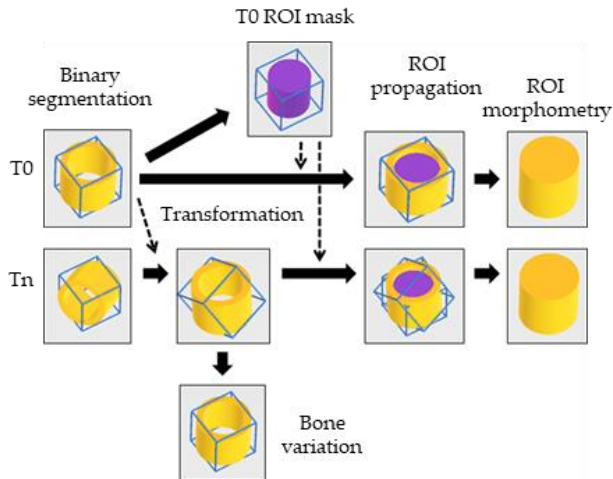
ACKNOWLEDGEMENTS

This work was supported through the use of imaging equipment provided by the Applied Molecular Imaging Erasmus University Medical Center facility.

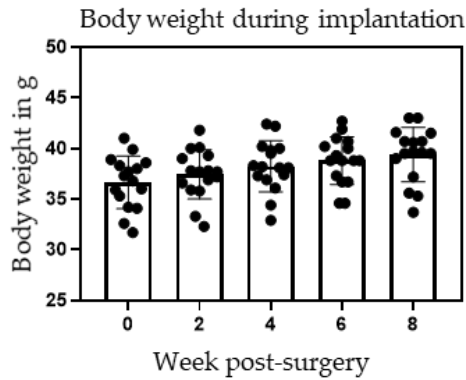
SUPPLEMENTARY DATA



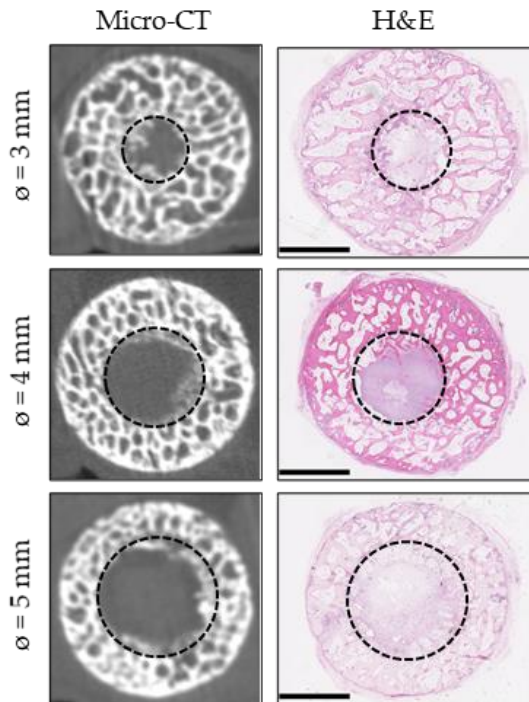
Supplementary Figure 1. Tissue density threshold selection. The selection of a consistent, global 335 mgHA/ccm threshold to quantify tissue calcification was performed qualitatively, and included the signal given both by fully mature bone and lower mineralised tissues. As a reference, the 700 mgHA/ccm threshold shown illustrates only the fully mature bone.



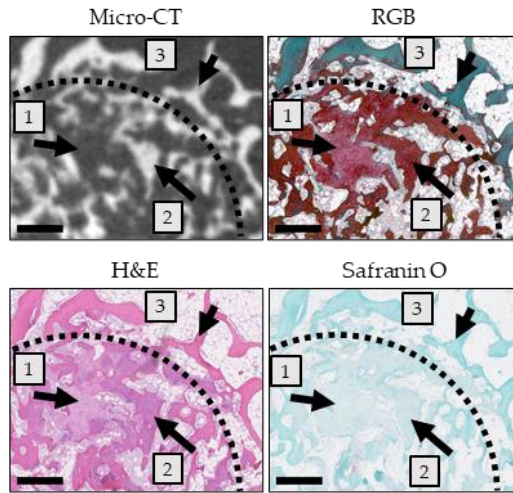
Supplementary Figure 2. Algorithm for automated segmentation and analysis of longitudinal scans of the bone constructs. The initial scan is binary segmented first (T0). Subsequently, after binarization, each follow-up scan (Tn) is transformed (reoriented) to maximise overlap with T0, thanks to the matching trabecular microarchitecture. 3D overlays are generated by aligning T0 and Tn pairs, allowing the visual representation of the bone variation in time. Then, T0 is used to create the time 0 region of interest (T0 ROI mask), corresponding to the defect volume. Next, the T0 ROI mask is propagated to all the transformed scans of the time series. Last the bone morphometric parameters of the volume defined by the ROI are evaluated.



Supplementary Figure 3. Weight variation of the mice during the duration of the experiment. 16 mice were used in total.



Supplementary Figure 4. Bone formation in constructs with defects of different diameter, 8 weeks after subcutaneous implantation in mice, assessed by micro-CT and H&E histology. N=4 constructs per condition. Dotted circles indicate the initial diameter of the defect. Scale bar: 2.5 mm



Supplementary Figure 5. *Correlative micro-CT and histology.* 1 unmineralised matrix. 2 calcified matrix. 3 mature bone. Dotted lines indicate the inner edge of the bone ring. Scale bar: 500 μm

CHAPTER 5 ANNEX

TSP-4 potential for bone regenerative therapies

ABSTRACT

Introduction

As the main constituent of the bone ECM, collagen type I (Col-I) has been used by bone tissue engineers as scaffolding material to guide bone regeneration, thanks to its great biocompatibility, osteoconductivity and moldability. In order to better mimic the bone microenvironment, these scaffolds have been incorporated with hydroxyapatite (HA), the major mineral component of the bone and functionalised with bioactive molecules to induce bone formation [249]. Among them, it is worth highlighting bone morphogenetic protein 2 (BMP-2) and vascular endothelial growth factor (VEGF), since their osteoinductive and proangiogenic abilities are key for this process.

As described in the Chapter 2 of this thesis, the multifunctional TSP-4 is an ECM protein present during developmental bone formation and fracture repair, and its expression precedes ossification. The proangiogenic activity of TSP-4 [83, 84] combined to its natural ability to bind collagen [77], makes TSP-4 an attractive alternative to VEGF –which lacks this collagen binding ability– to functionalise collagen-based scaffolds. Vascularisation is a key step in bone formation [250] and a challenge on which tissue engineering strategies have to succeed [251]. In addition, TSP-4 controls matrix assembly during tissue repair [78], modulates the TGF β -SMAD signalling pathway [67, 252], and –as found in the Chapter 3 of this thesis– it can stimulate the matrix production of chondrocytes, all of which are important steps during bone formation. For all the above, we hypothesise that bone formation might be promoted *in vivo* by TSP-4 when used in combination with a Col-I scaffold that has been functionalised with hydroxyapatite (ColHA). For this, we make use here of the semi-orthotopic bone formation model developed at the beginning of this Chapter to assess if such a TSP-4 functionalised scaffold may improve the healing of a critical-size bone defect.

MATERIALS AND METHODS

Fabrication of collagen-hydroxyapatite scaffolds

To fabricate highly porous collagen-based scaffolds, a lyophilisation method previously described by O'Brien FJ *et al.* was used [210]. Type I collagen-GAG scaffolds composed of type I collagen derived from bovine Achilles tendon [Collagen Matrix, USA] and hydroxyapatite (HA) particles [Sigma-Aldrich, Ireland] were added to the

collagen scaffold. Collagen-HA slurry was prepared by dissolving 1.8 g collagen and 3.6 g of HA in 360 ml of 0.5 M acetic acid as described to yield slurry with a final concentration of 0.5% (w/v) collagen and 1% (w/v) HA. Subsequently, 0.3 ml of the slurry was pipetted into a stainless-steel tray (internal dimensions: 9.5 mm diameter and 4 mm height) before being freeze-dried [Virtis Genesis 25EL, Biopharma, UK] at a constant cooling rate of 1°C/min to a final temperature of -40°C. Next, the porous scaffolds were dehydrothermally crosslinked in a vacuum oven [VacuCell, MMM, Germany] for 24h at a pressure of 0.05 bar and temperature 105°C.

Preparation of the bone ring constructs containing TSP-4

Bone rings were prepared from freshly harvested distal epiphyses of the metacarpal bones of 3 to 8-month-old calves, which were purchased from a slaughterhouse and processed within 5 hours. To produce the rings, the metacarpophalangeal joint (MCP) was opened, and the cruciate ligaments sectioned, to expose the articular cartilage surfaces. Next, 10 hollow cylindrical osteochondral plugs per bone were drilled by using an 8 mm diameter trephine drill [MF Dental, Weiherhammer, Germany] in which a central canal was drilled using a 4-mm steel drill. Tissue damage was minimised by avoiding the heating of the explant though low speed drilling and simultaneous cooling with sterile PBS. Then, 4 mm height rings were made by removing the articular cartilage and the proximal bone ends using a circular table saw. In this way, 8-mm diameter x 4-mm height bone rings were obtained. Next, the bone rings were transferred to 12-well plates containing α -MEM supplemented with 10% v/v FBS, 100 μ g/mL gentamycin and 3 μ g/mL amphotericin B [all from Thermo Fischer, Bleiswijk, The Netherlands] and incubated overnight in a humidified atmosphere at 37 °C and 5% CO₂. The following day, immediately before implantation, the core of the rings was filled with the dry scaffolds and rehydrated *in situ* with a saline solution (0.90% w/v of NaCl) containing or not 10 μ g of recombinant full-length TSP-4, which was produced according to Crosby *et al.* (2015) [91] and supplied by our collaborator F. Zaucke [Orthopaedic University Hospital Friedrichsheim, Frankfurt/Main, Germany]. The top and bottom ends of the rings were closed with two circular 8 mm diameter dense polytetrafluoroethylene membranes (dPTFE) [PermaMEM®, Botiss biomaterials, Zossen, Germany], to prevent direct in-growth of host cells into the testing pocket and fastened with a single 6-0 non-resorbable polyamide suture Ethilon® [Johnson & Johnson Medical, Livingston, UK]. (Fig. 1A, B). The viability of the explants at the moment of implantation was assumed, since previously observed that comparable explants obtained in a similar manner remain viable *in vitro* for one month [208].

Surgical implantation procedure and longitudinal micro-CT imaging.

Animal experiments were conducted in the experimental animal facility of the Erasmus University Medical Center with approval of the local animal ethics committee (under licence number 101002015114 and protocol number 15-114-09), which comply

with EU Directive 2010/63/EU, and were reported in compliance with the ARRIVE guidelines. The surgical procedure was performed on 10- to 14-week-old male immunodeficient NMRI-Foxn1 nu/nu mice purchased from Janvier [Le Genest-Saint-Isle, France]. This strain has previously been shown to be capable of hosting similar xenogenic implants [211-213]. 6 mice were used in total. This included experimental conditions from another study whereby the same control conditions were used in order to reduce total animal numbers. Of the 24 available subcutaneous pockets in these 6 mice, 12 pockets were used specifically for the study reported here. Mice were housed in groups of 3 and 4 in individually ventilated cages, and food was provided *ad libitum*. To avoid peri- and post-operative pain, mice received 0.05 mg/kg body weight of buprenorphine [Reckitt Benckiser, Hull, UK] 1 hour before the operation and 6-8 hours after implantation. The operation was performed under isoflurane inhalation anaesthesia. During the procedure, four incisions were made on the back of each mouse to create four subcutaneous pockets, where four constructs per mouse were placed bilaterally with respect to the thoracic and lumbar vertebrae. No blinding was performed, and each mouse received both the treatment and the control conditions. After construct placement, 4-0 non-resorbable polyamide suture Ethilon® [Norderstedt, Germany] was used to close the wounds. While still under anaesthesia, the four implants were scanned by micro-CT [Quantum GX, Perkin Elmer, USA], with a 36 mm Field of View (FOV) and 72 µm isotropic voxel size. After the scan, the sutures were immediately replaced by clips [AutoClips®, Fine Science Tools, Heidelberg, Germany], since the clips would otherwise introduce artifacts into the scan, and the mice received an injection of 25 mg/kg of ampicillin [Dopharma, Raamsdonksveer, The Netherlands]. The clips were removed 8-10 days after the operation, when the wounds had healed. At 2, 4, and 6 weeks after the surgical procedure, mice were scanned again under isoflurane anaesthesia. After 8 weeks, mice were sacrificed by cervical dislocation under isoflurane anaesthesia, scanned again and the constructs retrieved. The bone rings were fixed in 4% buffered formalin at room temperature for one week. During fixation, the caps were removed and the constructs were scanned again by the micro-CT for 4 minutes with a FOV of 18 mm and 36 µm isotropic voxel size. During the entirety of the experiment, the health condition of the mice used was closely monitored, and a humane endpoint was established if there was a drop in body weight of 15% in 2 days or 20% from the moment immediately after implantation. Moreover, the exclusion of all constructs from analysis was set up *a priori* if the humane endpoint was reached. No signs of distress were evident, all the mice survived and all the conditions intended for this study were included for analysis.

Micro-CT analysis

Bone morphometric analysis of the high resolution DICOM images generated was performed using specialised micro-CT software [SCANCO Medical AG, Brüttisellen, Switzerland]. Phantoms of known densities (0.25 g/cm³ and 0.75 g/cm³) were scanned in parallel and used to convert pixel intensity into mineral density. To assess the total bone

volume of each construct, the bone defect region was manually segmented from the neighbouring tissues. The resulting grey-scale images were Gaussian filtered with sigma of 0.8 and a support of 1 voxel, and the signal above a density threshold of 335 mg HA/ccm was considered as bone and used to produce binary images. Then, the bone morphometric parameter bone volume (BV) was evaluated using a three-dimensional analysis software [Image Processing Language, SCANCO Medical AG, Brüttisellen, Switzerland].

Histological assessment

After fixation, the constructs were decalcified in 10% w/v ethylenediaminetetraacetic acid (EDTA) pH 6.8-7.2 at room temperature for 4-5 weeks, where the EDTA was refreshed twice weekly. Subsequently, the samples were embedded in paraffin and 6 µm thick sections were collected for histology at different depths. Before histological assessment, sections were deparaffinised using a series of xylene, graded ethanol (100%, 96% and 70%) and distilled water.

H&E Staining. The histological sections were stained with Gill's haematoxylin [Sigma-Aldrich] for 5 minutes and incubated in 2% w/v eosin [Merck, Amsterdam, The Netherlands] in 50% v/v ethanol and 0.5% v/v acetic acid for 45 seconds. The sections were incubated in 70% ethanol for 10 seconds and afterwards dehydrated in 96% ethanol for 1 min, 100% ethanol for 1 min and two times xylene for 1 min, after which they were mounted with DPX, coverslipped and dried overnight at 37°C before imaging.

RGB Staining. RGB trichrome staining was performed as described by Gaytan F *et al* [216]. Briefly, sections were dewaxed using xylene and graded ethanol, rinsed in distilled water and stained for 20 minutes in 1% w/v Alcian Blue 8GX [Sigma] in 3% v/v acetic acid at pH 2.5. Then rinsed in tap water, followed by 20 minutes 1% w/v Fast Green [Sigma] in distilled water. Then, they were rinsed for 5 min in tap water, followed by 30 min 1% w/v Sirius Red [Direct Red 80, Sigma] in a saturated aqueous solution of picric acid. Then sections were carefully rinsed twice in 1% v/v acetic acid (3min each wash), followed by dehydration in subsequently 100% Ethanol (2x) and two times in Xylene. Slides were covered with DPX, coverslipped and dried overnight at 37°C before imaging.

Image acquisition

Composite tile scans from stainings were obtained with a NanoZoomer HT microscope (C9600-12) using the software NDP.scan v2.5.90 [Hamamatsu Photonics]. Hue and brightness were adjusted after acquisition using Adobe Photoshop CC 2018, following the recommendations described by Sedgewick [89].

Statistical analysis

Each construct was treated as a separate unit for means of measurement, independently of the position and the identity of the host mouse. Mice were considered as carriers of the constructs, and their interindividual variability assumed to play a negligible role into the construct's response to the presence of TSP-4. Single terminal time point data was compared via Mann-Whitney two-tailed test. A p-value of <0.05 was considered significant. GraphPad Prism (version 8.0.1 for Windows, GraphPad Software, La Jolla, California USA) was used to perform the statistics and to create the graphs.

RESULTS

TSP-4 does not significantly improve bone formation in the semi-orthotopic bone defect model

In order to investigate if the addition of TSP-4 into a Col-HA scaffold could promote bone formation, we compared in the semi-orthotopic bone defect model the Col-HA scaffold functionalised with and without 10 µg of recombinant TSP-4. After 8 weeks, bone formation had taken place inside the ring defect in both conditions, and most of the defect volume contained mineralised tissue (Fig. 1A). The quantification of the mineralised tissue revealed no statistically significant differences between the groups, suggesting that bone formation was not improved in the semi-orthotopic model by TSP-4 at the 8-week time point (Fig. 1B). The histological analysis confirmed the presence of the mineralised tissue at the defect site, and the active healing of the bone and the lack of difference between the two groups (Fig. 1C).

DISCUSSION

In this study, the bioactive properties of TSP-4 were investigated *in vivo* in the semi-orthotopic model for bone formation. In our experimental set-up the addition of TSP-4 to the ColHA scaffold did not significantly improve the amounts of bone formed. Here we selected a time frame of 8-weeks to allow bone formation, since in most models for bone regeneration bone formation is commonly assessed over a time frame of 8-12 weeks [205], and in order to share as controls and by having comparable times to those other grafts studied in Chapter 5. During this 8-week period of time, while vast amounts of calcified tissue formed at the defect site, the histological analysis indicated immature bone derived from cartilage undergoing endochondral ossification. This observation confirmed closing of the defect, although at this point in time, only small amounts of mature bone had already formed at the defect. This suggests that exogenous TSP-4 might at least not improve cartilage mineralisation. Therefore, the question whether TSP-4 might play a pro-osteogenic role later at the ossification stage remains open and would be interesting to be addressed in future studies. It is important to consider that, as found

in Chapter 2, TSP-4 is endogenously produced at different stages of fracture healing (in special at the cartilaginous callus), which might hinder the effects of exogenous TSP-4. Therefore, focussing attention to separate processes such as the degree of vascularisation during early stages of healing, the amounts of transient cartilage formed, and the final quality of the resulting bone would need to be considered. The use of contrast agents to quantify the degree of vascularisation by micro-CT and to combine it with a systematic quantitative analysis of the histology would be of interest. Finally, the use of other collagen-based scaffold formulations, and the addition of molecules that could act synergistically with TSP-4 such as proteins of the TGF- β superfamily, may significantly alter the effects caused by TSP-4 in bone formation, and should be evaluated in the future.

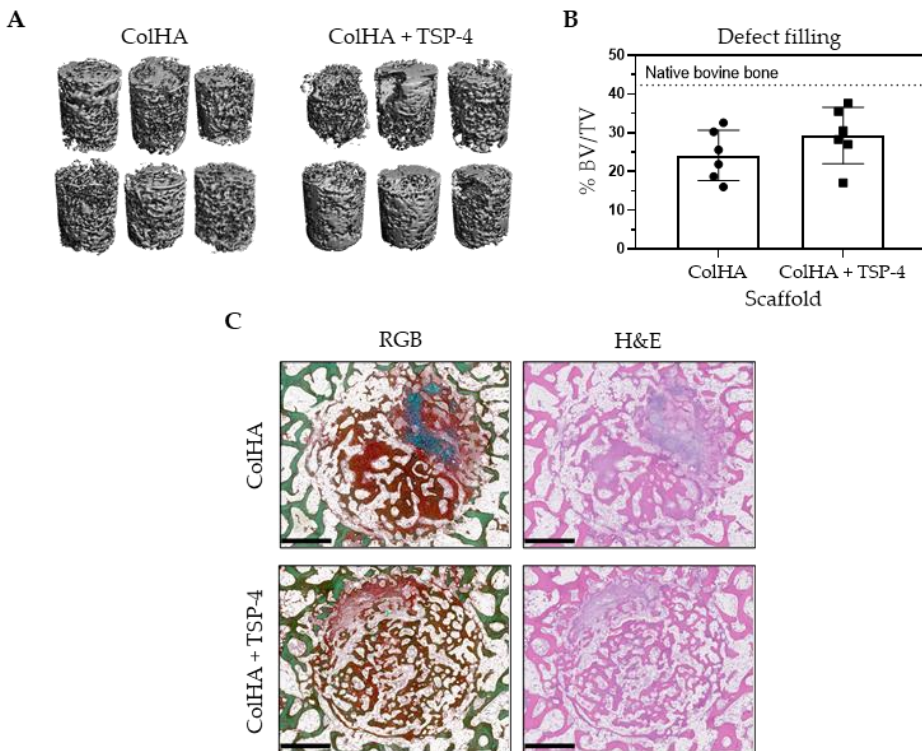


Figure 1. Functionalisation of a Collagen-HA scaffold with TSP-4. (A) Micro-CT 3D image reconstruction of the defect post-implantation. (B) Quantification of mineralisation per volume unit (% BV/TV) inside the defect 8 weeks post-implantation. Bars indicate the SD. (C) RGB and H&E-stained scaffolds showing the healing defects post-implantation. Scale bars: 1mm.

CONCLUSION

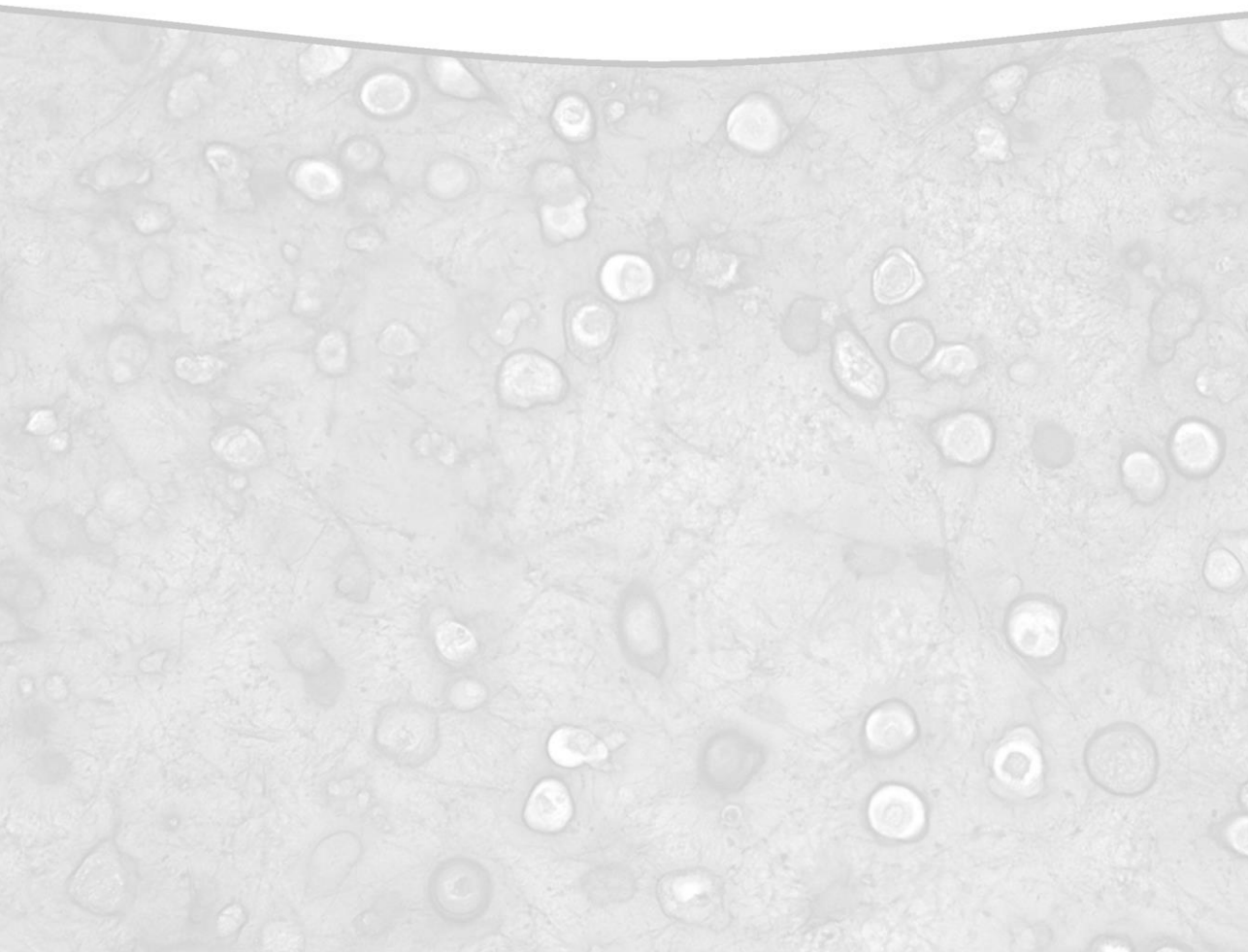
In this study we used the semi-orthotopic bone formation model developed at the beginning of this Chapter 5 to evaluate whether bone formation can be promoted by TSP-4, when used in combination with a collagen type I scaffold that has been functionalised with hydroxyapatite (ColHA). Unfortunately, we did not observe a significant improvement in bone formation after 8 weeks when TSP-4 was present. Further research on the role that TSP-4 plays in bone formation will be necessary to assess potential of TSP-4 for bone tissue engineering.

ACKNOWLEDGEMENTS

This work was supported through the use of imaging equipment provided by the Applied Molecular Imaging Erasmus University Medical Center facility.

CHAPTER 6

General discussion and conclusions



OVERVIEW

Mobility is crucial for human quality of life. However, different traumatic injuries and diseases of the skeletal system affect many people's lives and restrict their mobility. After a traumatic injury, the resection of bone tumours or infections, patients might be left with bone containing large defects that are unable to heal due to the size of the injury. These are serious complications, for which no effective treatments are available, that result in permanent disability and reduce the quality of life. To improve the therapeutic options, bone graft substitutes are being engineered to promote the healing by increasing the bone formation in fractures, bone defects and around surgical implants. To achieve this, bone tissue engineers make use of the intrinsic and extrinsic elements that induce bone formation during skeletal development and regeneration, in order to provide them to the patient. One of the components to replicate is the ECM, which provides support and guidance to the regenerative process. During skeletal development, the repair of bone fractures and certain pathological conditions, a transient cartilaginous ECM is generated, which directs bone formation via the process of endochondral ossification. Although many proteins and other factors present at the transitional cartilage matrix have been identified, their functions during bone formation are still largely unknown. For this reason, understanding the composition of the matrix and the role of its components during bone formation and repair is a key step necessary to replicate the 3D environment for better bone repair.

The aim of this thesis was to assess the role that two extracellular matrix proteins of the family of thrombospondins, TSP-4 and TSP-5, play in the skeletal system to later explore their potential therapeutic potential to modulate bone formation. For this reason, in **Chapter 2** I investigated what is the spatiotemporal location of these two proteins during physiological bone formation and fracture healing and evaluated how their presence may contribute to these two processes. Next, in **Chapter 3** I further explored the production and roles of TSP-4 and TSP-5 in the context of OA, since pathological bone formation is an etiological feature of this disease. Following this line, in **Chapter 4** I assessed the ability of three peptide fragments derived from TSP-5 to trigger responses observed during OA, some of which are related to EO. Then, in **Chapter 5** I proceeded by developing a novel semi-orthotopic bone defect model for bone formation *in vivo*, through which I concluded my work by assessing if a collagen-based biomaterial functionalised with TSP-4 could be capable of promoting bone formation. Last, here in **Chapter 6** I summarise and discuss the findings of this work, and present the conclusions and the future perspectives for research.

IDENTIFYING MATRIX FACTORS RELATED TO BONE FORMATION

The ECM is an essential component of the skeletal system. Among its multiple roles, it provides mechanical strength, mediates cellular interactions, and serves as storage of

growth factors [253]. To guide bone regeneration, tissue engineers aim to produce bone grafts that replicate a set of matrix features. For this, scaffolding materials such as demineralised bone matrix, collagen sponges or synthetic polymers can be used [24]. Then, in order to induce their transformation into bone, the scaffolds are further functionalised with ECM components, most of which are naturally found in the bone matrix and the cartilage matrix undergoing ossification. Examples of such components include chondroitin sulphate, hydroxyapatite, BMP-2 or VEGF [254]. By combining scaffolding elements and bioactive factors, their individual properties (structural support, osteoinduction, vasculogenesis, cell anchoring, etc.) can be exploited to guide regeneration. In practical terms, it is desirable to have a small number of components which can potentially induce bone regeneration. For example, the use of BMP-2 in combination with a collagen sponge has been used for specific clinical applications for bone regeneration. However, this necessitates the use of supraphysiological doses over a million times the physiological conditions, to compensate for the lack of the other components and comes with drawbacks [27]. For this reason, there has been an effort to find additional components to fine tune a formula for bone regeneration, taking into account their combined interactions and evolution on time.

The family of thrombospondins has been related to different functions in the skeletal system [38] and thus, constitutes a source of bioactive elements which can be potentially used in bone tissue engineering strategies. Graft vascularisation for example, is one of the things that bone tissue engineers aim to achieve. TSP-5 is produced at the cartilage matrix during endochondral ossification [70, 71] but no angiogenic function has been attributed to the protein. In 2010, Jeong BC *et al* improved bone formation by using a fusion protein composed of TSP-5 and angiopoietin-1 [255], which is a growth factor that can stabilise vasculature. Later, in 2016 Refaat M *et al* used a combination between a full-length TSP-5 and BMP-2, since the latter protein binds to TSP-5 and has both pro-osteogenic and pro-angiogenic functions [256]. When tested *in vivo* on a rat spinal fusion model, they found that TSP-5 was capable of promoting BMP-2 activity, thus lowering the amounts of BMP-2 protein required to achieve *de novo* bone formation. In order to better understand the biological role of the thrombospondins in bone, in this thesis I explored the skeletal function of TSP-5 and expanded the knowledge of its close relative TSP-4 from which not much was known in the skeletal system. Remarkably, this latter protein is the only known proangiogenic thrombospondin [84] and has already proven useful to promote therapeutic angiogenesis in brain ischaemia [257]. When assessing the spatiotemporal location of TSP-5 during bone development, I confirmed the previous descriptions [70, 71] and concluded that TSP-5 is associated with the formation and maintenance of the cartilage matrix template (**Chapters 2 and 3**). In fact, TSP-5 apparently disrupted vascularisation (data not shown, [196]). When further analysed in the context of osteoarthritis, disease-specific fragments of TSP-5 released during cartilage remodelling did not seem to possess any significant bioactive function (**Chapter 4**), such as those previously identified from the other ECM proteins aggrecan or fibronectin [179-181]. Regarding TSP-4, its presence during bone formation had been

previously noticed [81, 93], but the localisation and function of the protein during bone formation and skeletal healing were still unknown. In **Chapters 2 and 3** TSP-4 was found to emerge in the matrix immediately before ossification takes place –both during intramembranous and endochondral bone formation–, and also in osteoarthritic cartilage, which is known to recapitulate endochondral ossification. These findings expanded to the skeletal system the previous knowledge that TSP-4 is associated with tissue remodelling [66], both during development and disease. Due to its natural proangiogenic properties and presence in areas in which bone is being deposited, I hypothesised that TSP-4 could constitute a bioactive factor superior to TSP-5 to be used in bone tissue engineering strategies.

There is however no general regulatory mechanism that explains how the differential expression of TSP-4 and TSP-5 occurs [258]. In the case of TSP-5, both its *Comp* gene transcripts and protein increase rapidly after TGF- β stimulation, as previously reported [190]. For TSP-4 however, this appears to be more complex since an increase in the protein expression does not necessarily correlate with an increased transcription of its gene *Thbs4*. In **Chapter 2**, fracture healing measurements indicated that *Thbs4* mRNA synthesis is rapidly upregulated following a skeletal injury, which is accompanied by the production of TSP-4. Nevertheless, in **Chapter 3** it was shown that the levels of TSP-4 increase in osteoarthritic cartilage while its mRNA levels remain unchanged. Furthermore, when comparing TSP-4 and TSP-5, I observed that BMSCs undergoing hypertrophic chondrogenic differentiation *in vitro* (such as those used in **Chapter 5**) quickly upregulate the expression of TSP-5 upon TGF- β stimulation, while their TSP-4 mRNA levels are barely affected (data not shown). These observations are supported by previous research in endothelial cells, which attributed the mRNA-protein disparity to a regulatory mechanism at the level of protein stability [67]. For this, it can be hypothesised that specific tissues constitutively produce TSP-4 without accumulating the protein, so in the event of injury the protein can be rapidly available while preventing to trigger its intracellular functions. When possible, it would be advisable to complement gene expression analysis with additional proteomic and/or immunohistochemical analysis.

TSP-4 AND TSP-5: SIMILAR BUT NOT EQUAL

TSP-4 and TSP-5 share common mechanisms of action through the binding of several collagens [143], integrins [66, 96], notch receptors [101, 187] or TGF- β (TSP-5 in [75], TSP-4 first described in **Chapter 3**) thanks to their structural similarities [259]. On the other hand, they differentially bind relevant cartilage ECM proteins such as type IX collagen (TSP-5 binds Col-IX [161] but TSP-4 does not [163]). Moreover, depending on the context TSP-4 and TSP-5 elicit both similar and opposing cytological responses such as on cellular attraction. In **Chapter 2** TSP-4 but not TSP-5 attracted vascular cells, while none of them attracted BMSCs. In **Chapter 3** chondrocytes depleted from their ECM attached to TSP-5 but not TSP-4 confirming previous findings [97], and it was revealed that the chondrocytes migrated exclusively towards TSP-5. The reason for such

differences could be the specific set of ligands present on the cellular surface, such as CD36 or different integrin subsets. Further differences extend to when the two thrombospondins are complexed with other proteins. As found in **Chapter 3**, both proteins can induce similar levels of ERK phosphorylation in chondrocytes. However, when complexed with TGF- β it can be interpreted from the results that TSP-5 enhances ERK signalling in chondrocytes, while TSP-4 decreases the signalling. In addition to these differences, each thrombospondin can elicit cell-specific responses that can be opposite. In the case of TSP-5, when complexed with BMP-2 the SMAD signalling pathway in vascular smooth muscle cells was inhibited reducing their calcification [164]. However, this same TSP-5 + BMP-2 complex increased the SMAD signalling in myoblasts driving them to osteogenic differentiation [74]. In conclusion, it is evident that TSP-4 and TSP-5 exert differential effects over different cell types. All these differences may be increased further when taking into consideration that alternative splice variants of the two proteins exist [260], and that through limited proteolysis, specific domains of the proteins are naturally split and released into the matrix, as occurs with TSP-5 [183]. However, the functions of these variants are poorly understood, and would be an interesting topic to be further investigated.

THE ROLES OF TSP-4 AND TSP-5 IN BONE FORMATION

Prior to the studies presented in this work, the skeletal-specific functions of the two thrombospondins –TSP-4 in particular–, were poorly understood. In **Chapter 2**, it was shown that TSP-4 and TSP-5 are expressed at different stages of endochondral ossification. As previously mentioned, and according to **Chapter 3**, TSP-5 appears to contribute mainly to the formation and maintenance of the cartilage matrix template, where it functions to promote growth factor activity, collagen fibril formation and the secretion of its own ECM ligands [69]. In their journey towards hypertrophy, chondrocytes begin to produce TSP-4, which co-locates with TSP-5 at the chondrocyte periphery. Thus, it can be hypothesised that both proteins act in concert to enhance further the matrix production, which comes with chondrocyte hypertrophy [35]. As shown, when bound to a growth factor such as TGF- β , TSP-4 may modulate the intracellular signalling in an opposing manner to TSP-5, likely contributing to the phenotypic changes towards hypertrophy. Previous research also suggested that intracellular TSP-4 might positively regulate chondrocyte hypertrophy [261] by binding to the transcriptional factor ATF6 α and promoting its translocation to the nucleus [262]. Last, the TSP-4 incorporated to the matrix may act in a paracrine fashion to promote vascularisation, in which TSP-5 is not expected to play a significant role.

Interestingly, in **Chapter 2** TSP-4 but not TSP-5 was found to be produced during intramembranous ossification but in a different cell type –apparently, mesenchymal osteoprogenitor cells–. In this modality of ossification, it might contribute to structure the cranial suture by organising its collagenous matrix fibers, such as collagen type I and collagen type III [77, 263]. Furthermore, it may tune the specific signalling of the cells

present by modulating the functions of factors of the TGF- β superfamily [263] and Notch pathway [101, 264]. TSP-4 could therefore be involved in maintaining the patency of the cranial sutures, thus promoting the skull growth. Supporting this hypothesis, previous research found that TSP-4 expression can induce cellular proliferation and stem-like properties [100], which would point at a function where TSP-4 would be contributing to the maintenance of the pool of progenitor cells of the suture. As discussed before, the gene and protein expression of TSP-4 do not always correlate and thus, further research aimed at investigating the premature closure of the cranial sutures (craniosynostosis) could benefit from incorporating proteomic data on their analysis.

Since the fracture healing process typically involves both the intramembranous and endochondral ossification pathways to generate new bone, it is no surprise to observe TSP-4 and TSP-5 coexpressed at the cartilaginous callus, and TSP-4 (but not TSP-5) at the activated periosteum, likely playing equivalent roles as those during developmental bone formation. In relation to TSP-4, future research should analyse in-depth which are the molecular events that trigger the *de novo* expression of TSP-4 at the periosteum, which could shed light on the process behind a cell committing to form bone. Furthermore, the hypothesis that TSP-4 could be related to skeletal stemness and its association to chondrocyte hypertrophy, could lead to improve the understanding for example on the molecular changes that a chondrocyte experiences in order to transdifferentiate into an osteoblast [6]. Last, even though the topic of cancer was not covered by this work, it would be interesting for further studies to investigate the link between TSP-4 expression in tumours and their bone metastatic behaviour. Previous research showed that breast cancer and prostate cancer cells –which have a high tendency to metastasise to bone– become more invasive when expressing TSP-4 [265, 266]. It is therefore possible that TSP-4 may mediate certain interactions between the cancerous cells and the bone microenvironment.

TSP-4 AND TSP-5 IN OSTEOARTHRITIC DISEASE: FRIENDS OR FOES?

TSP-5 is a common protein of the articular cartilage, known since 1994 to increase during osteoarthritic disease [182] and currently being used as a biomarker of joint destruction [183]. In 2019, Maly *K et al* observed that the levels of not only TSP-5, but also TSP-4, increase during the progression of osteoarthritis [65]. Because of their ability to promote matrix deposition, in **Chapter 3** it was hypothesised that the production of both thrombospondins could constitute an attempt to repair the cartilage and thus, that the two proteins could play a protective role during the disease. In particular, TSP-5 appeared to promote the anchoring and migration of chondrocytes depleted of their ECM, while in **Chapter 4** some of its degradation fragments did not appear to contribute to the progression of the disease. Intriguingly, TSP-4 is never expressed to such high levels in healthy cartilage, and as found in **Chapter 2**, the co-expression of TSP-4 and TSP-5 occurs naturally only in the cartilage matrix during developmental bone formation

and fracture healing. As previously hypothesised, the expression of TSP-4 may lead the chondrocytes to transition to a hypertrophic phenotype while promoting vascularisation in a paracrine manner [267], ultimately leading to ossification of the cartilage. For this reason, it is paradoxical to observe the presence of TSP-4 at the osteoarthritic articular cartilage during its attempts to self-repair. Since one of the hallmarks of osteoarthritis is the recapitulation of endochondral ossification [5], it is possible that on the long term, the sustained levels of TSP-4 interfere with the normal function of the articular chondrocytes. Following this hypothesis, TSP-4 could be thus part of the osteophyte formation mechanism seen during the disease [19, 20]. While the expression of TSP-4 during the early stages of osteoarthritis might help to stabilise the cartilage, the increased matrix production triggered by TSP-4 might indicate an underlying pathological progression towards chondrocyte hypertrophy. Taking all of this into account, while TSP-5 appears to have a protective role during osteoarthritis, the sustained expression of TSP-4 could have long-term harmful consequences. Since the two proteins play both overlapping and opposing roles, it would be interesting for further research to explore how the combined presence of TSP-4 and TSP-5 modulates the function and phenotype of the chondrocytes. Last, the potential value of TSP-4 as a biomarker for osteoarthritis should not be underestimated, since its increased presence in the adult articular cartilage could be revealing underlying pathological endochondral events.

TOWARDS A CLINICAL USE OF THE ECM

After the findings of **Chapters 2, 3 and 4**, I hypothesised that TSP-4 could be a good candidate to promote bone healing *in vivo*, and tested this hypothesis in the **Addendum to Chapter 5**. Under the experimental conditions investigated, I did not find a significant increase in the amount of calcified tissue formed in the presence of TSP-4. It can be deduced then that the sole incorporation of TSP-4 into a collagen-hydroxyapatite scaffold may not be sufficient to improve bone formation further than with the biomaterial alone. This however, was the first step in assessing the suitability of TSP-4 to support bone healing. Further research using the semi-orthotopic bone model should consider both measuring the formation of mature bone at timepoints later than 8 weeks, and the induction of additional damage in the bovine ring bone in order to pose a bigger challenge to its regeneration. As I will be discussing later, the model system had a limited number of readouts. Additional parameters, such as the quantification of vascularisation, transient cartilage present and mature bone formation, should be incorporated in the near future, and these could reveal beneficial effects of TSP-4. Once the isolated function of TSP-4 is assessed, it will be key to study possible synergistic effects with other known ECM components. As previously mentioned, TSP-5 in combination with BMP-2 resulted in an increased ossification in a spinal fusion model. Due to the structural similarities between TSP-5 and TSP-4, it is highly likely that TSP-4 interacts with BMP-2 to modulate its activity. For this, further research should investigate these potential synergistic effects on bone formation.

Part of this work has focused on identifying ECM elements that are involved in the generation of bone tissue, with the purpose of producing new bone graft substitutes that can support the healing of the bones. While many other proteins have been found to regulate bone formation too, it is important to always keep in consideration whether their incorporation into a biomaterial will have a significantly positive clinical effect. Every protein present at the transient cartilage ECM can be related to a greater or lesser extent to a set of steps in bone formation, and can likely influence a variety of cellular behaviours when studied *in vitro*. However, when the goal is set to functionalise a bone graft substitute to fine tune bone formation, proteins may not significantly alter the regenerative process, if they are produced endogenously in sufficient amounts. In fact, they may potentially interfere with the healing process if delivered at an inappropriate timing or spatial location. For this reason, an increasing interest has grown towards the use of materials capable of adapting to the changing microenvironment of the healing site (smart biomaterials) [268]. If properly designed, these materials offer the promise to orchestrate the release of the factors contained within on-demand in a timely manner. In the case of TSP-4 for example, this would allow better mimicry of the temporal release pattern occurring during the bone formation and bone healing process observed in **Chapter 2**. When generalised to all the other proteins present in the matrix, their controlled release would promote a more potent and consistent healing response, and contribute to reduce their side-effects.

OPTIMISING FURTHER THE TESTING OF BONE GRAFTS

As discussed, ECM proteins can play both overlapping and opposing roles, which heavily relies on the protein network they are embedded in and the context where they are produced. Thus, when assessing their functions and possible medical uses, the overwhelming number of routes by which they might act poses a great challenge to the researcher. For practical reasons and aiming to reduce complexity, once the protein under research has been purified, first steps will analyse its possible functions in 2D/3D *in vitro* cultures, such as those performed in **Chapters 2, 3 and 4**. Then, its role is further analysed *in vivo* in order to display its effects in a more complex environment. However, the current *in vivo* methodologies are far less efficient than *in vitro* techniques, and pose a big bottleneck to how many candidates can be tested [204], both due to ethical reasons and economical limitations. For this reason, in **Chapter 5** I aimed to improve the efficiency of the *in vivo* testing of osteogenic grafts, in a more refined and possibly more economical manner than other current *in vivo* models. There, by following a systematic approach, I showed that it is possible to recapitulate the simultaneous healing of four bovine bone defects, by implanting bony constructs containing said defects into a murine host. There is still plenty of room for improvement, and a few steps should be followed to further exploit this model. For example, more information could be extracted from each condition tested. First, by using double thresholds for bone volume quantification, low mineralised tissues such as hypertrophic cartilage could be distinguished from the

highly mineralised mature bone, as done by Moreno-Jiménez I. *et al* [230]. Second, measurements on the degree of vascularisation could be simultaneously performed through the use of contrast agents, as done by Epple C. *et al* [232]. Third, a quantitative analysis of the histological samples using artificial intelligence algorithms [269] could allow the systematic analysis of the structures generated in the samples at a cellular resolution. Once those additional readout features are implemented, it would be highly desirable to perform studies that evaluate the characteristics of the system based on the ICH method development (reviewed in [270]). In particular, it will be necessary to explore the linearity, range, accuracy, precision, detection limit, quantitation limit and robustness of the system. For this, it would be interesting to start by characterising the response to BMP-2, since it is the most broadly studied osteogenic drug used to induce bone formation. These validation experiments will be fundamental to help deciding for which applications is the model suitable, and to give an orientation on the number of experimental replicates necessary to test their hypothesis.

A few questions about the model remain, such as which are the individual contributions of each species to the chimeric formation of the bone, how do the model outcomes compare to other models, and how does the model evolve past the 8-week timeframe that was analysed in this study. Worth the reminder, this semi-orthotopic bone formation model also constituted a proof-of-concept. Consequently, by including specific modifications, the current model could be adapted to recreate and study particular scenarios. For example, bone co-morbidities could be introduced into the bone rings implanted, such as those induced by radiation damage, cytotoxic chemotherapeutics, and anti-osteoporotic drugs. This would allow replication of the clinical situations where bone fails to heal. In addition, the use of human bone instead of bovine bone could be used to manufacture constructs to further increase the clinical relevance of the model. With regards to the host animal of the constructs, if the mouse was replaced by another of bigger size such as the pig (for which immunodeficient strains are available), the number of conditions that could be simultaneously tested would increase, as more constructs could be allocated subcutaneously per animal, and the sacrifice of the host animal after the termination of the experiment could be avoided. Last, if the origin of the bone ring was then matched to the host species, the study of allogeneic bone regeneration would be possible.

WHAT DOES THE PERFECT GRAFT LOOK LIKE?

In this work I explored how a matrix can be replicated from a few biochemical components to produce a chemically defined bone graft, aiming at developing new Class III medical device formulations. Among the advantages of this approach are the high control over the composition, properties and reproducibility of the graft. However, several methodologies can be followed to produce bone graft substitutes with different properties, each possessing its own advantages and limitations. Thus, in **Chapter 5** I explored how different approaches to produce bone grafts result in bone formation when

the resulting grafts are placed at a critical-size defect. Compared to the defects left untreated, collagen-based scaffolds permitted the ingrowth of tissues into the injured site, favouring the regeneration of the bone versus the formation of fibrous tissue. While this was sufficient to enhance bone regeneration in the *in vivo* model used, those collagen-based scaffolds were mechanically weak and incapable of withstanding compressive forces. Through a different approach, a new graft that replicated a transient cartilage matrix was produced. In this instance, instead of building it from single components, the complex matrix of tracheal tissue was repurposed by removing some of its components. While maintaining apparent good mechanical properties and being simple to produce, the graft supported its degradation while promoting bone formation, although at a slower rate than the collagen scaffolds. In both cases, the grafts promoted bone healing by guiding the surrounding bone endogenous repair mechanisms. Unfortunately, severe injuries where substantial amounts of bone are lost are often associated to other comorbidities resulting from infections or radiotherapy. For this reason, an increasing number of experimental treatments have been used to surpass the need to rely on the self-repair abilities of the patient. Progenitor cells have been added as an extra component to the graft, in addition to different molecules to guide their cellular processes [271]. Since these grafts make use of living cells, the new treatments making use of them are classified under the category of advanced therapeutical medicinal products (ATMPs) [23]. When these treatments were tested in **Chapter 5**, bone formation took place guided by living transient cartilage templates, at a rate comparable to cell-free collagen scaffolds [218, 219]. The cell-derived grafts however, possessed an evident higher mechanical strength than collagen scaffolds. It remains to be seen though, whether the costs associated with the cell-derived product would be justified. In conclusion, when selecting the most optimal graft one should always take into consideration the scenario where the graft is meant to be used, in order to determine its best composition and economical costs.

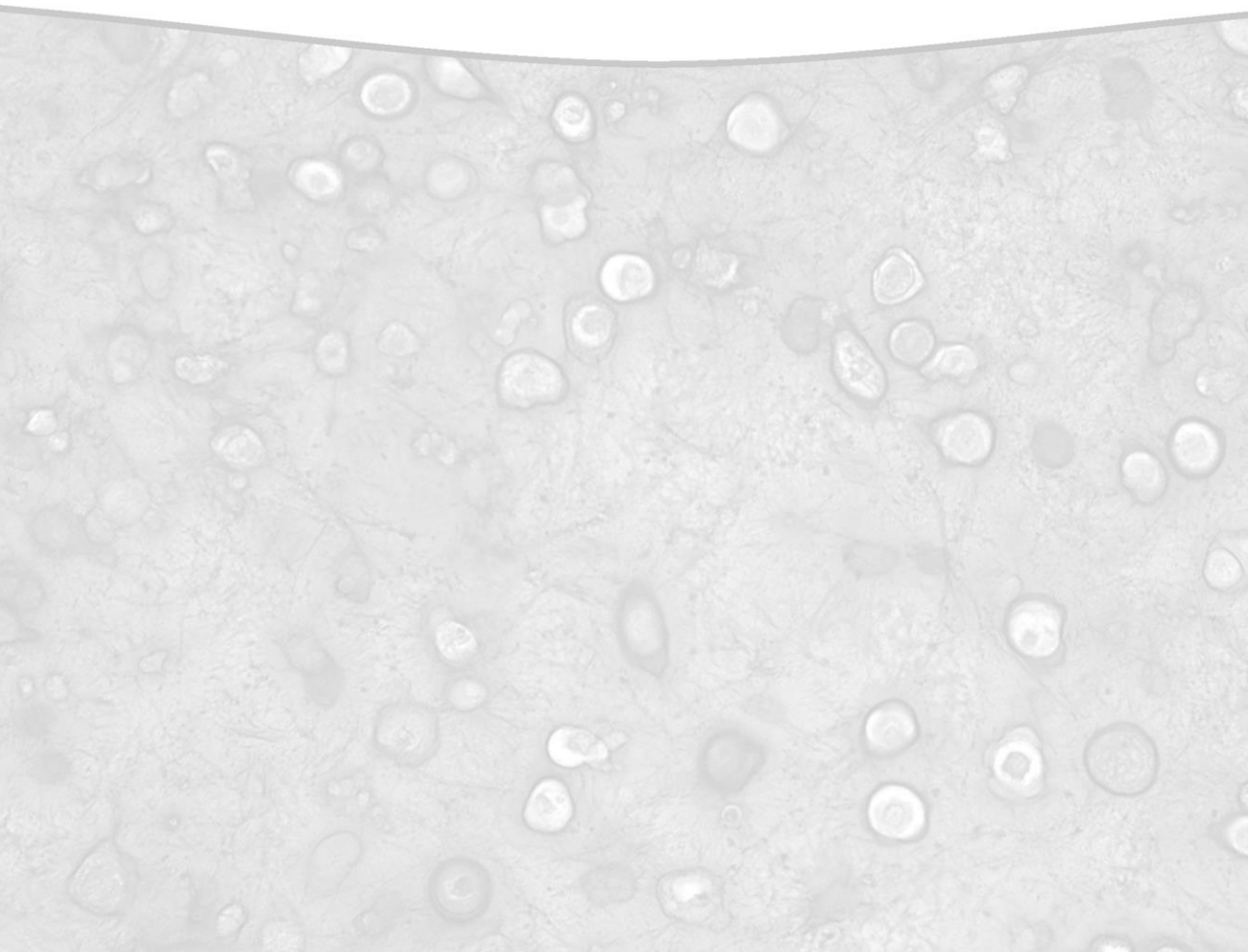
CONCLUSIONS AND FUTURE PERSPECTIVES

In conclusion, in this thesis I have contributed to elucidate the role that the two ECM proteins TSP-4 and TSP-5 play during skeletal formation and repair, and have provided with a new model to screen for new bone graft substitutes. While TSP-5 is associated with cartilage formation and maintenance, TSP-4 is present in skeletal regions committed to ossify. For this reason, TSP-4 might be of use for bone tissue engineering purposes, since it is likely to positively regulate bone formation. In addition, it may have value as biomarker for endochondral ossification which could be exploited for the early diagnosis of osteoarthritic disease. For this reason, further research should investigate in more detail the role that TSP-4 plays during endochondral ossification, and how it affects the cellular types involved. Regarding osteoarthritis, it will be key to assess the function of TSP-4 and its possible interference to that of TSP-5. With respect to novel bone tissue engineering strategies, it will be interesting to investigate first how TSP-4 interacts with

morphogens such as BMP-2. Then, to study if TSP-4 may have positive effects on bone regeneration, in particular those regarding vascularisation and mature bone formation. To aid in this endeavour, it would be convenient to further develop the semi-orthotopic bone formation model presented in this work, by including new readout measurements and modifications to better mimic the clinical set-up.

CHAPTER 7

Summary



THROMBOSPONDINS -4 AND -5 IN SKELETAL DEVELOPMENT, DISEASE AND REPAIR

Implications for Bone Tissue Engineering

Mobility is crucial for quality of life. However, after a traumatic injury or the resection of bone tumours, patients might be left with injured bones unable to fuse. For these serious complications that result in permanent disability and reduce the quality of life of the patient, no effective treatments are available. To improve the therapeutic options, new implants are being engineered to promote bone regeneration. During skeletal development and during the repair of bone fractures, our bodies generate transient cartilage structures to direct bone formation via the process of endochondral ossification. By replicating those cartilage structures, bone tissue engineers can design bone graft substitutes with improved properties. In particular, the extracellular matrix (ECM) of the transient cartilage is of great interest, since it naturally guides the regenerative process. Although many extracellular matrix proteins and other factors present in the transitional cartilage ECM have been identified, their functions during bone formation are still largely unknown. Thus, understanding the composition and the role that cartilage ECM components play during bone formation and repair is key to determine which components may be useful to promote bone healing. In this thesis I aimed first to gain more insight into the role that two ECM proteins –Thrombospondin-4 (TSP-4) and Thrombospondin-5 (TSP-5)–, play in the process of endochondral ossification. My second aim was to develop a method to assess their potential for bone tissue engineering.

My research began in **Chapter 2**, after discovering that humans produce TSP-4 during our skeletal growth. From there, I investigated how the spatial and temporal patterns of TSP-4 compare to its sibling protein TSP-5. Since humans and mice share similarities in skeletal development, I analysed the production of the two proteins during the growth of the mouse skeleton. I found that TSP-5 is present across all the transient cartilage during endochondral ossification, while TSP-4 is only produced at the hypertrophic zones adjacent to the forming bone. In parallel, I investigated the bones present at the head region, which form directly without the use of a cartilage template, via the process of intramembranous ossification. Nevertheless, there I found that prior to bone formation, TSP-4 is produced while TSP-5 is completely absent. These results made me wonder if during bone fracture healing –which makes use of the intramembranous and endochondral ossification programs– the same spatial and temporal patterns would be seen. Indeed, TSP-4 and TSP-5 followed the same patterns observed during skeletal development. With *in vitro* studies, I found that unlike TSP-5, one of TSP-4's role could be to attract blood vessels to the forming bone, which could be of great therapeutic value. Therefore, I concluded that the potential of the use of the two thrombospondins in bone tissue engineering should be further studied.

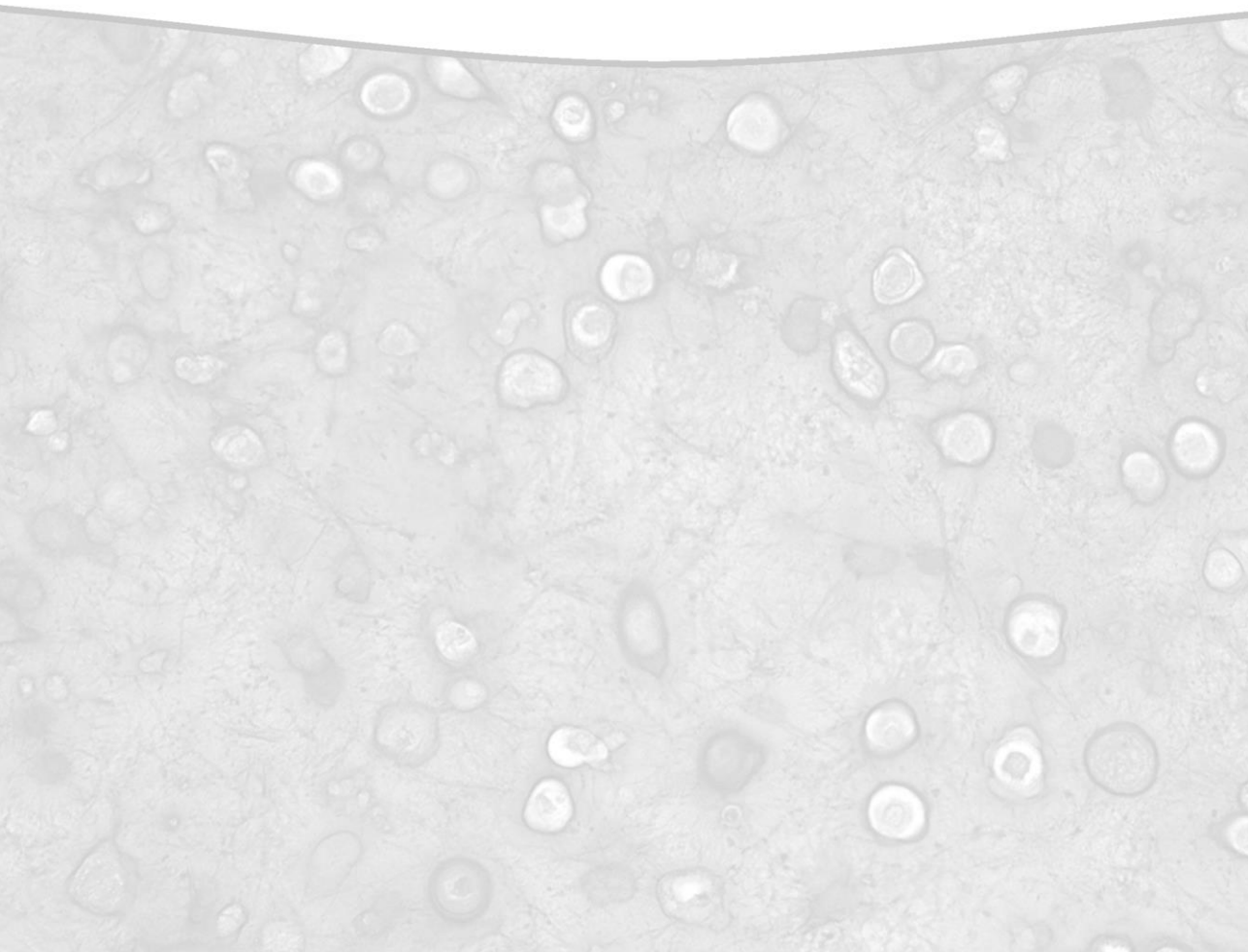
In **Chapter 3** I explored the production and roles of TSP-4 and TSP-5 in a context where pathological endochondral ossification is known to take place: in osteoarthritis. During this disease, sustained and irreversible cartilage damage occurs and the presence of both TSP-4 and TSP-5 increase at the affected joints. To understand how they modify the behaviour of the cells of the cartilage (chondrocytes), I investigated how the two proteins alter the signalling, production of ECM components and the migratory behaviour of chondrocytes. Interestingly, TSP-5 but not TSP-4, stimulated the migration of chondrocytes, whose ECM had been depleted. In addition, I observed that the two proteins act synergistically with the growth factor TGF- β to increase the matrix deposition, albeit through slightly different mechanisms. In relation to the previous chapter, it became evident that despite their structural similarities, TSP-4 and TSP-5 were playing both similar and different roles in skeletal formation and repair. While TSP-4 appeared to be mainly related to bone formation, this was still unclear for TSP-5. During cartilage remodelling and prior to cartilage ossification, part of the TSP-5 present at the ECM is fragmented in small peptides. Since other ECM protein fragments have shown to possess biological activity, in **Chapter 4** I asked if those derived from TSP-5 could have osteoarthritis-related functions, given the relationship between the disease and the pathological endochondral ossification. For this, I used synthetic versions of three TSP-5 peptides produced during the disease in different *in vitro* assays, and explored their possible effects on progenitor cells from the bone, endothelial cells and synovium. However, none of the peptides demonstrated bioactive properties.

TSP-4 appeared to be an attractive agent for application in a bone tissue engineering strategy and thus, worth testing further. Since bone formation cannot be evaluated in a comprehensive manner *in vitro*, it requires that the evaluation is carried out in living animals. Sadly, the *in vivo* models and techniques available at that time were laborious and had a big impact on animal welfare. For this reason, I developed a more refined and efficient methodology for the screening of bone grafts in **Chapter 5**, that could potentially reduce the number of necessary animals. In this new model, trabecular bone rings of bovine origin were subcutaneously implanted in mice. Thanks to this, the implants gained the ability to form new bone in their hollow cores. Regeneration happened only if therapeutically effective grafts were placed inside, which allowed the quantification of the induced regenerative response. After this, I validated this new model for bone formation, named as semi-orthotopic, by systematically evaluating the potential of different grafts to induce ossification. I concluded my doctoral research by starting the evaluation of TSP-4 as a therapeutic agent in the semi-orthotopic bone formation model. For this, I used a biomaterial based on collagen and hydroxyapatite, in which TSP-4 had been incorporated. While I did not observe a major improvement in bone formation upon the single addition of TSP-4, further studies will have to evaluate the synergistic effects that TSP-4 may have when administered in combination with the various growth factors present at the ECM.

In conclusion, during this research I have shed light on how different extracellular matrix components are altered in transient cartilage, and I have described how the presence and function of two similar ECM proteins overlap and differ depending on the context. Lastly, I have developed a new methodology for the testing of new therapies that will help to accelerate new discoveries in the field of bone grafts.

CHAPTER 8

References



1. Hirasawa, T. and S. Kuratani, *Evolution of the vertebrate skeleton: morphology, embryology, and development*. Zoological Lett, 2015. **1**: p. 2.
2. Berendsen, A.D. and B.R. Olsen, *Bone development*. Bone, 2015. **80**: p. 14-18.
3. Percival, C.J. and J.T. Richtsmeier, *Angiogenesis and intramembranous osteogenesis*. Dev Dyn, 2013. **242**(8): p. 909-22.
4. Mackie, E.J., et al., *Endochondral ossification: how cartilage is converted into bone in the developing skeleton*. Int J Biochem Cell Biol, 2008. **40**(1): p. 46-62.
5. Staines, K.A., et al., *Cartilage to bone transitions in health and disease*. J Endocrinol, 2013. **219**(1): p. R1-R12.
6. Wolff, L.I. and C. Hartmann, *A Second Career for Chondrocytes-Transformation into Osteoblasts*. Curr Osteoporos Rep, 2019. **17**(3): p. 129-137.
7. Newton, P.T., et al., *A radical switch in clonality reveals a stem cell niche in the epiphyseal growth plate*. Nature, 2019. **567**(7747): p. 234-238.
8. Wu, A.-M., et al., *Global, regional, and national burden of bone fractures in 204 countries and territories, 1990–2019: a systematic analysis from the Global Burden of Disease Study 2019*. The Lancet Healthy Longevity, 2021. **2**(9): p. e580-e592.
9. Einhorn, T.A. and L.C. Gerstenfeld, *Fracture healing: mechanisms and interventions*. Nat Rev Rheumatol, 2015. **11**(1): p. 45-54.
10. Bahney, C.S., et al., *Cellular biology of fracture healing*. J Orthop Res, 2019. **37**(1): p. 35-50.
11. Zura, R., et al., *Epidemiology of Fracture Nonunion in 18 Human Bones*. JAMA Surg, 2016. **151**(11): p. e162775.
12. Rogers, G.F. and A.K. Greene, *Autogenous bone graft: basic science and clinical implications*. J Craniofac Surg, 2012. **23**(1): p. 323-7.
13. Panagopoulos, G.N., et al., *Intercalary reconstructions after bone tumor resections: a review of treatments*. Eur J Orthop Surg Traumatol, 2017. **27**(6): p. 737-746.
14. Devescovi, V., et al., *Growth factors in bone repair*. Chir Organi Mov, 2008. **92**(3): p. 161-8.
15. Thompson, E.M., et al., *Recapitulating endochondral ossification: a promising route to in vivo bone regeneration*. J Tissue Eng Regen Med, 2015. **9**(8): p. 889-902.
16. Martel-Pelletier, J., et al., *Osteoarthritis*. Nat Rev Dis Primers, 2016. **2**: p. 16072.
17. Sacks, J.J., Y.H. Luo, and C.G. Helmick, *Prevalence of specific types of arthritis and other rheumatic conditions in the ambulatory health care system in the United States, 2001-2005*. Arthritis Care Res (Hoboken), 2010. **62**(4): p. 460-4.
18. Shane Anderson, A. and R.F. Loeser, *Why is osteoarthritis an age-related disease?* Best Pract Res Clin Rheumatol, 2010. **24**(1): p. 15-26.
19. van der Kraan, P.M. and W.B. van den Berg, *Osteophytes: relevance and biology*. Osteoarthritis Cartilage, 2007. **15**(3): p. 237-44.
20. Gelse, K., et al., *Osteophyte development--molecular characterization of differentiation stages*. Osteoarthritis Cartilage, 2003. **11**(2): p. 141-8.
21. Long, F. and D.M. Ornitz, *Development of the endochondral skeleton*. Cold Spring Harb Perspect Biol, 2013. **5**(1): p. a008334.
22. Melrose, J., et al., *The cartilage extracellular matrix as a transient developmental scaffold for growth plate maturation*. Matrix Biol, 2016. **52-54**: p. 363-383.

23. Ho-Shui-Ling, A., et al., *Bone regeneration strategies: Engineered scaffolds, bioactive molecules and stem cells current stage and future perspectives*. *Biomaterials*, 2018. **180**: p. 143-162.
24. Lin, X., et al., *The Bone Extracellular Matrix in Bone Formation and Regeneration*. *Front Pharmacol*, 2020. **11**: p. 757.
25. Rico-Llanos, G.A., et al., *Collagen Type I Biomaterials as Scaffolds for Bone Tissue Engineering*. *Polymers (Basel)*, 2021. **13**(4).
26. Axelrad, T.W. and T.A. Einhorn, *Bone morphogenetic proteins in orthopaedic surgery*. *Cytokine Growth Factor Rev*, 2009. **20**(5-6): p. 481-8.
27. El Bialy, I., W. Jiskoot, and M. Reza Nejadnik, *Formulation, Delivery and Stability of Bone Morphogenetic Proteins for Effective Bone Regeneration*. *Pharm Res*, 2017. **34**(6): p. 1152-1170.
28. James, A.W., et al., *A Review of the Clinical Side Effects of Bone Morphogenetic Protein-2*. *Tissue Eng Part B Rev*, 2016. **22**(4): p. 284-97.
29. Sophia Fox, A.J., A. Bedi, and S.A. Rodeo, *The basic science of articular cartilage: structure, composition, and function*. *Sports Health*, 2009. **1**(6): p. 461-8.
30. Mow, V.C., et al., *The influence of link protein stabilization on the viscometric properties of proteoglycan aggregate solutions*. *Biochim Biophys Acta*, 1989. **992**(2): p. 201-8.
31. Mow, V.C., M.H. Holmes, and W. Michael Lai, *Fluid transport and mechanical properties of articular cartilage: A review*. *Journal of Biomechanics*, 1984. **17**(5): p. 377-394.
32. Hardingham, T.E. and A.J. Fosang, *Proteoglycans: many forms and many functions*. *The FASEB Journal*, 1992. **6**(3): p. 861-870.
33. Bix, G. and R.V. Iozzo, *Novel interactions of perlecan: unraveling perlecan's role in angiogenesis*. *Microsc Res Tech*, 2008. **71**(5): p. 339-48.
34. Ortega, N., D.J. Behonick, and Z. Werb, *Matrix remodeling during endochondral ossification*. *Trends Cell Biol*, 2004. **14**(2): p. 86-93.
35. Hunziker, E.B., *Mechanism of longitudinal bone growth and its regulation by growth plate chondrocytes*. *Microsc Res Tech*, 1994. **28**(6): p. 505-19.
36. Ricard-Blum, S. and R. Salza, *Matricryptins and matrikines: biologically active fragments of the extracellular matrix*. *Exp Dermatol*, 2014. **23**(7): p. 457-63.
37. Ricard-Blum, S. and L. Ballut, *Matricryptins derived from collagens and proteoglycans*. *Front Biosci (Landmark Ed)*, 2011. **16**: p. 674-97.
38. Carminati, L. and G. Taraboletti, *Thrombospondins in bone remodeling and metastatic bone disease*. *Am J Physiol Cell Physiol*, 2020. **319**(6): p. C980-C990.
39. Hankenson, K.D., et al., *Thrombospondins and novel TSR-containing proteins, R-spondins, regulate bone formation and remodeling*. *Curr Osteoporos Rep*, 2010. **8**(2): p. 68-76.
40. Adams, J.C. and J. Lawler, *The thrombospondins*. *Cold Spring Harb Perspect Biol*, 2011. **3**(10): p. a009712.
41. Resovi, A., et al., *Current understanding of the thrombospondin-1 interactome*. *Matrix Biol*, 2014. **37**: p. 83-91.
42. Margosio, B., et al., *Fibroblast growth factor-2 binding to the thrombospondin-1 type III repeats, a novel antiangiogenic domain*. *Int J Biochem Cell Biol*, 2008. **40**(4): p. 700-9.

43. Rusnati, M., et al., *The calcium-binding type III repeats domain of thrombospondin-2 binds to fibroblast growth factor 2 (FGF2)*. *Angiogenesis*, 2019. **22**(1): p. 133-144.
44. Rosini, S., et al., *Thrombospondin-1 promotes matrix homeostasis by interacting with collagen and lysyl oxidase precursors and collagen cross-linking sites*. *Sci Signal*, 2018. **11**(532).
45. Shearer, D., et al., *TSP1 and TSP2 deficiencies affect LOX protein distribution in the femoral diaphysis and pro-peptide removal in marrow-derived mesenchymal stem cells in vitro*. *Connect Tissue Res*, 2019. **60**(5): p. 495-506.
46. Calabro, N.E., N.J. Kristofik, and T.R. Kyriakides, *Thrombospondin-2 and extracellular matrix assembly*. *Biochim Biophys Acta*, 2014. **1840**(8): p. 2396-402.
47. Bein, K. and M. Simons, *Thrombospondin type 1 repeats interact with matrix metalloproteinase 2. Regulation of metalloproteinase activity*. *J Biol Chem*, 2000. **275**(41): p. 32167-73.
48. Isenberg, J.S., et al., *Regulation of nitric oxide signalling by thrombospondin 1: implications for anti-angiogenic therapies*. *Nat Rev Cancer*, 2009. **9**(3): p. 182-94.
49. Murphy-Ullrich, J.E. and M.J. Suto, *Thrombospondin-1 regulation of latent TGF-beta activation: A therapeutic target for fibrotic disease*. *Matrix Biol*, 2018. **68-69**: p. 28-43.
50. Iruela-Arispe, M.L., et al., *Differential expression of thrombospondin 1, 2, and 3 during murine development*. *Dev Dyn*, 1993. **197**(1): p. 40-56.
51. Robey, P.G., et al., *Thrombospondin is an osteoblast-derived component of mineralized extracellular matrix*. *J Cell Biol*, 1989. **108**(2): p. 719-27.
52. Tooney, P.A., et al., *Restricted localization of thrombospondin-2 protein during mouse embryogenesis: A comparison to thrombospondin-1*. *Matrix Biology*, 1998. **17**(2): p. 131-143.
53. Carron, J.A., et al., *Expression of members of the thrombospondin family by human skeletal tissues and cultured cells*. *Biochem Biophys Res Commun*, 1999. **263**(2): p. 389-91.
54. Clezardin, P., et al., *Thrombospondin is synthesized and secreted by human osteoblasts and osteosarcoma cells. A model to study the different effects of thrombospondin in cell adhesion*. *Eur J Biochem*, 1989. **181**(3): p. 721-6.
55. van den Bos, T., et al., *Differences in matrix composition between calvaria and long bone in mice suggest differences in biomechanical properties and resorption: Special emphasis on collagen*. *Bone*, 2008. **43**(3): p. 459-68.
56. Kyriakides, T.R., et al., *The distribution of the matricellular protein thrombospondin 2 in tissues of embryonic and adult mice*. *J Histochem Cytochem*, 1998. **46**(9): p. 1007-15.
57. Hankenson, K.D. and P. Bornstein, *The secreted protein thrombospondin 2 is an autocrine inhibitor of marrow stromal cell proliferation*. *J Bone Miner Res*, 2002. **17**(3): p. 415-25.
58. Sherbina, N.V. and P. Bornstein, *Modulation of thrombospondin gene expression during osteoblast differentiation in MC3T3-E1 cells*. *Bone*, 1992. **13**(2): p. 197-201.
59. Zondervan, R.L., et al., *Thrombospondin-2 spatiotemporal expression in skeletal fractures*. *J Orthop Res*, 2021. **39**(1): p. 30-41.
60. Taylor, D.K., et al., *Thrombospondin-2 influences the proportion of cartilage and bone during fracture healing*. *J Bone Miner Res*, 2009. **24**(6): p. 1043-54.
61. DiCesare, P.E., et al., *Cartilage oligomeric matrix protein and thrombospondin 1. Purification from articular cartilage, electron microscopic structure, and chondrocyte binding*. *Eur J Biochem*, 1994. **223**(3): p. 927-37.

62. Lawler, J., et al., *Characterization of human thrombospondin-4*. J Biol Chem, 1995. **270**(6): p. 2809-14.
63. Qabar, A., et al., *Thrombospondin 3 is a pentameric molecule held together by interchain disulfide linkage involving two cysteine residues*. J Biol Chem, 1995. **270**(21): p. 12725-9.
64. Pellerin, S., et al., *The molecular structure of corticotropin-induced secreted protein, a novel member of the thrombospondin family*. Journal of Biological Chemistry, 1993. **268**(25): p. 18810-18817.
65. Maly, K., et al., *The Expression of Thrombospondin-4 Correlates with Disease Severity in Osteoarthritic Knee Cartilage*. Int J Mol Sci, 2019. **20**(2): p. 447.
66. Stenina-Adognravi, O. and E.F. Plow, *Thrombospondin-4 in tissue remodeling*. Matrix Biol, 2019. **75-76**: p. 300-313.
67. Muppala, S., et al., *Thrombospondin-4 mediates TGF-beta-induced angiogenesis*. Oncogene, 2017. **36**(36): p. 5189-5198.
68. Di Cesare, P.E., et al., *Expression of cartilage oligomeric matrix protein (COMP) by embryonic and adult osteoblasts*. J Orthop Res, 2000. **18**(5): p. 713-20.
69. Posey, K.L., F. Coustry, and J.T. Hecht, *Cartilage oligomeric matrix protein: COMPopathies and beyond*. Matrix Biol, 2018. **71-72**: p. 161-173.
70. Murphy, J.M., et al., *Distribution of cartilage molecules in the developing mouse joint*. Matrix Biology, 1999. **18**(5): p. 487-497.
71. DiCesare, P.E., et al., *Cartilage oligomeric matrix protein: isolation and characterization from human articular cartilage*. J Orthop Res, 1995. **13**(3): p. 422-8.
72. Schulz, J.N., et al., *COMP-assisted collagen secretion--a novel intracellular function required for fibrosis*. J Cell Sci, 2016. **129**(4): p. 706-16.
73. Halasz, K., et al., *COMP acts as a catalyst in collagen fibrillogenesis*. J Biol Chem, 2007. **282**(43): p. 31166-73.
74. Ishida, K., et al., *Cartilage oligomeric matrix protein enhances osteogenesis by directly binding and activating bone morphogenetic protein-2*. Bone, 2013. **55**(1): p. 23-35.
75. Haudenschild, D.R., et al., *Enhanced activity of transforming growth factor beta1 (TGF-beta1) bound to cartilage oligomeric matrix protein*. J Biol Chem, 2011. **286**(50): p. 43250-8.
76. Hauser, N., et al., *Tendon extracellular matrix contains pentameric thrombospondin-4 (TSP-4)*. FEBS Letters, 1995. **368**(2): p. 307-310.
77. Narouz-Ott, L., et al., *Thrombospondin-4 binds specifically to both collagenous and non-collagenous extracellular matrix proteins via its C-terminal domains*. J Biol Chem, 2000. **275**(47): p. 37110-7.
78. Subramanian, A. and T.F. Schilling, *Thrombospondin-4 controls matrix assembly during development and repair of myotendinous junctions*. Elife, 2014. **3**.
79. Sodersten, F., et al., *Thrombospondin-4 and cartilage oligomeric matrix protein form heterooligomers in equine tendon*. Connect Tissue Res, 2006. **47**(2): p. 85-91.
80. James, C.G., et al., *Microarray analyses of gene expression during chondrocyte differentiation identifies novel regulators of hypertrophy*. Mol Biol Cell, 2005. **16**(11): p. 5316-33.
81. Wilson, R., et al., *Changes in the chondrocyte and extracellular matrix proteome during post-natal mouse cartilage development*. Mol Cell Proteomics, 2012. **11**(1): p. M111 014159.

82. Rundle, C.H., et al., *Microarray analysis of gene expression during the inflammation and endochondral bone formation stages of rat femur fracture repair*. *Bone*, 2006. **38**(4): p. 521-9.
83. Lawler, P.R. and J. Lawler, *Molecular basis for the regulation of angiogenesis by thrombospondin-1 and -2*. *Cold Spring Harb Perspect Med*, 2012. **2**(5): p. a006627.
84. Santoshi Muppala, E.F., Roy Xiao, Irene Krukovets, Suzy Yoon, George Hoppe, Amit Vasanthi, Edward Plow, and Olga Stenina-Adognravi, *Proangiogenic Properties of Thrombospondin-4*. *Arterioscler Thromb Vasc Biol*, 2015. **35**(9): p. 1975-1986.
85. Bohm, A.M., et al., *Activation of Skeletal Stem and Progenitor Cells for Bone Regeneration Is Driven by PDGFRbeta Signaling*. *Dev Cell*, 2019. **51**(2): p. 236-254 e12.
86. Maes, C., et al., *Placental growth factor mediates mesenchymal cell development, cartilage turnover, and bone remodeling during fracture repair*. *J Clin Invest*, 2006. **116**(5): p. 1230-42.
87. Maes, C., et al., *Osteoblast precursors, but not mature osteoblasts, move into developing and fractured bones along with invading blood vessels*. *Dev Cell*, 2010. **19**(2): p. 329-44.
88. Hedbom, E., et al., *Cartilage Matrix Proteins an acidic oligomeric protein (COMP) detected only in cartilage*. *Journal of Biological Chemistry*, 1992. **267**(9): p. 6132-6136.
89. Sedgewick, J., *Acquisition and Post-Processing of Immunohistochemical Images*. *Methods Mol Biol*, 2017. **1554**: p. 75-106.
90. Ruthard, J., et al., *COMP does not directly modify the expression of genes involved in cartilage homeostasis in contrast to several other cartilage matrix proteins*. *Connect Tissue Res*, 2014. **55**(5-6): p. 348-56.
91. Crosby, N.D., et al., *Thrombospondin-4 and excitatory synaptogenesis promote spinal sensitization after painful mechanical joint injury*. *Exp Neurol*, 2015. **264**: p. 111-20.
92. Knuth, C.A., et al., *Isolating Pediatric Mesenchymal Stem Cells with Enhanced Expansion and Differentiation Capabilities*. *Tissue Eng Part C Methods*, 2018. **24**(6): p. 313-321.
93. Tucker, R.P., J.C. Adams, and J. Lawler, *Thrombospondin-4 is expressed by early osteogenic tissues in the chick embryo*. *Dev Dyn*, 1995. **203**(4): p. 477-90.
94. Arber, S. and P. Caroni, *Thrombospondin-4, an extracellular matrix protein expressed in the developing and adult nervous system promotes neurite outgrowth*. *J Cell Biol*, 1995. **131**(4): p. 1083-94.
95. Meyer, M.H., W. Etienne, and R.A. Meyer, Jr., *Altered mRNA expression of genes related to nerve cell activity in the fracture callus of older rats: A randomized, controlled, microarray study*. *BMC Musculoskelet Disord*, 2004. **5**: p. 24.
96. Chen, F.H., et al., *Cartilage oligomeric matrix protein/thrombospondin 5 supports chondrocyte attachment through interaction with integrins*. *J Biol Chem*, 2005. **280**(38): p. 32655-61.
97. Jeschke, A., et al., *Deficiency of Thrombospondin-4 in Mice Does Not Affect Skeletal Growth or Bone Mass Acquisition, but Causes a Transient Reduction of Articular Cartilage Thickness*. *PLoS One*, 2015. **10**(12): p. e0144272.
98. Maly, K., et al., *COMP and TSP-4: Functional Roles in Articular Cartilage and Relevance in Osteoarthritis*. *Int J Mol Sci*, 2021. **22**(5): p. 2242.
99. Whited, J.L., et al., *Dynamic expression of two thrombospondins during axolotl limb regeneration*. *Dev Dyn*, 2011. **240**(5): p. 1249-58.

100. Hou, Y., H. Li, and W. Huo, *THBS4 silencing regulates the cancer stem cell-like properties in prostate cancer via blocking the PI3K/Akt pathway*. *Prostate*, 2020. **80**(10): p. 753-763.
101. Benner, E.J., et al., *Protective astrogenesis from the SVZ niche after injury is controlled by Notch modulator Thbs4*. *Nature*, 2013. **497**(7449): p. 369-73.
102. Phng, L.K. and H. Gerhardt, *Angiogenesis: a team effort coordinated by notch*. *Dev Cell*, 2009. **16**(2): p. 196-208.
103. Zheng, Y., et al., *Notch signaling in regulating angiogenesis in a 3D biomimetic environment*. *Lab Chip*, 2017. **17**(11): p. 1948-1959.
104. Adorno-Cruz, V. and H. Liu, *Regulation and functions of integrin alpha2 in cell adhesion and disease*. *Genes Dis*, 2019. **6**(1): p. 16-24.
105. Svensson, L., et al., *Cartilage oligomeric matrix protein-deficient mice have normal skeletal development*. *Mol Cell Biol*, 2002. **22**(12): p. 4366-71.
106. Posey, K.L., et al., *Skeletal abnormalities in mice lacking extracellular matrix proteins, thrombospondin-1, thrombospondin-3, thrombospondin-5, and type IX collagen*. *Am J Pathol*, 2008. **172**(6): p. 1664-74.
107. Bhosale, A.M. and J.B. Richardson, *Articular cartilage: structure, injuries and review of management*. *Br Med Bull*, 2008. **87**: p. 77-95.
108. Athanasiou, K.A., Darling, E.M., DuRaine, G.D., Hu, J.C., & Reddi, A.H., *Articular Cartilage*. 2013: CRC Press: Boca Raton, FL, USA.
109. Eyre, D.R., *Collagens and cartilage matrix homeostasis*. *Clin Orthop Relat Res*, 2004(427 Suppl): p. S118-22.
110. Kempson, G.E., M.A. Freeman, and S.A. Swanson, *Tensile properties of articular cartilage*. *Nature*, 1968. **220**(5172): p. 1127-8.
111. Gottardi, R., et al., *Supramolecular Organization of Collagen Fibrils in Healthy and Osteoarthritic Human Knee and Hip Joint Cartilage*. *PLoS One*, 2016. **11**(10): p. e0163552.
112. Hagg, R., P. Bruckner, and E. Hedbom, *Cartilage fibrils of mammals are biochemically heterogeneous: differential distribution of decorin and collagen IX*. *J Cell Biol*, 1998. **142**(1): p. 285-94.
113. Gregory, K.E., et al., *Developmental distribution of collagen type XII in cartilage: association with articular cartilage and the growth plate*. *J Bone Miner Res*, 2001. **16**(11): p. 2005-16.
114. Yamagata, M., et al., *The complete primary structure of type XII collagen shows a chimeric molecule with reiterated fibronectin type III motifs, von Willebrand factor A motifs, a domain homologous to a noncollagenous region of type IX collagen, and short collagenous domains with an Arg-Gly-Asp site*. *J Cell Biol*, 1991. **115**(1): p. 209-21.
115. Eyre, D.R., M.A. Weis, and J.J. Wu, *Articular cartilage collagen: an irreplaceable framework?* *Eur Cell Mater*, 2006. **12**: p. 57-63.
116. Luckman, S.P., E. Rees, and A.P. Kwan, *Partial characterization of cell-type X collagen interactions*. *Biochem J*, 2003. **372**(Pt 2): p. 485-93.
117. Aspden, R.M., *Fibre reinforcing by collagen in cartilage and soft connective tissues*. *Proc Biol Sci*, 1994. **258**(1352): p. 195-200.
118. Gibson, G.J., C.H. Bearman, and M.H. Flint, *The Immunoperoxidase Localization of Type X Collagen in Chick Cartilage and Lung*. *Collagen and Related Research*, 1986. **6**(2): p. 163-184.

119. Bonen, D.K. and T.M. Schmid, *Elevated extracellular calcium concentrations induce type X collagen synthesis in chondrocyte cultures*. J Cell Biol, 1991. **115**(4): p. 1171-8.
120. Koelling, S., et al., *Cartilage oligomeric matrix protein is involved in human limb development and in the pathogenesis of osteoarthritis*. Arthritis Res Ther, 2006. **8**(3): p. R56.
121. Goldring, M.B., *Chondrogenesis, chondrocyte differentiation, and articular cartilage metabolism in health and osteoarthritis*. Ther Adv Musculoskelet Dis, 2012. **4**(4): p. 269-85.
122. Loeser, R.F., et al., *Osteoarthritis: a disease of the joint as an organ*. Arthritis Rheum, 2012. **64**(6): p. 1697-707.
123. Neogi, T., *The epidemiology and impact of pain in osteoarthritis*. Osteoarthritis and Cartilage, 2013. **21**(9): p. 1145-1153.
124. Sofat, N., *Analysing the role of endogenous matrix molecules in the development of osteoarthritis*. Int J Exp Pathol, 2009. **90**(5): p. 463-79.
125. Grimmer, C., et al., *Regulation of type II collagen synthesis during osteoarthritis by prolyl-4-hydroxylases: possible influence of low oxygen levels*. Am J Pathol, 2006. **169**(2): p. 491-502.
126. Lippiello, L., D. Hall, and H.J. Mankin, *Collagen synthesis in normal and osteoarthritic human cartilage*. J Clin Invest, 1977. **59**(4): p. 593-600.
127. Grimaud, E., D. Heymann, and F. R dini, *Recent advances in TGF-  effects on chondrocyte metabolism*. Cytokine & Growth Factor Reviews, 2002. **13**(3): p. 241-257.
128. Zhu, Y., et al., *Transforming growth factor-beta1 induces type II collagen and aggrecan expression via activation of extracellular signal-regulated kinase 1/2 and Smad2/3 signaling pathways*. Mol Med Rep, 2015. **12**(4): p. 5573-9.
129. Recklies, A.D., L. Baillargeon, and C. White, *Regulation of cartilage oligomeric matrix protein synthesis in human synovial cells and articular chondrocytes*. Arthritis & Rheumatism, 1998. **41**(6): p. 997-1006.
130. Thielen, N.G.M., P.M. van der Kraan, and A.P.M. van Caam, *TGFbeta/BMP Signaling Pathway in Cartilage Homeostasis*. Cells, 2019. **8**(9).
131. Fortier, L.A., et al., *The role of growth factors in cartilage repair*. Clin Orthop Relat Res, 2011. **469**(10): p. 2706-15.
132. Gao, Y., et al., *The ECM-cell interaction of cartilage extracellular matrix on chondrocytes*. Biomed Res Int, 2014. **2014**: p. 648459.
133. Kim, K.O., et al., *Ski inhibits TGF-beta/phospho-Smad3 signaling and accelerates hypertrophic differentiation in chondrocytes*. J Cell Biochem, 2012. **113**(6): p. 2156-66.
134. Ferguson, C.M., et al., *Smad2 and 3 mediate transforming growth factor-beta1-induced inhibition of chondrocyte maturation*. Endocrinology, 2000. **141**(12): p. 4728-35.
135. Blaney Davidson, E.N., et al., *Increase in ALK1/ALK5 ratio as a cause for elevated MMP-13 expression in osteoarthritis in humans and mice*. J Immunol, 2009. **182**(12): p. 7937-45.
136. Lian, C., et al., *Collagen type II suppresses articular chondrocyte hypertrophy and osteoarthritis progression by promoting integrin beta1-SMAD1 interaction*. Bone Res, 2019. **7**: p. 8.
137. Fava, R., et al., *Active and latent forms of transforming growth factor beta activity in synovial effusions*. J Exp Med, 1989. **169**(1): p. 291-6.

138. Hall, A.C., *The Role of Chondrocyte Morphology and Volume in Controlling Phenotype-Implications for Osteoarthritis, Cartilage Repair, and Cartilage Engineering*. *Curr Rheumatol Rep*, 2019. **21**(8): p. 38.
139. Zaucke, F., et al., *Cartilage oligomeric matrix protein (COMP) and collagen IX are sensitive markers for the differentiation state of articular primary chondrocytes*. *Biochem J*, 2001. **358**(Pt 1): p. 17-24.
140. Miosge, N., et al., *Expression of collagen type I and type II in consecutive stages of human osteoarthritis*. *Histochem Cell Biol*, 2004. **122**(3): p. 229-36.
141. Kirsch, T., B. Swoboda, and H. Nah, *Activation of annexin II and V expression, terminal differentiation, mineralization and apoptosis in human osteoarthritic cartilage*. *Osteoarthritis Cartilage*, 2000. **8**(4): p. 294-302.
142. von der Mark, K., et al., *Upregulation of type X collagen expression in osteoarthritic cartilage*. *Acta Orthopaedica Scandinavica*, 2009. **66**(sup266): p. 125-129.
143. Gebauer, J.M., et al., *COMP and TSP-4 interact specifically with the novel GXKQHR motif only found in fibrillar collagens*. *Sci Rep*, 2018. **8**(1): p. 17187.
144. Rosenberg, K., et al., *Cartilage oligomeric matrix protein shows high affinity zinc-dependent interaction with triple helical collagen*. *J Biol Chem*, 1998. **273**(32): p. 20397-403.
145. Agarwal, P., et al., *Collagen XII and XIV, new partners of cartilage oligomeric matrix protein in the skin extracellular matrix suprastructure*. *J Biol Chem*, 2012. **287**(27): p. 22549-59.
146. Di Cesare, P.E., et al., *Matrix-matrix interaction of cartilage oligomeric matrix protein and fibronectin*. *Matrix Biology*, 2002. **21**(5): p. 461-470.
147. Mann, H.H., et al., *Interactions between the cartilage oligomeric matrix protein and matrilins. Implications for matrix assembly and the pathogenesis of chondrodysplasias*. *J Biol Chem*, 2004. **279**(24): p. 25294-8.
148. Tan, K. and J. Lawler, *The interaction of Thrombospondins with extracellular matrix proteins*. *J Cell Commun Signal*, 2009. **3**(3-4): p. 177-87.
149. Hansen, U., et al., *A secreted variant of cartilage oligomeric matrix protein carrying a chondrodysplasia-causing mutation (p.H587R) disrupts collagen fibrillogenesis*. *Arthritis Rheum*, 2011. **63**(1): p. 159-67.
150. Budde, B., et al., *Altered integration of matrilin-3 into cartilage extracellular matrix in the absence of collagen IX*. *Mol Cell Biol*, 2005. **25**(23): p. 10465-78.
151. Dunkle, E.T., F. Zaucke, and D.O. Clegg, *Thrombospondin-4 and matrix three-dimensionality in axon outgrowth and adhesion in the developing retina*. *Exp Eye Res*, 2007. **84**(4): p. 707-17.
152. Koelling, S., et al., *Migratory chondrogenic progenitor cells from repair tissue during the later stages of human osteoarthritis*. *Cell Stem Cell*, 2009. **4**(4): p. 324-35.
153. Seol, D., et al., *Chondrogenic progenitor cells respond to cartilage injury*. *Arthritis Rheum*, 2012. **64**(11): p. 3626-3637.
154. Frolova, E.G., et al., *Thrombospondin-4 regulates fibrosis and remodeling of the myocardium in response to pressure overload*. *FASEB J*, 2012. **26**(6): p. 2363-73.
155. Mustonen, E., et al., *Thrombospondin-4 expression is rapidly upregulated by cardiac overload*. *Biochem Biophys Res Commun*, 2008. **373**(2): p. 186-91.

156. Giannoni, P.S., M.; Hunziker, E.B.; Wong, M, *The mechanosensitivity of cartilage oligomeric matrix protein (COMP)*. *Biorheology*, 2003. **40**: p. 101-109.
157. Wong, M., M. Siegrist, and X. Cao, *Cyclic compression of articular cartilage explants is associated with progressive consolidation and altered expression pattern of extracellular matrix proteins*. *Matrix Biology*, 1999. **18**(4): p. 391-399.
158. Gratz, K.R., et al., *The effects of focal articular defects on cartilage contact mechanics*. *J Orthop Res*, 2009. **27**(5): p. 584-92.
159. Moo, E.K., et al., *Extracellular matrix integrity affects the mechanical behaviour of in-situ chondrocytes under compression*. *J Biomech*, 2014. **47**(5): p. 1004-13.
160. Caron, M.M.J., et al., *Aggrecan and COMP Improve Periosteal Chondrogenesis by Delaying Chondrocyte Hypertrophic Maturation*. *Front Bioeng Biotechnol*, 2020. **8**: p. 1036.
161. Holden, P., et al., *Cartilage oligomeric matrix protein interacts with type IX collagen, and disruptions to these interactions identify a pathogenetic mechanism in a bone dysplasia family*. *J Biol Chem*, 2001. **276**(8): p. 6046-55.
162. Thur, J., et al., *Mutations in cartilage oligomeric matrix protein causing pseudoachondroplasia and multiple epiphyseal dysplasia affect binding of calcium and collagen I, II, and IX*. *J Biol Chem*, 2001. **276**(9): p. 6083-92.
163. Brachvogel, B., et al., *Comparative proteomic analysis of normal and collagen IX null mouse cartilage reveals altered extracellular matrix composition and novel components of the collagen IX interactome*. *J Biol Chem*, 2013. **288**(19): p. 13481-92.
164. Du, Y., et al., *Cartilage oligomeric matrix protein inhibits vascular smooth muscle calcification by interacting with bone morphogenetic protein-2*. *Circ Res*, 2011. **108**(8): p. 917-28.
165. Gordon, M.K., et al., *Type XII collagen. A large multidomain molecule with partial homology to type IX collagen*. *Journal of Biological Chemistry*, 1989. **264**(33): p. 19772-19778.
166. Font, B., et al., *Characterization of the interactions of type XII collagen with two small proteoglycans from fetal bovine tendon, decorin and fibromodulin*. *Matrix Biology*, 1996. **15**(5): p. 341-348.
167. Darling, E.M., et al., *Mechanical properties and gene expression of chondrocytes on micropatterned substrates following dedifferentiation in monolayer*. *Cell Mol Bioeng*, 2009. **2**(3): p. 395-404.
168. Wang, C., et al., *Cartilage oligomeric matrix protein improves in vivo cartilage regeneration and compression modulus by enhancing matrix assembly and synthesis*. *Colloids Surf B Biointerfaces*, 2017. **159**: p. 518-526.
169. Zawel, L., et al., *Human Smad3 and Smad4 Are Sequence-Specific Transcription Activators*. *Molecular Cell*, 1998. **1**(4): p. 611-617.
170. van der Kraan, P.M., et al., *Age-dependent alteration of TGF-beta signalling in osteoarthritis*. *Cell Tissue Res*, 2012. **347**(1): p. 257-65.
171. Xia, M. and Y. Zhu, *Fibronectin fragment activation of ERK increasing integrin alpha(5) and beta(1) subunit expression to degenerate nucleus pulposus cells*. *J Orthop Res*, 2011. **29**(4): p. 556-61.
172. Daheshia, M. and J.Q. Yao, *The interleukin 1beta pathway in the pathogenesis of osteoarthritis*. *J Rheumatol*, 2008. **35**(12): p. 2306-12.

173. Magdaleno, F., et al., *Cartilage oligomeric matrix protein participates in the pathogenesis of liver fibrosis*. J Hepatol, 2016. **65**(5): p. 963-971.
174. Cingolani, O.H., et al., *Thrombospondin-4 is required for stretch-mediated contractility augmentation in cardiac muscle*. Circ Res, 2011. **109**(12): p. 1410-4.
175. Pfander, D., et al., *Expression of thrombospondin-1 and its receptor CD36 in human osteoarthritic cartilage*. Ann Rheum Dis, 2000. **59**(6): p. 448-54.
176. Motaung, S.C., P.E. Di Cesare, and A.H. Reddi, *Differential response of cartilage oligomeric matrix protein (COMP) to morphogens of bone morphogenetic protein/transforming growth factor-beta family in the surface, middle and deep zones of articular cartilage*. J Tissue Eng Regen Med, 2011. **5**(6): p. e87-96.
177. Skioldebrand, E., et al., *Cartilage oligomeric matrix protein neopeptide in the synovial fluid of horses with acute lameness: A new biomarker for the early stages of osteoarthritis*. Equine Vet J, 2017. **49**(5): p. 662-667.
178. Brooks, P.C., et al., *Disruption of Angiogenesis by PEX, a Noncatalytic Metalloproteinase Fragment with Integrin Binding Activity*. Cell, 1998. **92**(3): p. 391-400.
179. Lees, S., et al., *Bioactivity in an Aggrecan 32-mer Fragment Is Mediated via Toll-like Receptor 2*. Arthritis Rheumatol, 2015. **67**(5): p. 1240-9.
180. López-Moratalla, N., et al., *Activation of human lymphomononuclear cells by peptides derived from extracellular matrix proteins*. Biochimica et Biophysica Acta (BBA) - Molecular Cell Research, 1995. **1265**(2-3): p. 181-188.
181. Stanton, H., L. Ung, and A.J. Fosang, *The 45 kDa collagen-binding fragment of fibronectin induces matrix metalloproteinase-13 synthesis by chondrocytes and aggrecan degradation by aggrecanases*. Biochem J, 2002. **364**(Pt 1): p. 181-90.
182. Lohmander, L.S., T. Saxne, and D.K. Heinegard, *Release of cartilage oligomeric matrix protein (COMP) into joint fluid after knee injury and in osteoarthritis*. Ann Rheum Dis, 1994. **53**(1): p. 8-13.
183. Lorenzo, P., et al., *Quantification of cartilage oligomeric matrix protein (COMP) and a COMP neopeptide in synovial fluid of patients with different joint disorders by novel automated assays*. Osteoarthritis Cartilage, 2017. **25**(9): p. 1436-1442.
184. Calamia, V., et al., *Development of a multiplexed assay for the targeted analysis of cartilage endogenous peptides in synovial fluid and serum from osteoarthritis patients [Abstract]*. Osteoarthritis and Cartilage, 2016. **24**.
185. Fu, Y., et al., *Shift of Macrophage Phenotype Due to Cartilage Oligomeric Matrix Protein Deficiency Drives Atherosclerotic Calcification*. Circ Res, 2016. **119**(2): p. 261-76.
186. Klatt, A.R., et al., *Matrilin-3 activates the expression of osteoarthritis-associated genes in primary human chondrocytes*. FEBS Lett, 2009. **583**(22): p. 3611-7.
187. Ma, B., et al., *Cartilage oligomeric matrix protein is a novel notch ligand driving embryonic stem cell differentiation towards the smooth muscle lineage*. J Mol Cell Cardiol, 2018. **121**: p. 69-80.
188. Geng, H., et al., *Incomplete B cell tolerance to cartilage oligomeric matrix protein in mice*. Arthritis Rheum, 2013. **65**(9): p. 2301-9.
189. Saxne, T. and D. Heinegard, *Cartilage oligomeric matrix protein: a novel marker of cartilage turnover detectable in synovial fluid and blood*. Br J Rheumatol, 1992. **31**(9): p. 583-91.

190. Li, H., et al., *Comparative analysis with collagen type II distinguishes cartilage oligomeric matrix protein as a primary TGFbeta-responsive gene*. *Osteoarthritis Cartilage*, 2011. **19**(10): p. 1246-53.
191. Orth, P., L. Gao, and H. Madry, *Microfracture for cartilage repair in the knee: a systematic review of the contemporary literature*. *Knee Surg Sports Traumatol Arthrosc*, 2020. **28**(3): p. 670-706.
192. Mapp, P.I. and D.A. Walsh, *Mechanisms and targets of angiogenesis and nerve growth in osteoarthritis*. *Nat Rev Rheumatol*, 2012. **8**(7): p. 390-8.
193. Walsh, D.A., et al., *Angiogenesis and nerve growth factor at the osteochondral junction in rheumatoid arthritis and osteoarthritis*. *Rheumatology (Oxford)*, 2010. **49**(10): p. 1852-61.
194. Williams, F.M. and T.D. Spector, *Biomarkers in osteoarthritis*. *Arthritis Res Ther*, 2008. **10**(1): p. 101.
195. Ahrman, E., et al., *Novel cartilage oligomeric matrix protein (COMP) neoepitopes identified in synovial fluids from patients with joint diseases using affinity chromatography and mass spectrometry*. *J Biol Chem*, 2014. **289**(30): p. 20908-16.
196. Andrés Sastre, E., et al., *Cartilage Oligomeric Matrix Protein inhibits angiogenesis in vitro, depending upon its oligomerisation state [Abstract]*, in *Tissue Engineering and Regenerative Medicine International Society (TERMIS)*. 2019, TERMIS-EU: Rhodes. Greece.
197. Zhen, E.Y., et al., *Characterization of metalloprotease cleavage products of human articular cartilage*. *Arthritis Rheum*, 2008. **58**(8): p. 2420-31.
198. Kennedy, J., et al., *COMP mutation screening as an aid for the clinical diagnosis and counselling of patients with a suspected diagnosis of pseudoachondroplasia or multiple epiphyseal dysplasia*. *Eur J Hum Genet*, 2005. **13**(5): p. 547-55.
199. Briggs, M.D., et al., *Diverse mutations in the gene for cartilage oligomeric matrix protein in the pseudoachondroplasia-multiple epiphyseal dysplasia disease spectrum*. *Am J Hum Genet*, 1998. **62**(2): p. 311-9.
200. Jakkula, E., et al., *A recurrent R718W mutation in COMP results in multiple epiphyseal dysplasia with mild myopathy: clinical and pathogenetic overlap with collagen IX mutations*. *J Med Genet*, 2003. **40**(12): p. 942-8.
201. Fernandez-Puente, P., et al., *Analysis of Endogenous Peptides Released from Osteoarthritic Cartilage Unravels Novel Pathogenic Markers*. *Mol Cell Proteomics*, 2019. **18**(10): p. 2018-2028.
202. Dimitriou, R., et al., *Bone regeneration: current concepts and future directions*. *BMC Med*, 2011. **9**: p. 66.
203. Roberts, T.T. and A.J. Rosenbaum, *Bone grafts, bone substitutes and orthobiologics: the bridge between basic science and clinical advancements in fracture healing*. *Organogenesis*, 2012. **8**(4): p. 114-24.
204. Ehnert, S., et al., *Use of in vitro bone models to screen for altered bone metabolism, osteopathies, and fracture healing: challenges of complex models*. *Arch Toxicol*, 2020. **94**(12): p. 3937-3958.
205. Scott, M.A., et al., *Brief review of models of ectopic bone formation*. *Stem Cells Dev*, 2012. **21**(5): p. 655-67.

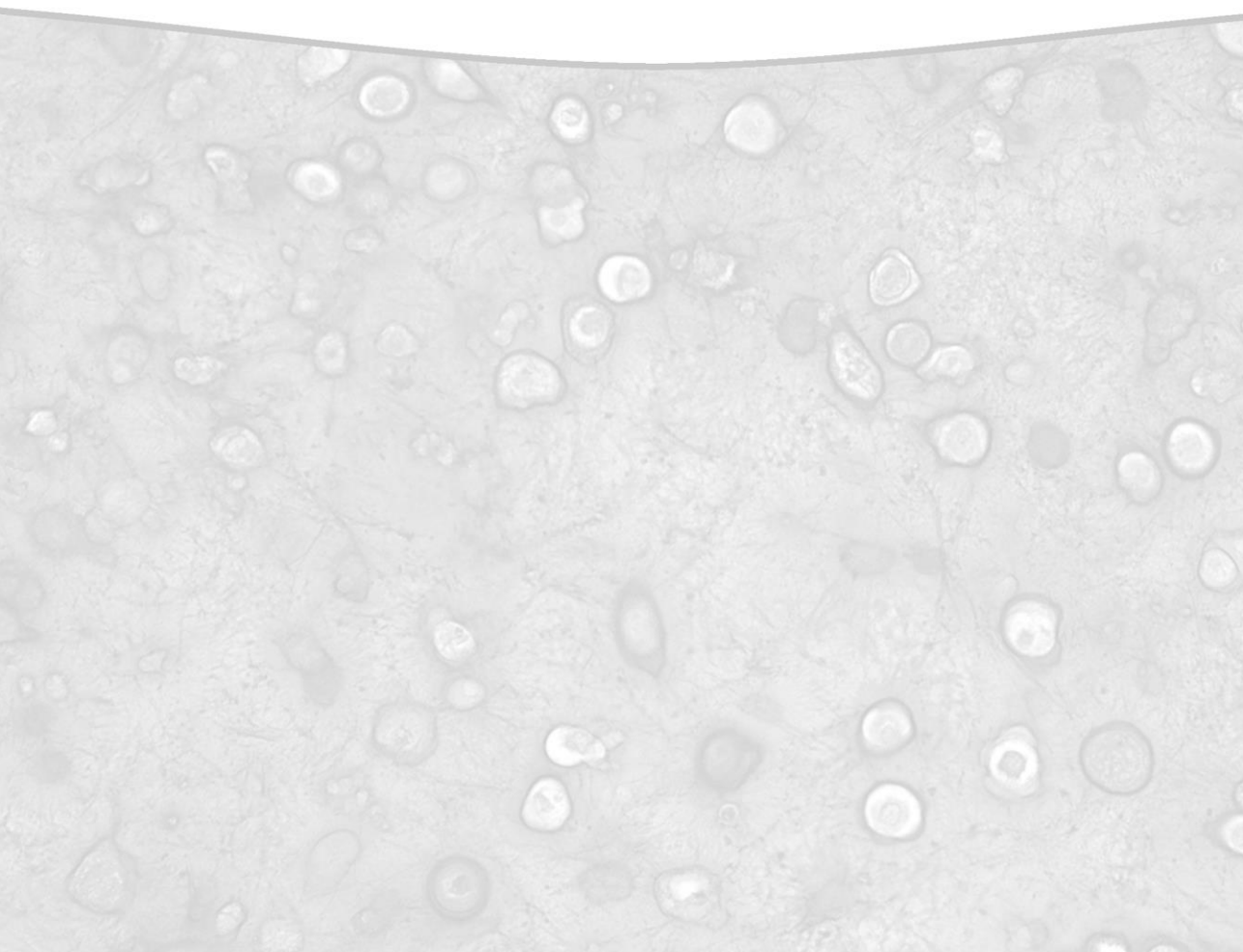
206. Schindeler, A., et al., *Preclinical models for orthopedic research and bone tissue engineering*. J Orthop Res, 2018. **36**(3): p. 832-840.
207. Chalmers, J., D.H. Gray, and J. Rush, *Observations on the Induction of Bone in Soft Tissues*. The Journal of Bone and Joint Surgery. British volume, 1975. **57-B**(1): p. 36-45.
208. de Vries-van Melle, M.L., et al., *An osteochondral culture model to study mechanisms involved in articular cartilage repair*. Tissue Eng Part C Methods, 2012. **18**(1): p. 45-53.
209. Zaffe, D. and F. D'Avenia, *A novel bone scraper for intraoral harvesting: a device for filling small bone defects*. Clin Oral Implants Res, 2007. **18**(4): p. 525-33.
210. O'Brien, F., *Influence of freezing rate on pore structure in freeze-dried collagen-GAG scaffolds*. Biomaterials, 2004. **25**(6): p. 1077-1086.
211. Lolli, A., et al., *Silencing of Antichondrogenic MicroRNA-221 in Human Mesenchymal Stem Cells Promotes Cartilage Repair In Vivo*. Stem Cells, 2016. **34**(7): p. 1801-11.
212. Lolli, A., et al., *Hydrogel-based delivery of anti-miR-221 enhances cartilage regeneration by endogenous cells*. Journal of Controlled Release, 2019. **309**: p. 220-230.
213. Vainieri, M.L., et al., *Evaluation of biomimetic hyaluronic-based hydrogels with enhanced endogenous cell recruitment and cartilage matrix formation*. Acta Biomater, 2020. **101**: p. 293-303.
214. Christen, P. and R. Muller, *In vivo Visualisation and Quantification of Bone Resorption and Bone Formation from Time-Lapse Imaging*. Curr Osteoporos Rep, 2017. **15**(4): p. 311-317.
215. Waarsing, J.H., et al., *Detecting and tracking local changes in the tibiae of individual rats: a novel method to analyse longitudinal in vivo micro-CT data*. Bone, 2004. **34**(1): p. 163-9.
216. Gaytan, F., et al., *A novel RGB-trichrome staining method for routine histological analysis of musculoskeletal tissues*. Sci Rep, 2020. **10**(1): p. 16659.
217. Johnstone, B., et al., *In Vitro Chondrogenesis of Bone Marrow-Derived Mesenchymal Progenitor Cells*. Experimental Cell Research, 1998. **238**(1): p. 265-272.
218. Alhag, M., et al., *Evaluation of the ability of collagen-glycosaminoglycan scaffolds with or without mesenchymal stem cells to heal bone defects in Wistar rats*. Oral Maxillofac Surg, 2012. **16**(1): p. 47-55.
219. Lyons, F.G., et al., *The healing of bony defects by cell-free collagen-based scaffolds compared to stem cell-seeded tissue engineered constructs*. Biomaterials, 2010. **31**(35): p. 9232-43.
220. Thompson, E.M., et al., *An Endochondral Ossification-Based Approach to Bone Repair: Chondrogenically Primed Mesenchymal Stem Cell-Laden Scaffolds Support Greater Repair of Critical-Sized Cranial Defects Than Osteogenically Stimulated Constructs In Vivo*. Tissue Eng Part A, 2016. **22**(5-6): p. 556-67.
221. Sorgente N, K.K., Soble LW, Eisenstein R, *The resistance of certain tissues to invasion. II. Evidence for extractable factors in cartilage which inhibit invasion by vascularized mesenchyme*. Lab Invest, 1975. **32**: p. 217-222.
222. Hubrecht, R.C. and E. Carter, *The 3Rs and Humane Experimental Technique: Implementing Change*. Animals (Basel), 2019. **9**(10).
223. Haffner-Luntzer, M., et al., *Mouse Models in Bone Fracture Healing Research*. Current Molecular Biology Reports, 2016. **2**(2): p. 101-111.
224. Zwingenberger, S., et al., *Establishment of a femoral critical-size bone defect model in immunodeficient mice*. J Surg Res, 2013. **181**(1): p. e7-e14.

225. Yu, X., et al., *Controlling the structural organization of regenerated bone by tailoring tissue engineering scaffold architecture*. Journal of Materials Chemistry, 2012. **22**(19).
226. Gauthier, O., et al., *In vivo bone regeneration with injectable calcium phosphate biomaterial: a three-dimensional micro-computed tomographic, biomechanical and SEM study*. Biomaterials, 2005. **26**(27): p. 5444-53.
227. Kim, H.W., et al., *Bone formation on the apatite-coated zirconia porous scaffolds within a rabbit calvarial defect*. J Biomater Appl, 2008. **22**(6): p. 485-504.
228. Lee, E.H., et al., *A combination graft of low-molecular-weight silk fibroin with Choukroun platelet-rich fibrin for rabbit calvarial defect*. Oral Surg Oral Med Oral Pathol Oral Radiol Endod, 2010. **109**(5): p. e33-8.
229. Wang, X.L., et al., *Exogenous phytoestrogenic molecule icaritin incorporated into a porous scaffold for enhancing bone defect repair*. J Orthop Res, 2013. **31**(1): p. 164-72.
230. Moreno-Jimenez, I., et al., *The chorioallantoic membrane (CAM) assay for the study of human bone regeneration: a refinement animal model for tissue engineering*. Sci Rep, 2016. **6**: p. 32168.
231. de Vries-van Melle, M.L., et al., *Chondrogenesis of Mesenchymal Stem Cells in an Osteochondral Environment Is Mediated by the Subchondral Bone*. Tissue Engineering Part A, 2014. **20**(1-2): p. 23-33.
232. Epple, C., et al., *Prefabrication of a large pedicled bone graft by engineering the germ for de novo vascularization and osteoinduction*. Biomaterials, 2019. **192**: p. 118-127.
233. Ismail, T., et al., *Engineered, axially-vascularized osteogenic grafts from human adipose-derived cells to treat avascular necrosis of bone in a rat model*. Acta Biomater, 2017. **63**: p. 236-245.
234. Ismail, T., et al., *Platelet-rich plasma and stromal vascular fraction cells for the engineering of axially vascularized osteogenic grafts*. J Tissue Eng Regen Med, 2020. **14**(12): p. 1908-1917.
235. Betts, D.C. and R. Muller, *Mechanical regulation of bone regeneration: theories, models, and experiments*. Front Endocrinol (Lausanne), 2014. **5**: p. 211.
236. Papi, P., et al., *The Use of a Non-Absorbable Membrane as an Occlusive Barrier for Alveolar Ridge Preservation: A One Year Follow-Up Prospective Cohort Study*. Antibiotics (Basel), 2020. **9**(3).
237. Korzinskas, T., et al., *In Vivo Analysis of the Biocompatibility and Macrophage Response of a Non-Resorbable PTFE Membrane for Guided Bone Regeneration*. Int J Mol Sci, 2018. **19**(10).
238. Mori, G., et al., *The Interplay between the bone and the immune system*. Clin Dev Immunol, 2013. **2013**: p. 720504.
239. Schlundt, C., et al., *Individual Effector/Regulator T Cell Ratios Impact Bone Regeneration*. Front Immunol, 2019. **10**: p. 1954.
240. El Khassawna, T., et al., *T Lymphocytes Influence the Mineralization Process of Bone*. Front Immunol, 2017. **8**: p. 562.
241. Schlundt, C., et al., *The multifaceted roles of macrophages in bone regeneration: A story of polarization, activation and time()*. Acta Biomater, 2021.
242. Stefanowski, J., et al., *Spatial Distribution of Macrophages During Callus Formation and Maturation Reveals Close Crosstalk Between Macrophages and Newly Forming Vessels*. Front Immunol, 2019. **10**: p. 2588.

243. Schlundt, C., et al., *Macrophages in bone fracture healing: Their essential role in endochondral ossification*. *Bone*, 2018. **106**: p. 78-89.
244. Knuth, C., et al., *Understanding tissue-engineered endochondral ossification; towards improved bone formation*. *Eur Cell Mater*, 2019. **37**: p. 277-291.
245. Farrell, E., et al., *In-vivo generation of bone via endochondral ossification by in-vitro chondrogenic priming of adult human and rat mesenchymal stem cells*. *BMC Musculoskelet Disord*, 2011. **12**: p. 31.
246. Jo, S.H., et al., *Tracheal calcification*. *CMAJ*, 2008. **179**(3): p. 291.
247. Claassen, H., et al., *Different Patterns of Cartilage Mineralization Analyzed by Comparison of Human, Porcine, and Bovine Laryngeal Cartilages*. *J Histochem Cytochem*, 2017. **65**(6): p. 367-379.
248. Stevens, M.M., *Biomaterials for bone tissue engineering*. *Materials Today*, 2008. **11**(5): p. 18-25.
249. Walsh, D.P., et al., *Rapid healing of a critical-sized bone defect using a collagen-hydroxyapatite scaffold to facilitate low dose, combinatorial growth factor delivery*. *J Tissue Eng Regen Med*, 2019. **13**(10): p. 1843-1853.
250. Filipowska, J., et al., *The role of vasculature in bone development, regeneration and proper systemic functioning*. *Angiogenesis*, 2017. **20**(3): p. 291-302.
251. Auger, F.A., L. Gibot, and D. Lacroix, *The pivotal role of vascularization in tissue engineering*. *Annu Rev Biomed Eng*, 2013. **15**: p. 177-200.
252. Qian, W., et al., *Thrombospondin-4 critically controls transforming growth factor beta1 induced hypertrophic scar formation*. *J Cell Physiol*, 2018. **234**(1): p. 731-739.
253. Karamanos, N.K., et al., *A guide to the composition and functions of the extracellular matrix*. *FEBS J*, 2021.
254. Blackwood, K.A., et al., *Scaffolds for Growth Factor Delivery as Applied to Bone Tissue Engineering*. *International Journal of Polymer Science*, 2012. **2012**: p. 1-25.
255. Jeong, B.C., et al., *COMP-Ang1, a chimeric form of Angiopoietin 1, enhances BMP2-induced osteoblast differentiation and bone formation*. *Bone*, 2010. **46**(2): p. 479-86.
256. Refaat, M., et al., *Binding to COMP Reduces the BMP2 Dose for Spinal Fusion in a Rat Model*. *Spine (Phila Pa 1976)*, 2016. **41**(14): p. E829-36.
257. Zhang, Q., et al., *Promoting therapeutic angiogenesis of focal cerebral ischemia using thrombospondin-4 (TSP4) gene-modified bone marrow stromal cells (BMSCs) in a rat model*. *J Transl Med*, 2019. **17**(1): p. 111.
258. Stenina-Adognravi, O., *Invoking the power of thrombospondins: regulation of thrombospondins expression*. *Matrix Biol*, 2014. **37**: p. 69-82.
259. Carlson, C.B., J. Lawler, and D.F. Mosher, *Structures of thrombospondins*. *Cell Mol Life Sci*, 2008. **65**(5): p. 672-86.
260. Vilorio, K. and N.J. Hill, *Embracing the complexity of matricellular proteins: the functional and clinical significance of splice variation*. *Biomol Concepts*, 2016. **7**(2): p. 117-32.
261. Guo, F., et al., *ATF6a, a Runx2-activable transcription factor, is a new regulator of chondrocyte hypertrophy*. *J Cell Sci*, 2016. **129**(4): p. 717-28.
262. Lynch, J.M., et al., *A thrombospondin-dependent pathway for a protective ER stress response*. *Cell*, 2012. **149**(6): p. 1257-68.
263. Opperman, L.A. and J.T. Rawlins, *The extracellular matrix environment in suture morphogenesis and growth*. *Cells Tissues Organs*, 2005. **181**(3-4): p. 127-35.

264. Pakvasa, M., et al., *Notch signaling: Its essential roles in bone and craniofacial development*. Genes Dis, 2021. **8**(1): p. 8-24.
265. McCart Reed, A.E., et al., *Thrombospondin-4 expression is activated during the stromal response to invasive breast cancer*. Virchows Arch, 2013. **463**(4): p. 535-45.
266. Liu, J., et al., *Reciprocal regulation of long noncoding RNAs THBS4003 and THBS4 control migration and invasion in prostate cancer cell lines*. Mol Med Rep, 2016. **14**(2): p. 1451-8.
267. Bonnet, C.S. and D.A. Walsh, *Osteoarthritis, angiogenesis and inflammation*. Rheumatology (Oxford), 2005. **44**(1): p. 7-16.
268. Montoya, C., et al., *On the road to smart biomaterials for bone research: definitions, concepts, advances, and outlook*. Bone Res, 2021. **9**(1): p. 12.
269. Malhan, D., et al., *An Optimized Approach to Perform Bone Histomorphometry*. Front Endocrinol (Lausanne), 2018. **9**: p. 666.
270. Stockl, D., H. D'Hondt, and L.M. Thienpont, *Method validation across the disciplines--critical investigation of major validation criteria and associated experimental protocols*. J Chromatogr B Analyt Technol Biomed Life Sci, 2009. **877**(23): p. 2180-90.
271. Amini, A.R., C.T. Laurencin, and S.P. Nukavarapu, *Bone tissue engineering: recent advances and challenges*. Crit Rev Biomed Eng, 2012. **40**(5): p. 363-408.

APPENDICES



TROMBOSPONDINES -4 EN-5 IN ONTWIKKELING, ZIEKTE EN HERSTEL VAN HET SKELET

Implicaties voor tissue engineering van bot

Mobiliteit is cruciaal voor de kwaliteit van leven. Echter, na een ongeluk of na het verwijderen van een bottumor, kunnen patiënten botletsels hebben die niet genezen. Voor deze ernstige complicaties die blijvende invaliditeit tot gevolg hebben en de kwaliteit van leven van de patiënt verminderen, zijn geen effectieve behandelingen beschikbaar. Om de therapeutische opties te verbeteren, worden nieuwe implantaten ontwikkeld die de vorming van nieuw bot stimuleren. Tijdens de ontwikkeling van ons skelet als we groeien en tijdens het "normale" herstel van een botbreuk maakt ons lichaam tijdelijke kraakbeenstructuren om de botvorming te sturen via een proces dat we endochondrale verbening noemen. Door die kraakbeenstructuren te repliceren, kunnen we implantaten ontwikkelen die gebruikt kunnen worden voor de genezing van botletsels die uit zichzelf niet goed genezen. Vooral de extracellulaire matrix (ECM) van de kraakbeenstructuur is van groot belang, omdat het van nature botvorming begeleidt. Hoewel we al veel kennis hebben van de ECM eiwitten en andere factoren die aanwezig zijn in deze tijdelijke kraakbeenstructuur, is van een deel van de ECM eiwitten de functie tijdens botvorming nog grotendeels onbekend. Het begrijpen van de samenstelling en de rol die ECM eiwitten in kraakbeen spelen tijdens botvorming en botherstel kan helpen te bepalen welke componenten bruikbaar kunnen zijn voor het bevorderen van botherstel. In dit proefschrift wilde ik meer inzicht krijgen in de rol die twee ECM eiwitten –Trombospondine-4 (TSP-4) en Trombospondine-5 (TSP-5)– spelen in het proces van endochondrale verbening. Mijn tweede doel was een methode ontwikkelen om hun potentieel voor botvorming te beoordelen.

Mijn onderzoek begon in **Hoofdstuk 2**, nadat ik had ontdekt dat mensen TSP-4 aanmaken tijdens de groei van het skelet. Van daaruit heb ik onderzocht waar en wanneer TSP-4 voorkomt en hoe zich dat verhoudt tot TSP-5, een ECM eiwit van dezelfde eiwitfamilie. Omdat mensen en muizen overeenkomsten vertonen in skeletontwikkeling, analyseerde ik de productie van de twee eiwitten tijdens de groei van het muizenskelet. Ik ontdekte dat TSP-5 aanwezig is in alle tijdelijke kraakbeenstructuren tijdens endochondrale verbening, terwijl TSP-4 alleen wordt geproduceerd in een speciale zone die direct naast het vormende bot ligt, de zogenaamde hypertrofe zone. Tegelijkertijd heb ik botten in het hoofdgebied bestudeerd, die zich vormen zonder het gebruik van een kraakbeenstructuur, via een proces dat intramembraneuze verbening wordt genoemd. Desalniettemin vond ik dat daar voorafgaand aan de botvorming TSP-4 wordt geproduceerd terwijl TSP-5 volledig afwezig is. Deze resultaten brachten me tot de vraag of tijdens de genezing van botbreuken –waarbij gebruik wordt gemaakt van de programma's voor intramembraneuze en endochondrale verbening– dezelfde ruimtelijke en tijdelijke patronen zouden worden gezien. Inderdaad bleken TSP-4 en TSP-5 dezelfde patronen te

volgen als tijdens de ontwikkeling van het skelet. Met verder laboratoriumonderzoek kwam ik tot de conclusie dat één van de rollen van TSP-4, in tegenstelling tot TSP-5, zou kunnen zijn om bloedvaten naar het vormende bot aan te trekken, wat van grote therapeutische waarde zou kunnen zijn. Ik heb daarom geconcludeerd dat het potentiële gebruik van de twee thrombospondins in botvorming, verder moeten worden bestudeerd.

In **Hoofdstuk 3** heb ik de aanmaak en de rol van TSP-4 en TSP-5 onderzocht in een situatie waar pathologische endochondrale verbening plaatsvindt tijdens artrose. In artrose wordt het kraakbeen in de gewrichten onherstelbaar beschadigd en is er meer TSP-4 en TSP-5 aanwezig. Mijn onderzoek liet zien dat TSP-5 de migratie van kraakbeencellen kan stimuleren, maar TSP-4 niet. Verder ontdekte ik dat de twee eiwitten synergetisch kunnen werken met de groeifactor TGF- β om kraakbeenmatrix aan te maken, maar dat ze dat doen via enigszins verschillende mechanismen. Gerelateerd aan de resultaten in Hoofdstuk 2 werd het duidelijk dat ondanks dat de chemische structuur van TSP-4 en TSP-5 veel op elkaar lijkt, deze eiwitten zowel vergelijkbare als verschillende functies hebben in de vorming van weefsels van het skelet. Hoewel TSP-4 met name verband leek te houden met botvorming, was dit onduidelijk voor TSP-5. Tijdens de verbening van kraakbeen, wordt het kraakbeen geremodelleerd en worden er TSP-5-fragmenten gevormd. Omdat bekend is dat ECM-eiwitfragmenten biologische activiteit kunnen hebben, heb ik in **Hoofdstuk 4** onderzocht of drie TSP-5 fragmenten die bij artrose worden gevormd, een rol kunnen spelen in de pathologische botvorming die gezien wordt bij deze ziekte. Hiervoor gebruikte ik synthetische versies van drie TSP-5 peptiden die geproduceerd worden tijdens artrose en bestudeerde ik in het laboratorium hun mogelijke effecten op voorlopercellen uit het bot, cellen van de bloedvatwand en gewrichtsslijmvlies. Van geen van de peptides kon ik echter bioactieve eigenschappen aantonen.

We vonden TSP-4 de moeite waard om verder te testen voor toepassing in implantaten voor het verbeteren van botweefselaanmaak. Aangezien in een kweekschachtje in het laboratorium botvorming niet goed kan worden beoordeeld, moet de evaluatie bij levende dieren worden uitgevoerd. Helaas waren de technieken die beschikbaar waren omslachtig en hadden ze een grote impact op het dierenwelzijn. Om deze reden heb ik in **Hoofdstuk 5** een meer verfijnde en efficiëntere methode ontwikkeld voor het testen van botimplantaten, dat in potentie het aantal benodigde dieren zou kunnen verminderen. Voor dit nieuwe model worden cilindervormige structuren van runderbotten gemaakt, die we van het slachthuis verkrijgen. In het midden van de cilinder wordt een holle ruimte gemaakt die kan worden opgevuld met een botimplantaat en vervolgens worden de cilindervormige structuren onder de huid bij muizen geplaatst. Ik heb dit nieuwe botvormingsmodel gevalideerd door systematisch verschillende implantaten te evalueren voor hun potentieel om botgenezing te induceren. Botherstel vond alleen plaats als er geschikte implantaten in de ring werden geplaatst. Ik sloot mijn promotieonderzoek af door in dit model te testen of TSP-4 gebruikt kon worden om

botvorming te stimuleren. Daarvoor voegde ik TSP-4 toe aan een biomateriaal gebaseerd op collageen en hydroxyapatite. Helaas liet deze eerste test geen grote verbetering in botvorming zien met TSP-4 en zijn verdere studies nodig om de effecten te evalueren die TSP-4 kan hebben als het wordt toegediend in combinatie met andere groeifactoren die aanwezig zijn in de ECM.

Samenvattend, heb ik met dit onderzoek licht geworpen op hoe twee vergelijkbare ECM-eiwitten veranderen in kraakbeenstructuren die gevormd worden tijdens endochondrale verbening en heb ik beschreven hoe hun functies overlappen en verschillen afhankelijk van de situatie. Tot slot heb ik een methode ontwikkeld voor het testen van nieuwe therapieën die toekomstige ontdekkingen op het gebied van botgenezing zullen helpen versnellen.

TROMBOSPONDINAS -4 Y -5 EN EL DESARROLLO, ENFERMEDAD Y REPARACIÓN DEL ESQUELETO

Implicaciones para la ingeniería de tejidos óseos

La movilidad es crucial para la calidad de vida humana. Sin embargo, tras un traumatismo grave o la resección de tumores óseos, algunos pacientes quedan con huesos lesionados incapaces de fusionarse. Estas secuelas resultan en discapacidades permanentes y reducen la calidad de vida. Desafortunadamente, carecemos de tratamientos efectivos para esos pacientes. Con el fin de aumentar las opciones terapéuticas, se están diseñando nuevos implantes para guiar la regeneración de los huesos afectados. Durante el desarrollo esquelético y la curación de fracturas, nuestros cuerpos generan estructuras de cartílago transitorias que dirigen la formación de hueso a través del proceso de osificación endocondral. Replicando esas estructuras, los ingenieros de tejidos pueden diseñar sustitutos óseos con propiedades particulares. Para producir esos sustitutos, la matriz extracelular (MEC) del cartílago de transición es de especial interés, puesto que sus componentes guían el proceso regenerativo de forma natural. Sin embargo, son muchas las proteínas cuyas funciones relativas a la formación de hueso que todavía se desconocen. Por tanto, comprender la composición y la función de las proteínas de la MEC del cartílago de transición es fundamental para determinar cuáles de ellas pueden ser útiles para mejorar la regeneración ósea. En esta tesis, mis objetivos han sido: primero, profundizar en el papel que juegan durante la osificación endocondral dos proteínas de la MEC –la Trombospondina-4 (TSP-4) y la Trombospondina-5 (TSP-5)–; y segundo, desarrollar un método para evaluar su potencial terapéutico.

Mi investigación partió del **Capítulo 2**, tras descubrir que los humanos producimos TSP-4 durante nuestro crecimiento esquelético. Entonces, investigué cómo los patrones espaciales y temporales de la TSP-4 difieren respecto a su proteína hermana TSP-5. Dado que humanos y ratones desarrollamos nuestros esqueletos de forma similar, analicé la producción de las dos proteínas en ratones durante su crecimiento. Observé que la TSP-5 ocupa todo el cartílago transitorio durante la osificación endocondral, mientras que la TSP-4 solo se produce en las zonas hipertróficas adyacentes al hueso en formación. En paralelo, analicé los huesos presentes en la región de la cabeza, que se forman directamente sin la guía de dicho cartílago, a través del proceso de osificación intramembranosa. Sin embargo, ahí descubrí que la TSP-4 se produce también previa formación de hueso, mientras que la TSP-5 permanece ausente. Tras estos resultados me pregunté si los patrones espaciales y temporales observados aparecerían durante la curación de una fractura ósea, cuyo proceso regenerativo combina el uso de los mecanismos de osificación intramembranosa y endocondral. Y, de hecho, la TSP-4 y la TSP-5 se expresaron en la fractura imitando los patrones seguidos durante el desarrollo esquelético. Mediante estudios *in vitro* inferí que, a diferencia de la TSP-5, una de las

funciones de la TSP-4 podría ser la de atraer vasos sanguíneos al hueso en formación, lo cual podría tener gran valor terapéutico. Por todo esto, concluí que seguir investigando las dos trombospondinas sería clave para determinar sus posibles usos en ingeniería de tejidos óseos.

En el **Capítulo 3** exploré la producción y las funciones de la TSP-4 y la TSP-5 en un contexto donde ocurre una osificación endocondral patológica: la osteoartritis. Durante esta enfermedad se produce un daño prolongado e irreversible del cartílago, y aumenta la presencia de TSP-4 y TSP-5 en las articulaciones afectadas. Para comprender cómo las dos proteínas modifican el comportamiento de las células del cartílago (conocidas como condrocitos), investigué los efectos de ambas proteínas sobre el comportamiento migratorio, señalización intracelular y producción de componentes de la MEC de los condrocitos. Curiosamente, la TSP-5, pero no la TSP-4, estimuló la migración de condrocitos cuya MEC había sido eliminada. Además, observé que las dos proteínas actúan sinérgicamente con el factor de crecimiento TGF- β para incrementar la integración de la matriz, aunque a través de vías de señalización ligeramente diferentes. En relación con el capítulo anterior, se hizo evidente que, a pesar de sus similitudes estructurales, la TSP-4 y la TSP-5 desempeñan funciones tanto semejantes como dispares en la formación y reparación del esqueleto. Mientras que la TSP-4 parecía alinearse con la formación de hueso, no estaba claro hasta qué punto la TSP-5 también lo hacía. Durante la remodelación del cartílago y en los momentos previos a su osificación, parte de la TSP-5 presente en la MEC se fragmenta en pequeños péptidos. Puesto que ciertos fragmentos proteicos de la MEC han demostrado poseer actividad biológica, en el **Capítulo 4** me pregunté si los derivados de la TSP-5 podrían tener funciones relevantes en la osteoartritis, dada la relación de la enfermedad con la osificación endocondral patológica. Para ello, utilicé versiones sintéticas de tres péptidos de la TSP-5 producidos durante la enfermedad en diferentes ensayos *in vitro*, y exploré sus posibles efectos sobre las células progenitoras del hueso, las células endoteliales y la membrana sinovial. Sin embargo, ninguno de los péptidos demostró poseer propiedades bioactivas durante los ensayos.

Por otro lado, la TSP-4 parecía atractiva para ser aplicada en una estrategia de ingeniería de tejido óseo, por lo que decidí realizar más pruebas con ella. Dado que la formación de hueso no se puede evaluar de manera integral *in vitro*, es necesario hacerlo en animales vivos. Lamentablemente, los modelos y técnicas *in vivo* disponibles en aquel momento eran laboriosos y tenían un gran impacto sobre el bienestar animal. Por eso, en el **Capítulo 5** desarrollé una metodología más refinada y eficiente para evaluar la efectividad terapéutica de injertos óseos, que permitiera reducir potencialmente el número de animales de experimentación necesarios. En este nuevo modelo, anillos de hueso trabecular de origen bovino fueron implantados subcutáneamente en ratones. De esta manera, los implantes adquirieron la capacidad de formar hueso nuevo en sus centros huecos. La regeneración ocurrió solo al colocar injertos terapéuticamente eficaces en su interior, permitiendo así cuantificar la respuesta regenerativa inducida. Tras ello,

validé este nuevo modelo de formación ósea, que designé como semiortotópico, evaluando sistemáticamente en él el potencial osteogénico de diferentes injertos. En la última parte de mi investigación doctoral, usé el nuevo modelo de formación ósea semiortotópica para comenzar la evaluación de la TSP-4 como agente terapéutico. Para ello, usé un biomaterial basado en colágeno e hidroxiapatita, en el que incorporé TSP-4. Mientras que la adición individual de TSP-4 no incrementó sustancialmente la formación de hueso, estudios subsiguientes deberán evaluar los efectos sinérgicos de la TSP-4 al administrarla junto con los diversos factores de crecimiento presentes en la MEC.

En conclusión, en esta investigación he aportado nuevos datos sobre cómo diferentes componentes de la matriz extracelular varían en el cartílago de transición, y he descrito cómo la presencia y la función de dos proteínas similares de la MEC se superponen y difieren según su contexto. Por último, he desarrollado una nueva metodología capaz de probar nuevas terapias que ayudará a acelerar nuevos descubrimientos en el campo de los injertos óseos.

TROMBOSPONDINES -4 I -5 EN EL DESENVOLUPAMENT, MALALTIA I REPARACIÓ DE L'ESQUELET

Implicacions en enginyeria de teixits ossis

La mobilitat és crucial per a la qualitat de vida humana. No obstant això, després d'un traumatisme greu o la resecció de tumors ossis, alguns pacients poden quedar-se amb ossos lesionats incapaços de fusionar-se. Estes seqüeles resulten en discapacitats permanents i reduïxen la qualitat de vida. Desafortunadament, no disposem de tractaments efectius per aquests pacients. Amb la fi d'augmentar les opcions terapèutiques, s'estan dissenyant nous implants per a guiar la regeneració dels ossos afectats. Durant el desenvolupament esquelètic i la curació de fractures, els nostres cossos generen estructures de cartílag transitòries que dirigixen la formació d'os a través del procés d'ossificació endocondral. Replicant eixes estructures, els enginyers de teixits poden dissenyar substituïts ossis amb propietats particulars. Per a produir estos substituïts, la matriu extracel·lular (MEC) del cartílag de transició és de especial interès, atés que els seus components guien el procés regeneratiu de manera natural. Tot i això, són moltes les proteïnes amb funcions relatives a la formació d'os que encara es desconeixen. Per tant, comprendre la composició i la funció de les proteïnes de la MEC del cartílag de transició és fonamental per a determinar quines d'elles poden ser útils per a millor la regeneració òssia. En aquesta tesi, els meus objectius han sigut: primer, aprofundir en el paper que juguen durant l'ossificació endocondral dues proteïnes de la MEC –la Trombospondina-4 (TSP-4) i la Trombospondina-5 (TSP-5); i segon, desenvolupar un mètode per avaluar el seu potencial terapèutic.

La meua investigació partí del **Capítol 2**, després de descobrir que els humans produïm TSP-4 durant el nostre creixement esquelètic. Aleshores, investiguí com els patrons espacials i temporals de la TSP-4 diferixen respecte a la seua proteïna germana TSP-5. Atés que humans i ratolins desenvolupem els nostres esquelets de manera similar, analitzí la producció d'ambdues proteïnes en ratolins durant el seu creixement. Observí que la TSP-5 ocupa tot el cartílag transitori durant l'ossificació endocondral, mentres que la TSP-4 només es produïx a les zones hipertrofiques adjacents a l'os en formació. Paral·lelament, analitzí els ossos presents a la regió del cap, que es formen directament sense la guia d'aquest cartílag, a través del procés d'ossificació intramembranosa. No obstant això, ací descobrí que la TSP-4 es produïx també prèvia formació d'os, mentres que la TSP-5 roman absent. Després d'estos resultats em preguntí si els patrons espacials i temporals observats apareixerien durant la curació d'una fractura òssia, el procés regeneratiu de la qual combina l'ús dels mecanismes d'ossificació intramembranosa i endocondral. I, de fet, la TSP-4 i la TSP-5 s'expressaren en la fractura imitant els patrons seguits durant el desenvolupament esquelètic. Mitjançant estudis *in vitro* inferí que, a diferència de la TSP-5, una de les funcions de la TSP-4 podria ser la d'atraure vasos sanguinis a l'os en formació, la qual cosa podria tindre gran valor terapèutic. Per tot açò,

conclouí que seguir investigant les dos trombospondines seria clau per determinar els seus possibles usos en enginyeria de teixits ossis.

En el **Capítol 3** explorí la producció i les funcions de la TSP-4 i la TSP-5 en un context on ocorre una ossificació endocondral patològica: la osteoartritis. Durant aquesta malaltia, es produïx un dany prolongat i irreversible del cartílag, i augmenta la presència de TSP-4 i TSP-5 en les articulacions afectades. Per a comprendre com les dues proteïnes modifiquen el comportament de les cèl·lules del cartílag (conegudes com condrocits), investiguí els efectes d'ambdues proteïnes sobre el comportament migratori, senyalització intracel·lular, i producció de components de la MEC dels condrocits. Curiosament, la TSP-5, però no la TSP-4, estimulà la migració de condrocits la MEC dels quals havia sigut eliminada. A més, observí que les dues proteïnes actuen sinèrgicament amb el factor de creixement TGF- β per a incrementar la integració de la matriu, tot i que a través de vies de senyalització lleugerament diferents. En relació amb el capítol anterior, es féu evident que, malgrat les seues similituds estructurals, la TSP-4 i la TSP-5 exercien funcions tant semblants com dispers en la formació i reparació de l'esquelet. Mentre que la TSP-4 pareixia alinear-se amb la formació d'os, no estava clar fins a quin punt la TSP-5 també ho feia. Durant la remodelació del cartílag i en els moments previs a la seua ossificació, part de la TSP-5 present en la MEC es fragmenta en xicotets pèptids. Com que uns certs fragments proteics de la MEC han demostrat posseir activitat biològica, en el **Capítol 4** em preguntí si els derivats de la TSP-5 podrien tindre funcions rellevants en la osteoartritis, donada la relació de la malaltia amb l'ossificació endocondral patològica. Amb aquest fi, utilitzí versions sintètiques dels tres pèptids de la TSP-5 produïts durant la malaltia en diferents assajos *in vitro*, i explorí els seus possibles efectes sobre les cèl·lules progenitores de l'os, les cèl·lules endotelials i la membrana sinovial. No obstant això, cap dels pèptids demostrà posseir propietats bioactives durant els assajos.

D'altra banda, la TSP-4 semblava atractiva per a ser aplicada en una estratègia d'enginyeria de teixit ossi, per la qual cosa decidí realitzar més proves amb ella. Atés que la formació d'os no es pot avaluar de manera integral *in vitro*, és necessari fer-ho en animals vius. Lamentablement, els models i tècniques *in vivo* disponibles en aquell moment eren laboriosos i tenien un gran impacte sobre el benestar animal. Per això, en el **Capítol 5** desenvolupí una metodologia més refinada i eficient per avaluar l'efectivitat terapèutica d'empelts ossis, que permetera reduir potencialment el nombre d'animals d'experimentació necessaris. En aquest nou model, anells d'os trabecular d'origen boví foren implantats subcutàniament en ratolins. D'aquesta manera, els implants adquiriren la capacitat de formar os nou en els seus centres buits. La regeneració ocorregué només en col·locar empelts terapèuticament eficaços en el seu interior, permetent així quantificar la resposta regenerativa induïda. Després d'això, validí aquest nou model de formació òssia, que designí com semiortotòpica, avaluant sistemàticament en ell el potencial osteogènic de diferents empelts. En l'última part de la meua investigació doctoral, utilitzí el nou model de formació òssia semiortotòpica per a començar

l'avaluació de la TSP-4 com a agent terapèutic. Amb aquest fi, utilitzí un biomaterial basat en col·lagen i hidroxiapatita, en el qual incorporí TSP-4. Mentre que l'addició individual de TSP-4 no incrementà substancialment la formació d'os, estudis subsegüents hauran d'avaluar els efectes sinèrgics de la TSP-4 en administrar-la juntament amb els diversos factors de creixement presents en la MEC.

En conclusió, en aquesta investigació he aportat noves dades sobre com diferents components de la matriu extracel·lular varien en el cartílag de transició, i he descrit com la presència i la funció de dues proteïnes similars de la MEC se superposen i diferixen segons el seu context. Finalment, he desenvolupat una nova metodologia capaç de provar noves teràpies que ajudarà a accelerar nous descobriments en el camp dels empelts ossis.

List of publications

Knuth C.A., **Andrés Sastre E.**, Fahy N.B., Witte-Bouma J., Ridwan Y., Strabbing E.M., Koudstaal M.J., van de Peppel J., Wolvius E.B., Narcisi R., Farrell E., *Collagen type X is essential for successful mesenchymal stem cell mediated cartilage formation and subsequent endochondral ossification*. Eur Cell Mater. 2019 Sep 18; 38:106-122

Andrés Sastre E., Zaucke F., Witte-Bouma J., van Osch G.J.V.M., Farrell E., *Cartilage oligomeric matrix protein-derived peptides secreted by cartilage do not induce responses commonly observed during osteoarthritis*. Cartilage. 2020 Sep 29:1947603520961170

Maly K., **Andrés Sastre E.**, Farrell E., Meurer A., Zaucke F., *COMP and TSP-4: functional roles in articular cartilage and relevance in osteoarthritis*. Int J Mol Sci. 2021 Feb 24; 22(5):2242

Andrés Sastre E., Maly K., Zhu M., Witte-Bouma J., Trompet D., Böhm A.M., Brachvogel B., van Nieuwenhoven C., Maes C., van Osch G.J.V.M., Zaucke F., Farrell E., *Spatiotemporal distribution of thrombospondin-4 and -5 in cartilage during endochondral bone formation and repair*. Bone. 2021 Sep; 150:115999

Andrés Sastre E., Nossin Y., Jansen I., Kops N., Intini C., Witte-Bouma J., van Rietbergen B., Hofmann S., Ridwan Y., Gleeson J.P., O'Brien F.J., Wolvius E.B., van Osch G.J.V.M., Farrell E., *A new minimally invasive semi-orthotopic bone defect model for cell and biomaterial testing in regenerative medicine*. Biomaterials. 2021 Dec; 279:121187

Acknowledgements

When I enrolled in this PhD project, I was not aiming at the recognition that eventually it would entitle, but I rather aimed at the experience of the process itself. I wanted to experience the good and the bad days, failure and success, and the memories and friendships that I would build along the way. After a long journey, another amazing chapter of my life has finally come to an end, and what a successful one! Without each one of you, important pieces would have gone missing; and now, I would like to thank all of you that contributed to shape it and accompanied me through this adventure.

My first words go to the person that mentored me, **Dr. Eric Farrell**. It never mattered what plans we agreed the day before, because on the following day they were all scrambled and doubled in size –and that is all on me–. Eric, thanks for the patience and support you always showed me, even when failure was knocking on the door. With your guidance, I always felt safe to try, to fail, and to try better again. As it is said, ideas might be crazy until they are not, and that freedom you gave me was the key to put them into practice. Always standing next to you, **Prof. dr. Gerjo van Osch**. Gerjo, your passion, hard work and care for the people around are remarkable. I hope more people will keep seeing you as a source of inspiration and motivation on the years to come. Following your recommendation, I will keep celebrating every achievement, no matter how small it might seem. Thank you both from my heart for helping me grow both as a researcher and as a person during these last years.

To my two paranymphs, **Yannick** and **Virginia**. The three of us are now at the end of this PhD rollercoaster and still surviving to celebrate. Yannick, when we met in that competitive interview, who would have imagined all that was to come after? That car trip across Ireland, the expat meetings, or the day we found that Belgian beers are not like German ones. I still have my doubts on who aged better though, either us or our home-made honey wine. But the best, is the good friendship we developed across these years. I will only regret not having got on time our hands on a few ostrich eggs. Virginia, *qué gusto haber compartido esta media década de aventura. Siempre fuiste guarida emocional y sin ti, ¿a quién hubiera ido yo a quejarme o a contar mis locuras? Contigo nunca eché en falta un buen cotilleo, ni –justificado– escaqueo. Aunque de ciencia más bien poco, lo que sí me enseñaste fue a no combinar el azul oscuro con el negro. Por tu culpa ya no me río igual, y con la tontería, al final he acabado confundiendo hasta mi propio acento.*

Prof. dr. Frank Zaucke, how could I have ever imagined the entire universe exists inside the cartilage matrix? The game of finding its secrets turned to be addictively fun. Thank you for helping me navigate in this project and for welcoming me in your lab. Also, thanks to the other senior researchers -Doctors and Professors- that helped shaping the CarBon consortium with Eric and Gerjo. In particular: **Andy, Bent, Christa, Danny,**

John, Liesbet, Linda and Roberta. I will miss all the fun meetings we had across Europe, packed with science, new ideas and good food and wine.

My words of gratitude extend further to the members of the **Committee**, thanks for accepting the invitation and taking the time to read and to evaluate my dissertation.

Next, I would also like to acknowledge the main two departments of the Erasmus MC Rotterdam that provided the frame to allow cross-disciplinary scientific discussions. First one and where I belonged, the department of Oral and Maxillofacial Surgery, that took the lead in translational meetings. Within the department, a special mention to **Prof. dr. Eppo van Wolvius**; your input was key to direct my projects straight towards practical applications. And second, the department of Internal Medicine, more focused on the fundamental research side. **Bram, Jeroen and Marjolein**, it was always fun to mix a little the groups, to get constructive comments and to row together!

While innovative ideas are fundamental to progress, materialising them is the next step on the process. With regards to this, the three lab technicians of our Connective Tissue Repair Lab where those who brought them to life. **Wendy**, without your care for duty and order, how chaotic would have been everything around? **Janneke**, you taught me a lot during these years, and supported me on each crazy project I jumped in. With your tips and tricks, my life in the lab turned to be much easier. And **Nicole** (only person lucky enough to have seen the true stressed version of me), from you I learned the importance to keep calm when experiments start to go wrong. At the end of the day, laughing at the small stumbles along the path makes the journey more fun, doesn't it?

Also of great help, thanks **Yanto** for the support with the micro-CT scanner. With those great images as starting point, our manuscript turned into a piece of art. Key for this project were also our other collaborators from Eindhoven **Sandra** and **Bert**, thanks for your guidance and assistance automating those image analyses.

The amount of things that need to be organised at any great project sometimes lack the recognition that they deserve. For this, I would like to show my gratitude to the project managers that collaborated on the CarBon project: **Marloes** and **Francesca**; and later **Niamh**: thanks for taking over when help was needed. Also, to the two **Sandra** secretaries, from the Orthopaedics and Oral and Maxillofacial Surgery departments. Thank you all for the reminders and for helping me to navigate through all the administration.

When I arrived in 2017 to the lab, I felt immediately welcomed by colleagues coming from all around the world. As it is natural, we always meet at different stages of our careers. From the bachelor level to the postdoc level, it was a great inspiration to see you fighting for your projects and progressing along the way. To those that already left: **Yvonne, Kavitha, Diego, Johannes, Niamh, Shorouk, Callie, Sohrab, Panithi, Lizette, Caiomhe** and **Pedro**. Thank you for the wonderful memories during the time you were around, and I wish you good luck on your studies and jobs. To those who stayed:

Roberto and **Andrea**, the two Italians that against all odds, convinced me to put on my sneakers to go running every now and then. I am sure you will keep the lab growing and will get great success on your careers. And to the rest of PhD student colleagues of the lab. **Mauricio**, siempre disfruté de tus pensamientos en voz alta. Qué buena la energía y vida que trajiste al llegar, que tan vivo nos volvió a todo el grupo. **Chantal** and **Tim**, it was good that you both brought some calmness to our Spanish-Dutch office. Now, after absorbing more and more of the Dutch culture (I'm past the level of cheese sandwiches), wow, I see how the noise levels went sometimes off-hand. **Imke**, it was a pleasure supervising you during your master internship and see you grow along the way. I wish all those of you finishing your PhD's good luck, and all the best in your future endeavours. And last, to the new people that came to the lab during the times of corona. I only regret not having had the chance to get to know you a little more, and I wish you a lot of fun shaping the lab and developing your career.

My thoughts go also to the other PhD students of the CarBon project. **Kathi**, we had the chance to work side-by-side for a large part of our projects, and I would like to thank you for your support and help during my secondments at Germany. **Mengjie** and **Claudio**, thanks too for your help which resulted in very nice publications! And to the rest of colleagues from Carbon: **Cansu**, **Raphaëlle**, **Soraia**, **Farhad**, **Martina**, **Nicolás**, **Satanik** and **Dionysia** (plus **Yannick** and **Mauricio**). Let's be honest, our group ruled. I loved getting together at every consortium meeting and congress possible. From our scientific discussions to the awesome dinners and parties that followed after, I got very good memories from these times. I hope you keep progressing on your jobs and that we all stay in touch!

Y mi grupo de españoles del hospital: **Ana**, **Jesús**, **Gonzalo**, **Leticia**, **Antonio** (y **Virginia**). Con vosotros, la falta de sol y de comidas calientes sí que se podía tratar como algo serio. Echaré de menos las veces que quedábamos a compartir orgullosos nuestras tortillas de patatas o nuestras reservas de jamón, extrañando nuestro lejano hogar. Teneros cerca fue un gusto, y ahora que cada uno ha seguido su propio camino, os deseo lo mejor y que nos volvamos a encontrar.

Papà i **Mamà**, sense tindre-vos, qui haguera imaginat tot el que es faria realitat? Em vàreu ensenyar, acompanyar i animar a volar. Sempre posàreu la meua felicitat per davant de la vostra, i sols Déu sap fins a quin punt m'heu volgut. Com les oronetes, en l'ànima porte el tornar. **Javi** i **Chelo**, encara que en la distància, sempre vos porte al cor. Espere que allà on aneu sigau feliços. Mai oblideu que sempre em tindreu. I les iaies **Consuelo** i **Carmen**. Que bo que hàgeu arribat a llegir açò, el record escrit de la meua passió científica.

And now, what? **Martha**, you are the reason why I stayed here after all of this. The one that kept me sane during the quarantine. The only person capable to make me want to learn Dutch. The one I seek to grow together with. I love you.

PhD portfolio

Personal details

Name PhD Student: Enrique Andrés Sastre

Erasmus MC department: Department of Oral and Maxillofacial Surgery

PhD period: March 2017 – December 2020

Research School: Postgraduate School Molecular Medicine

Promotor: Prof. dr. Gerjo J.V.M. van Osch

Co-Promotor: Dr. Eric Farrell

PhD Training

Courses and Workshops		Workload (ECTS)
2017	Biomedical Research Techniques	1.5
2017	ExCarbon Summer School, Regensburg	1
2017	FELASA C	4
2018	Research Integrity	0.3
2018	Personal Leadership, Management and Communication	1
2019	Supervising students	0.3
2019	Presentation skills	1
2020	Biomedical English Writing and Communication	3
2017-2020	CarBon Training program (biannually)	1
2020	Medicine by design Summer School, online	0.5

(Inter)national Conferences

2017	21 th Molecular Medicine Day, Rotterdam. Poster presentation	0.5
2018	Annual DGMB meeting, Stuttgart. Poster presentation	1
2018	22 th Molecular Medicine Day, Rotterdam. Poster presentation	0.5
2018	Annual NVMB meeting, Lunteren. Poster presentation	1
2019	Annual NVMB meeting, Lunteren. Oral presentation	1
2019	23 th Molecular Medicine Day, Rotterdam. Poster presentation	0.5

2019	TERMIS-EU Conference, Rhodes. Oral and poster presentation	1
2019	28 th annual NBTE meeting, Lunteren. Oral presentation	1
2020	Annual NVMB meeting, online. Poster presentation.	1

CarBon , Department and Research Group presentations and meetings

2017-2020	CarBon EU project consortium meetings (biannually), Europe	2
2017-2020	Research meetings dept Internal Medicine (weekly)	2
2017-2020	Research meetings Connective Tissue Repair Lab (depts Orthopaedics and Sports Medicine, Otorhinolaryngology, & Oral and Maxillofacial Surgery (weekly)	2
2017-2020	Journal Club (monthly)	1
2017-2020	Oral and Maxillofacial Surgery Dept. Day (annually)	0.5
2019-2020	Willem de Kooning Academy (Rotterdam, Netherlands). Lecture given for the major in Advertising (annually)	0.5
2020	Science Gallery Rotterdam (Rotterdam, Netherlands). Collaborative online presentation	0.5

Student Supervision

2020	Imke Jansen	1
2020	Jayant Jagessar-Tewari	0.5

Miscellaneous

2019	Early-Stage Researcher organization committee member, Dutch society for matrix biology (NVMB)	0.5
------	---	-----

Awards

2018	Best Scientific Poster (Molecular Medicine Day)	
2018	Van den Hoof Award for the best discussion (Dutch Society for Matrix Biology)	
2019	Pauline van Wachem Award for the best oral presentation (Dutch Society for Matrix Biology)	

Curriculum Vitae

Enrique Andrés Sastre was born on the 27th of July 1992 in Valencia (Spain). He is the oldest of three siblings. At the age of 3 he began his musical studies, and attended to the school Madre Josefa Campos until adulthood. During this time, the accidental finding of some chemistry equipment in the attic and the chance to play with it, piqued his interest in science. This brought Enrique to start in 2010 his Bachelor in Biotechnology at the University of Valencia. In parallel, he undertook his liberal studies at the University Francisco de Vitoria (Madrid), while spending his summers in various European countries volunteering in social projects. In 2014, he obtained his bachelor degree upon completing his thesis on lung cancer under the supervision of Dr. Javier Pereda. His wish to travel and to live new experiences, brought Enrique to enrol in a master in Regenerative Biology and Medicine at the Technical University Dresden, in Germany. There, he worked in different laboratories. First, at the Center for Regenerative Therapies Dresden he evaluated the potential of different drugs to treat diabetes. Then, he studied the cytocompatibility of bone calcium cements at the Medical Theoretical Center. Following those experiences, he conducted his master thesis at the Carl Gustav Carus Hospital, exploring the role of an iron-sensing protein in bone under the supervision of Dr. Ulrike Baschant. After this experience, Enrique was awarded with a Marie-Curie ITN Scholarship in the Netherlands and joined in 2017 the international consortium of PhD students *CarBon* aiming to find new treatments for skeletal diseases. In his project, based at the Erasmus MC Rotterdam, Department of Oral and Maxillofacial Surgery, he sought for novel extracellular matrix compounds that could improve skeletal regeneration under the supervision of Dr. Eric Farrell and Prof. dr. Gerjo van Osch. As a result of his work, Enrique received three awards and co-authored five publications. In 2019 Enrique started living together with his girlfriend Martha, and adopted an independent but surprisingly affectionate cat. Without them, the lockdown imposed during the 2020 health crisis would have been unbearable. During his academic career, Enrique has met people all around the world which have resulted in life-lasting friendships. Currently, Enrique is working at Janssen Pharmaceutical contributing to bring the latest medical therapies to patients.